AARHUS UNIVERSITY

Aarhus University
Mechanical Production & Engineering

Modelling solar, wind and hydro time series impacted by climate change and investigating energy droughts

M.Sc. Mechanical Engineering Thesis

Supervisor:	Marta Victoria
Co-supervisor:	Ebbe Kyhl Gøtske
Author:	Waleed Arshad
Student ID:	202010807
Deadline:	03-01-2023

January 3, 2023

Acknowledgements

Firstly, my most profound appreciation and gratitude goes to Associate Professor Marta Victoria and co-supervisor PhD Fellow Ebbe Kyhl Gøtske, for their supervision, guidance and time in helping me throughout this thesis.

Then, I would also like to thank Aarhus University for these two years, which proved to be an amazing learning journey with plenty of challenges.

Last but not least, I would like to thank my family for their love and support.

Abstract

The rise of Earth's temperature represents one of the biggest challenges of the modern world. If this upheaval is tackled in the appropriate way, it could lead to a sustainable and self-sufficient world. This thesis analyses that in order to reduce future anthropogenic climate changes, the global energy systems need to include, in a systematic and calculated way, a higher share of renewable energies i.e. solar, wind and hydro. However, the availability, intermittency and generation capacity of these renewable energy sources strongly depend on the climate. Therefore, the consequences caused by a shift in the climate, i.e. energy droughts and extreme events, is a major concern in terms of production and profitability for the energy system. This study investigates the impacts of climate change on solar, wind and hydro resources. The beginning and end of the century evolution of solar, wind and hydro resources is investigated by means of a multi-model ensemble comprised of 5 global circulation models. In addition, the most recent scenarios of greenhouse gases emissions, the Shared Socioeconomic Pathways (SSPs), are considered i.e. SSP1-2.6 (sustainability), SSP2-4.5 (middle of the road) and SSP5-8.5 (fossil-fueled development), from Phase 6 of the Coupled Model Intercomparison Project (CMIP6) in order to quantify the climate risks towards the end of the century. This thesis uses climate data and then converts that into time series representative for the generation of solar, wind and hydro energy at a country level. The conversion from weather parameters into energy production is done with ATLITE. In addition, capacity factors, i.e. ratio between the delivered powered and the installed capacity, time series is modelled for solar and wind energy for 38 European countries, while runoff time series is modelled for hydro energy for 22 European countries.

A hindcast analysis within the period from 2001 and 2015 is carried out in order to validate and calibrate modelled data for solar, wind and hydro. Then a comparison for the modelled data is made for two periods. The first period corresponds to the Beginning of the Century (BOC) from 2001 til 2030 and the second period corresponds to the End of the Century (EOC) from 2071 til 2100. Changes due to climate change in terms of yearly averaged capacity factors and runoff are investigated. In addition, seasonal changes and extreme events such as periods of drought and overflow are analysed.

Regarding solar energy, the ensemble climate model, for the worst case, predicts a decrease for Northern Europe in terms of capacity factor and an increase for Southern Europe with strong inter-model agreement. The Nordics, i.e. Norway, Sweden and Finland, encounter a decrease in relative capacity factors within the range from -7% to -11%. Meanwhile, the Alps, i.e. France, Switzerland, Austria and Italy show an increase within the range from +3% to +5%. The Mediterranean, i.e. Spain and Portugal, show an increase ranging from +5% to +7%. This study also finds that for SSP1-2.6, mitigating emissions improves solar power generation by 5%, while no significant changes are noticeable for SSP2-4.5. When it comes to intra-annual analysis, the seasonality of PV production becomes more pronounced as the generation grows more strongly in winter compared to summer (SSP1-2.6) or grows in summer and decreases in winter (SSP 5-8.5). With the exception that for Southern Europe, PV generation decreases in summer while it increases in winter for SSP5-8.5. The reduction in the capacity factors that occurs in the Nordics, causes more frequent and longer periods of drought (defined as $< 10^{\text{th}}$ percentile of historical values). In addition, Mediterranean countries also forecast an increase in days with a higher clearness index, i.e. days with clear-sky radiation, while the Nordics forecast the

opposite.

Moreover, when it comes to the wind resource, SSP5-8.5 projects a decrease, despite large interannual and intermodel variability, across the whole European continent (10%-20%), particularly for the Nordics and the British Isles. Even though, SSP1-2.6 and SSP2-4.5 predict that towards the end of the century small localized areas might experience an increase in wind energy (15%-30% in easter Ukraine and Turkey), all other European countries will experience a significant decrease (5%-15%). The general decrease in the capacity factors that occurs for SSP5-8.5, causes more frequent and longer periods of drought for all of Europe, with Italy representing the country with the highest number of total days in a year with drought. In addition, the results also indicate an increase in the frequency and duration of overflow periods (defined as $> 90^{\text{th}}$ percentile of historical values) for Northeast Europe, i.e. Latvia, Russia, Lithuania, Estonia, while a decrease for Southern Europe, i.e. Spain, Austria. This study also suggests an increase in the intra-annual variability in the British Isles, Turkey, Iberia and Northeast Europe.

Furthermore, hydro energy also is expected to significantly change towards the end of the century. SSP5-8.5 suggests an increase in annual inflow in Northern Europe by 20% and a decrease in Southern Europe by 30%. Intra-annual analysis forecasts that inflow decreases during spring and summer, while it increases during fall and winter. More frequent and prolonged droughts are expected in Iberia.

The results show that for future work it has significant importance to include climate affected-weather data in power system simulations, as this will impact the optimization of a future energy system based on the scenario considered.

Table of Contents

1 INTRODUCTION **1**
1.1 Research questions . . . 2
1.2 Thesis overview . . . 3
1.3 Definition of terms . . . 3

2 Literature review **5**
2.1 Solar energy . . . 5
2.2 Wind energy . . . 6
2.3 Hydro energy . . . 7

3 Methodology **9**
3.1 Models . . . 10
3.2 Methods . . . 11
3.2.1 Interannual daily mean . . . 11
3.2.2 Interranual monthly mean . . . 11
3.2.3 Interranual yearly mean . . . 11
3.2.4 Standard deviation . . . 12
3.2.5 Normalised root mean square error . . . 12
3.2.6 Clearness Index . . . 12
3.2.7 Irradiance . . . 14
3.2.8 PV time-series modelling . . . 16
3.2.9 Wind time-series modelling . . . 17
3.2.10 Upstream basin determination and runoff aggregation . . . 18

4 Historical validation **20**
4.1 Solar energy hindcast . . . 20
4.2 Wind energy hindcast . . . 22
4.3 Hydro energy hindcast . . . 23

5 Evaluation of climate change signal **25**
5.1 Solar energy projection . . . 25
5.2 Wind energy projection . . . 29
5.3 Hydro energy projection . . . 32

6 Energy droughts and extreme events **36**
6.1 Solar energy extreme events . . . 36
6.2 Wind energy extreme events . . . 38

7 Discussion **41**

8 Conclusions **44**

9 Future Work **46**

Appendices **50**

Appendix A Solar energy **51**
A.1 Intra-annual analysis for SSP2-4.5 . . . 51
A.2 Intra-annual analysis for SSP1-2.6 . . . 52
A.3 Energy droughts and extreme events for SSP2-4.5 . . . 53
A.4 Energy droughts and extreme events for SSP1-2.6 . . . 55

Appendix B Wind energy **57**
B.1 Intra-annual analysis for SSP2-4.5 . . . 57
B.2 Intra-annual analysis for SSP1-2.6 . . . 58
B.3 Energy droughts and extreme events for SSP2-4.5 . . . 59
B.4 Energy droughts and extreme events for SSP1-2.6 . . . 61

Appendix C Hydro energy **63**
C.1 Intra-annual analysis for SSP2-4.5 . . . 63
C.2 Intra-annual analysis for SSP1-2.6 . . . 64

List of Figures

3.1 Solar and wind energy climate projection methodology explained with a flowchart . . . 9
3.2 Hydro energy climate projection methodology explained with a flowchart. The validation and calibration step with ERA5 was not finalised during this Master Thesis . . . 10
3.3 Representation of Solar Radiation Components (Souza et al., 2019) . . . 15
3.4 Power curve of the wind turbine Vestas V112-3.3 MW (Petrakopoulou, Robinson, and Loizidou, 2016) . . . 18

4.1 Solar energy climate model hindcast for Spain, Norway and Germany. This figure includes data for five GCMs and ERA5 prior to calibration . . . 21
4.2 Solar energy climate model hindcast for Spain, Norway and Germany. This figure includes data for the averaged ensemble and ERA5 after calibration 21
4.3 Wind energy climate model hindcast for Spain, Norway and Germany. This figure includes data for five GCMs and ERA5 prior to calibration . . . 22
4.4 Wind energy climate model hindcast for Spain, Norway and Germany. This figure includes data for the averaged ensemble and ERA5 after calibration 23
4.5 Hydro energy climate model hindcast for Spain, Norway and Germany. This figure includes data for five GCMs prior to calibration . . . 24

5.1 Ensemble mean relative change in capacity factors between EOC and BOC for solar energy. The results are for SSP5-8.5, SSP2-4.5 and SSP1-2.6 . . . 26
5.2 Ensemble mean intra-annual relative change in capacity factors between EOC and BOC for solar energy. The results are for SSP5-8.5 . . . 27
5.3 Kernel density estimations of the probability density functions for the yearly solar energy capacity factors in Spain, Norway and Germany at the BOC (blue) and EOC (yellow) periods for the SSP5-8.5 scenario . . . 28

5.4 Kernel density estimations of the probability density functions for the daily solar energy capacity factors in Spain, Norway and Germany at the BOC (blue) and EOC (yellow) periods for the SSP5-8.5 scenario 29
5.5 Ensemble mean relative change in capacity factors between EOC and BOC for wind energy. The results are for SSP5-8.5, SSP2-4.5 and SSP1-2.6 . . . 30
5.6 Ensemble mean intra-annual relative change in capacity factors between EOC and BOC for wind energy. The results are for SSP5-8.5 31
5.7 Kernel density estimations of the probability density functions for the yearly wind energy capacity factors in Spain, Norway and Germany at the BOC (blue) and EOC (yellow) periods for the SSP5-8.5 scenario 32
5.8 Ensemble mean relative change in runoff between EOC and BOC for hydro energy. The results are for SSP5-8.5, SSP2-4.5 and SSP1-2.6 33
5.9 Ensemble mean intra-annual relative change in runoff between EOC and BOC for hydro energy. The results are for SSP5-8.5 34
5.10 Kernel density estimations of the probability density functions for the yearly hydro energy runoff in Spain, Norway and Germany at the BOC (blue) and EOC (yellow) periods for the SSP5-8.5 scenario 35

6.1 Duration and frequency of solar energy drought periods, determined as consecutive days with capacity factors less than the 10th percentile of capacity factors at the BOC, evaluated for the BOC and EOC periods under the SSP5-8.5 scenario 37
6.2 Duration and frequency of solar energy overflow periods, determined as consecutive days with capacity factors more than the 90th percentile of capacity factors at the BOC, evaluated for the BOC and EOC periods under the SSP5-8.5 scenario 38
6.3 Duration and frequency of wind energy drought periods, determined as consecutive days with capacity factors less than the 10th percentile of capacity factors at the BOC, evaluated for the BOC and EOC periods under the SSP5-8.5 scenario 39
6.4 Duration and frequency of wind energy overflow periods, determined as consecutive days with capacity factors more than the 90th percentile of capacity factors at the BOC, evaluated for the BOC and EOC periods under the SSP5-8.5 scenario 40

A.1 Ensemble mean intra-annual relative change in capacity factors between EOC and BOC for solar energy. The results are for SSP2-4.5 51
A.2 Ensemble mean intra-annual relative change in capacity factors between EOC and BOC for solar energy. The results are for SSP1-2.6 52
A.3 Duration and frequency of solar energy drought periods, determined as consecutive days with capacity factors less than the 10th percentile of capacity factors at the BOC, evaluated for the BOC and EOC periods under the SSP2-4.5 scenario 53
A.4 Duration and frequency of solar energy overflow periods, determined as consecutive days with capacity factors more than the 90th percentile of capacity factors at the BOC, evaluated for the BOC and EOC periods under the SSP2-4.5 scenario 54

A.5 Duration and frequency of solar energy drought periods, determined as consecutive days with capacity factors less than the 10th percentile of capacity factors at the BOC, evaluated for the BOC and EOC periods under the SSP1-2.6 scenario . . . 55
A.6 Duration and frequency of solar energy overflow periods, determined as consecutive days with capacity factors more than the 90th percentile of capacity factors at the BOC, evaluated for the BOC and EOC periods under the SSP1-2.6 scenario . . . 56

B.1 Ensemble mean intra-annual relative change in capacity factors between EOC and BOC for wind energy. The results are for SSP2-4.5 . . . 57
B.2 Ensemble mean intra-annual relative change in capacity factors between EOC and BOC for wind energy. The results are for SSP1-2.6 . . . 58
B.3 Duration and frequency of wind energy drought periods, determined as consecutive days with capacity factors less than the 10th percentile of capacity factors at the BOC, evaluated for the BOC and EOC periods under the SSP2-4.5 scenario . . . 59
B.4 Duration and frequency of wind energy overflow periods, determined as consecutive days with capacity factors more than the 90th percentile of capacity factors at the BOC, evaluated for the BOC and EOC periods under the SSP2-4.5 scenario . . . 60
B.5 Duration and frequency of wind energy drought periods, determined as consecutive days with capacity factors less than the 10th percentile of capacity factors at the BOC, evaluated for the BOC and EOC periods under the SSP1-2.6 scenario . . . 61
B.6 Duration and frequency of wind energy overflow periods, determined as consecutive days with capacity factors more than the 90th percentile of capacity factors at the BOC, evaluated for the BOC and EOC periods under the SSP1-2.6 scenario . . . 62

C.1 Ensemble mean intra-annual relative change in runoff between EOC and BOC for hydro energy. The results are for SSP2-4.5 . . . 63
C.2 Ensemble mean intra-annual relative change in runoff between EOC and BOC for hydro energy. The results are for SSP1-2.6 . . . 64

List of Tables

3.1 Overview of GCMs, institution and resolution . . . 11

C.1 Overview of yearly (2014-2019) solar energy historical capacity factors from IRENA for 38 European countries . . . 65
C.2 Overview of IRENA and ensemble solar energy capacity factors with relative percentage difference for 38 European countries . . . 66
C.3 Overview of yearly averaged solar energy capacity factors standard deviation at BOC and EOC with relative percentage change column . . . 67
C.4 Overview of NRMSE values for solar energy before and after calibration. The calibration significantly improves the match with ERA5 data . . . 68

C.5 Overview of NRMSE values for wind energy before and after calibration. The calibration significantly improves the match with ERA5 data 69
C.6 Overview of yearly averaged wind energy capacity factors standard deviation at BOC and EOC with relative percentage change column 70
C.7 Overview of yearly averaged hydro energy capacity factors standard deviation at BOC and EOC with relative percentage change column 71

List of Abbreviations

GHG	Greenhouse Gases
BOC	Beginning of the century
EOC	End of the century
GCM	General circulation model
SSP	Shared Socioeconomic Pathways
CMIP	Coupled Model Intercomparison Project
Cordex	Coordinated Regional Climate Downscaling Experiment
MAPE	Mean absolute percentage error
RMSE	Root mean square error
NRMSE	Normalised root mean square error
PV	Photovoltaics
RCM	Regional climate model
RCP	Representative concentration pathway

1 INTRODUCTION

Ever since the start of the industrial revolution, energy usage has increased drastically. The energy sources used were mainly represented by fossil fuels such as coil, oil and gas. However, these fuels, when used to produce energy, emit greenhouse gases such as CO_2, CH_4 and N_2O. When these gases become highly concentrated in the atmosphere, the consequence is an alteration of the balance between incoming and outgoing radiation. In fact, infrared radiation get trapped inside the atmosphere, creating a second source of radiation to warm the Earth's surface. This causes Earth to become warmer than it would otherwise be (CSI, 2022).

In order to mitigate the effects caused by an alarming amount of carbon dioxide released into the atmosphere, world leaders at the UN Climate Change Conference (COP21) in Paris reached an agreement in December 2015, known also as the Paris Agreement (UN, 2015)(UNFCCC, 2022). This Agreement sets long-term goals for all countries to reduce greenhouse gas (GHG) emissions to limit the global temperature increase in the 21^{st} century to $2°C$, while pursuing efforts to limit the increase even further to $1.5°C$.

In line with the Paris Agreement, the EU 2030 Climate Target Plan (EU, 2020) sets a more ambitious and cost-effective path to achieve climate neutrality by 2050. The Commission proposes for EU countries to reduce GHG emissions to at least 55% below 1990 levels by 2030.

In addition, the impact assessment of this proposal paves the way for adapting climate and energy policies to achieve decarbonization of the European economy. This means that the vast majority of the share used to produce energy will be comprised by renewable energies, e.g solar, wind and hydro energy.

A change in the climate will have an impact both on the energy generation and the energy consumption. In fact, climate change will alter energy generation from the renewable energies mentioned above as they are weather dependent. Moreover, an increase in the mean temperature of the Earth will affect the heating and cooling sectors during summer and winter.

In particular, solar photovoltaics (PV) power generation is linked to atmospheric parameters such as cloud coverage and optical thickness, aerosols and water vapor. Previous studies have analysed the impact of climate change on solar energy under different climate change models, generally finding relatively low ranges of change in solar potential (Wild et al., 2015; Jerez et al., 2015; Gaetani et al., 2014; Panagea et al., 2014; Crook et al., 2011). These results are based on the Climate Modelling Intercomparison Project Phase 5 (CMIP5), where general circulation models (GCMs) and the Coordinated Downscaling Experiment (EURO-CORDEX) are used to simulate global climate data. However, most EURO-CORDEX models are not accurate in predicting surface solar radiation since aerosols are kept constant in the majority of the regional climate models used for downscaling (Gutiérrez et al., 2020; Bartók et al., 2017). In addition, coarser spatial resolutions

limit the accuracy attained for solar PV modelled results, since the clouds are smaller than the grid resolution.

Moreover, previous studies regarding wind energy have shown that wind speed correlation generally appears to increase (Schlott et al., 2018), that the wind resource increases in the Northern Europe and decreases over Southern Europe, and an increase in the intra-annual variability (seasonality) (Carvalho, Rocha, Gómez-Gesteira, et al., 2017; Reyers, Moemken, and Pinto, 2016; Pryor and Barthelmie, 2010). The wind energetic potential varies with the wind speed cubed, therefore even small variations in the wind speed will greatly affect the energy produced by wind turbines. Considering that the lifetime of wind farms can even be of 30 years, estimating the impacts of global warming scenarios on wind energy resources becomes even more crucial for the reliability, profitability and stability of the wind produced electricity (Pryor and Barthelmie, 2010).

Hydropower also has an important role in an energy system with a high penetration of renewable energies. In fact, it can be crucial in order to balance the solar and wind intermittent weather-dependent renewable energies. Using pumped hydroelectric storage facilities, it is possible to store excessive energy and, more importantly, by using hydroelectric reservoirs it is possible to dispatch energy when the demand is not met by the wind and solar energy generation. Hydroelectricity in itself contributes to 15.0% of the global energy production and therefore plays an important role in a highly renewable energy system (IEA, 2020). Previous studies regarding hydroelectric energy have shown that the climate impact causes a north-south Europe split, where the north is characterized by an increase in the annual inflow while the south is characterized by a decrease (M. van Vliet, Vögele, and Rübbelke, 2013; Schlott et al., 2018; Gøtske and Victoria, 2021).

1.1. Research questions

This master thesis investigates, validates and calibrates the historical values for the three renewable energies. For the period between 2001 and 2015, annually-averaged capacity factors for wind and solar can be calculated from the modelled time series and compared to historical values based on the historical electricity generation and installed capacity, which has been retrieved from Irena (IRENA, 2022) and reanalysis data from ERA5, to validate the time series. Similarly, historical inflow values for hydropower can also be compared to BOC modelled inflow values, in order to answer research question 1(RQ1)

- RQ1: *What is the deviation between modelled and actual historical data for solar, wind and hydroelectric energy?*

In addition, this master thesis also investigates how the solar, wind and hydro energy sources depend on climate change in Europe at the Beginning of the Century (BOC) and at the End of the Century (EOC) for different climate models included in CMIP6, to answer research question 2 (RQ2)

- RQ2: *How are solar, wind and hydro energies impacted by different CMIP6 climate change scenarios in Europe at BOC and EOC?*

Anthropogenic climate changes can affect the behaviour and configuration of a highly renewable energy system, since electricity generation and consumption depend on the weather. Therefore, this master thesis investigates the effects of climate change on future

solar, wind and hydro energy resources, to answer research question 3 (RQ3).

- RQ3: *How is the potential future climate change impact in solar, wind and hydro energy resources expected to affect:*
  a) interannual variability?
  b) intra-annual variability?
  c) intermodel variability?

Lastly, this thesis also compares the energy droughts and extreme events at BOC and EOC for solar, wind and hydro energy, to answer research question 4 (RQ4).

- RQ4: *How does climate change affect frequency and magnitude of extreme events for solar, wind and energy ?*

1.2. Thesis overview

This report will first present a brief literature review (Chapter 2), in which a description of the current state of the art for solar, wind and hydro energy resources is provided. Subsections for each of the energy sources are present to describe relevant papers.

Thereafter, Chapter 3 analyses the historical validation and calibration for solar, wind and hydro energy resources to answer (RQ1).

Moreover, Chapter 4 investigates how these renewable energy sources will behave with respect to three scenarios of greenhouse gases emissions, the Shared Socioeconomic Pathways (SSPs), i.e. SSP1-2.6, SSP2-4.5 and SSP5-8.5, in order to quantify the climate risks towards the end of the century to answer (RQ2)

In addition, Chapter 5 focuses in depth on the main consequences of climate change in terms of intermodel, interannual and intra-annual variability in order to answer (RQ3). Also, this chapter includes the energy droughts and extreme events analysis in order to answer (RQ4).

Individual method and data sections can be found in each chapter, with Chapter 6 presenting results and key findings of this study.

1.3. Definition of terms

In the following subsections, key terms used in this master thesis are explained.

Capacity factors

The capacity factor of an energy resource is given by the ratio between the mean power generation in a considered temporal period and the cumulative installed capacity, i.e. the rated power of that technology.

$$\text{Capacity Factor} = \frac{\text{Average power delivered by the system}}{\text{Installed power capacity}} \tag{1.1}$$

Shared Socioeconomic Pathways (SSPs)

To quantify the climate risks towards the end of the century, three most recent scenarios of greenhouse gases emissions, the Shared Socioeconomic Pathways (SSPs), are considered i.e. SSP1-2.6 (sustainability), SSP2-4.5 (middle of the road) and SSP5-8.5 (fossil-fueled development), from Phase 6 of the Coupled Model Intercomparison Project (CMIP6). These SSPs represent an update of the CMIP5 scenarios, which were called Representative Concentration Pathways (RCPs). Here it is possible to find a description of the three scenarios used according to (Nazarenko et al., 2022; Riahi et al., 2017):

1. SSP1-2.6: optimistic scenario representing sustainable development with radiative forcing of 2.6 W/m^2 by the year 2100 is a remake of the scenario RCP2.6. Designed with the aim of representing a development in line with the $2°C$ target. In fact, the higher peak temperature will be of $1.9°C$ during the 21^{st} century compared to the 1850-1880 period. This scenario assumes that strong climate protection measures will be taken into consideration

2. SSP2-4.5: middle of the road scenario with radiative forcing of 4.5 W/m^2 by the year 2100 is a remake of the scenario RCP4.5. Designed with the aim of representing a development with a higher peak temperature of $2.7°C$ during the 21^{st} century compared to the 1850-1880 period. This scenario assumes that climate protection measures will be taken into consideration

3. SSP5-8.5: worst case scenario representing fossil-fueled development with radiative forcing of 8.5 W/m^2 by the year 2100 is a remake of the scenario RCP8.5. Designed with the aim of representing a development with a higher peak temperature of $5.2°C$ during the 21^{st} century compared to the 1850-1880 period. This scenario assumes that climate protection measures will be taken into consideration

Types of hydropower plant

In this Master Thesis three types of hydropower plants are considered:

1. Hydroelectric reservoir: most common hydro power plant, which utilises a dam to store and obtain a hydraulic head. By dispatching water through some turbines, electric energy is produced.

2. Run-of river: converts kinetic energy of the river into electric energy by diverting a portion of the river flow through turbines

3. Pumped hydroelectric storage: works by using excess electricity generation to pump water from a low reservoir to a higher one. Then, when electricity is needed, water is dispatched from the high to the low reservoir

   The hydroelectric reservoir represent the scope of this study, but data from run-of-river power plants is included for countries which do not have data for the hydro-electric reservoir.

2 Literature review

This chapter summarizes the current state of the art within prediction of solar, wind and energy resources towards the end of the century. Firstly, the reader is introduced to two papers outlining the main findings regarding solar energy for Europe from CMIP5 and CMIP6. Then, three papers simulating climate change impact on wind energy for Europe and North America are described. In addition, two papers examining the future operation of hydropower in Europe under climate change are also reported. In the end, a table summarizing these papers is also present, with relevant temporal and spatial resolution, SSPs used and main findings.

2.1. Solar energy

(Hou et al., 2021) analyses how PV potential changes according to two different mitigation scenarios in Europe during the 21^{st} century. SSP1-2.6 and SSP5-8.5 from CMIP6 are used in order to quantify the climate risks for solar energy. To account for model uncertainty, 28 GCMs are considered in this study. Daily and monthly data with a model resolution of $\mathbf{2.5}^\circ \times \mathbf{2.5}^\circ$ (≈ 250 km $\times$ 250 km) is used. In addition, four different climate variables are analysed:

- Surface downwelling shortwave radiation under all-sky conditions (rsds)
- Surface temperature (tas)
- Surface downwelling shortwave radiation under clear-sky conditions (rsdscs)
- Total cloud fraction (clt)

Bias correction is done by using meteorological reanalysis and satellite data with temporal resolution of daily data. In addition, a seasonal analysis approach is also used to analyze summer (June, July and August) and winter (December, January and February) changes separately. This intra-annual analysis is helpful to investigate potential impacts on a seasonal cycle which would be otherwise masked by the annual means. Moreover, two different 20-year periods are used: 1995-2014 from the historical CMIP6 simulations and 2081-2100 from the SSPs scenarios. The results show that for SSP1-2.6 a general positive change is expected for PV electricity production throughout Europe, leading to approximately 5% more power generation by the end of the century compared to historical values. The intra-annual analysis forecasts that PV generation is expected to grow independently of seasons or region with a generally high model agreement. Whereas, SSP5-8.5 predicts a more complex PV change pattern for Europe. The annual means suggest that Southern and Mediterranean Europe will experience an increase in PV generation, while the Nordics will experience a decrease. The intra-annual analysis predicts a summer PV production increase in central and Northern Europe but a decrease in the south, while

this pattern in flipped in winter similarly to results from previous studies (Müller et al., 2019).

Similarly, (Schlott et al., 2018) uses three ensemble members of the EURO-CORDEX project to analyse the impacts of climate change on solar, wind and hydroelectricity in a cost-optimal highly renewable European electricity network. The RCP8.5 scenario is used, which is associated with a strong climate change forecasting a temperature increase of 2.6-4.8 $^{\circ}C$ until the end of the century. Compared to CMIP6, this study shows small changes for PV capacity factors, which are mostly decreasing for the whole Europe with the exception of Spain, parts of Italy and France.

2.2. Wind energy

(Carvalho, Rocha, Costoya, et al., 2021) investigates how future European wind resources change with two different CMIP6 climate projections: SSP2-4.5 and SSP5-8.5. In addition, daily and monthly wind data (sfcWind variable in CMIP6) is used for 15 GCMs which have a horizontal resolution higher than $\mathbf{1.25}^{\circ}$ ($\approx$ 125 km) in latitude and longitude, and with data for the historical period. This study investigates future changes in the European wind resource with respect to its large-scale changes. In fact, the GCMs spatial resolutions are typically too coarse in order to accurately quantify the wind resource of a given area. All the GCMs are aggregated into a multi-model ensemble (MME), which is a better and more reliable method of showing results than single-model experiments since it minimizes individual model uncertainties. Large scale changes are indicative of what can be expected at smaller scales. Furthermore, three 20-year time periods are considered: 1995-2014 (historical), 2046-2065 (medium-range future) and 2081-2100 (long-range future).

Reanalysis data from ERA5 is used in order to validate the wind data from all CMIP6 models. CMIP6 only has wind data available at a height of 10 m and ERA5 data is obtained for a height of 100 m to resemble real-life wind turbines heights. Therefore, the wind power law is used to extrapolate the CMIP6 10 m wind data to 100 m. Afterwards, CMIP6 100 m wind speed data is validated with ERA5 data by analyzing the overlap percentage (OP), which measures the degree of similarity between the modeled and reference wind speed data probability density function. In addition to OP, the Mann-Whitney non-parametric test with a 5% significance level is also used to evaluate the differences between the CMIP6 models and ERA5 wind speed medians. The seven CMIP6 models which show higher OP values and lower wind speed median differences are used to build the MME.

For the mid-term (long-term) future, SSP2-4.5 indicates that the wind power density (WPD) increases in eastern Ukraine and Turkey of around 10-20% (15-30%). In the rest of Europe there is instead a decrease of around 5-15% (10-20%), with some exceptions showing a higher decrease. SSP5-8.5 predicts a decrease of the wind resource practically for all European countries, with changes of around 10-20% for the vast majority of the European territory. In addition, Norway, Poland and western Ukraine show a higher decrease ranging between 25-30%. Compared with CMIP5 analysis done in other studies, this study shows that CMIP6, due to stronger radiative forcing scenarios, predicts enhanced differences when compared with milder scenarios and shows significantly different spatial patterns of the wind resource changes.

Intra-annual analysis for SSP2-4.5 does not project significant changes in the WPD, except for regions such as Iberia and the adjacent offshore area, where WPD increase in summer and decreases in all other seasons, and in eastern Ukraine, where WPD increases in fall and winter. On the other hand, SSP5-8.5 shows relevant differences compared with SSP2-4.5 when it comes to seasonality: Turkey and the Balkans show an increase only during summer and a decrease in all other seasons; WPD decrease is stonger in summer across Europe (except for Iberia, Balkans and Turkey); during winter some areas in the northeastern Europe show an increase in WPD. These finding are more pronounced towards the end of the century.

Moreover, the study also conducts an analysis on the non-useable wind speed events: when the wind speed is below cut-in (3-3.5 m/s) and above cut-off wind speeds (25 m/s). Both future climate projections show an increase in occurrences of non-useable wind speeds for all of Europe. The results are more pronounced in SSP5-8.5 for countries such as Italy (and the Mediterranean Sea), Norway and Iceland.

(Schlott et al., 2018) also analyses the effects of climate change on the wind resource. As for the solar energy analysis, three ensemble members of the EURO-CORDEX project are used in combination with the RCP8.5 scenario. A general decrease in offshore capacity factors is predicted, except for the Baltic Sea. Contrasting results between models are seen for onshore wind, which is a noticeable difference compared to CMIP6.

Similarly to (Carvalho, Rocha, Costoya, et al., 2021), (Martinez and Iglesias, 2022) investigates the climate change impacts on wind energy resources in North America based on CMIP6 projections. Two different scenarios of climate change are considered in this study: SSP2-4.5 and SSP5-8.5. In addition, 18 GCMs with daily-averaged values are used for both scenarios. In this study, data validation of the different GCMs with ERA5 is conducted by means of the Kolmogorov-Smirnow (K-S) test and the top five GCMs are used to construct the MME.

Both scenarios predict a drop in overall wind power density, with SSP5-8.5 predicting an average drop of approximately 15% by 2100, with certain regions reaching 40%. Also, an increased intra-annual variability is forecasted, with monthly averages changing up to +120% and -60%.

2.3. Hydro energy

(Gøtske and Victoria, 2021) analyses the future operation of hydropower in Europe under high renewable penetration and climate change. This paper uses five different general circulation models in combination with two regional climate models to estimate future reservoir inflow at three $C0_2$ emission scenarios. Runoff from these climate models is converted into inflow time series for the EOC period. The absolute change in mean daily runoff at EOC period relative to BOC shows a consistent signal. In fact, the runoff increases in Northern Europe and decreases in Southern Europe. For the RCP8.5 scenario, Mediterranean countries show a large reduction at EOC while the Nordic countries show a large increase.

An analysis for intermodel and interannual variability is also carried out. For Norway the interranual variability is projected to increase from 8.9% to 10.8% and for Spain it is projected to decrease from 30.4 to 26.1%.

The 10 climate models are grouped into an ensemble in order to evaluate changes by EOC. For EOC, a statistically significant change is found in annual inflow for 20 out of 22 European countries. Despite large interannual and intermodel variations, a change in the inflow caused by climate change is found. Annual inflow is projected to decrease by 31% in Southern countries and 21% in Northern countries for the high-emission scenario. Moreover, Spain, Portugal and the Balkan countries (except Romania) are expected to suffer from more frequent and prolonged droughts. While Finland is expected to be characterized by an increase in the frequency of overflow events.

3 Methodology

A Python library named ATLITE is used to convert weather data into time series for solar, wind and hydro energy. The library is an open light-version of the Aarhus University RE Atlas, covered in (Andresen, Søndergaard, and Greiner, 2015). From the Earth System Grid Federation (ESGF) data portal (*WCRP* 2022), data for variables rsds, rsus and tas is downloaded for solar. While the variables sfcWind and mrro are respectively used for wind and hydro energy.

Figure 3.1 presents the overall methodology in this study for solar and wind energy regarding the conversion of climate data to capacity factors at BOC and EOC for 38 European countries.

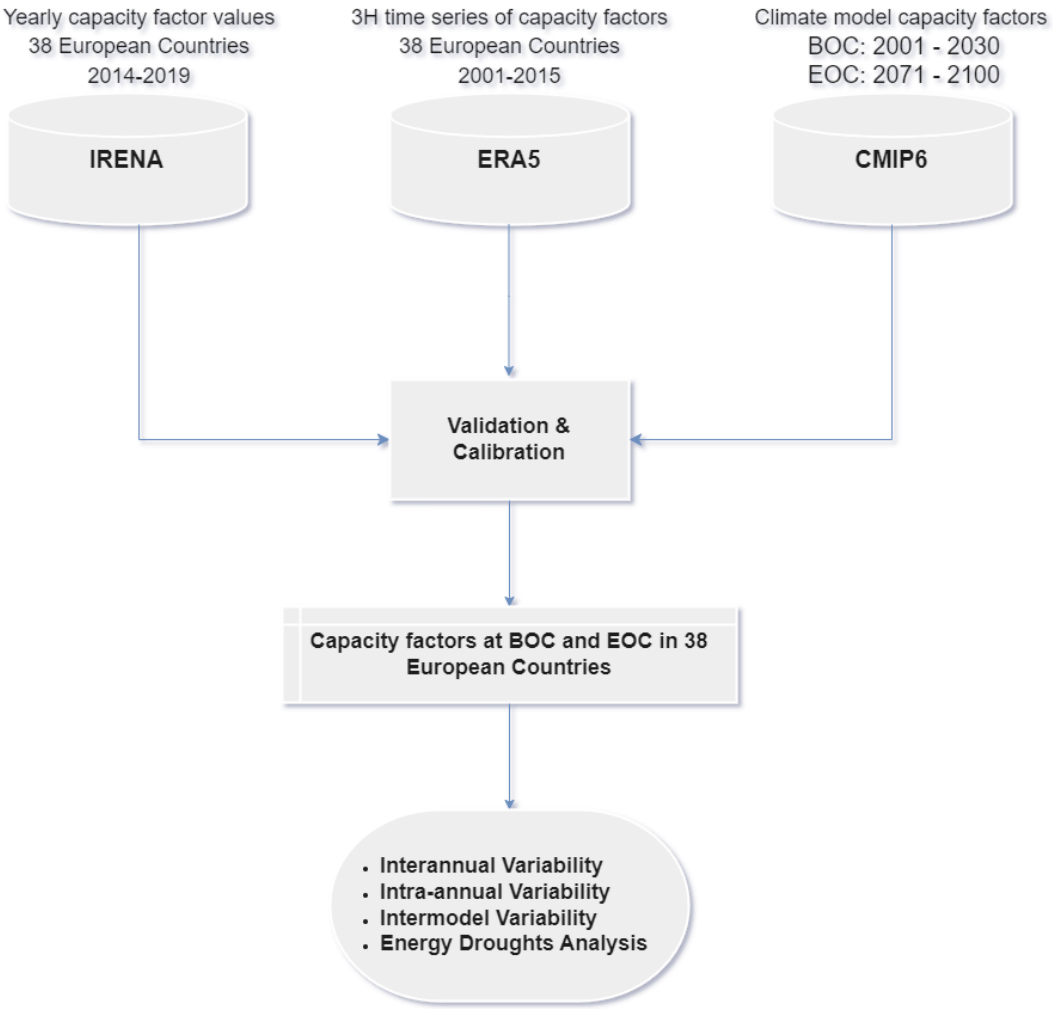

Figure 3.1: Solar and wind energy climate projection methodology explained with a flowchart

In addition, Figure 3.2 shows the overall methodology for hydro energy regarding the conversion of climate data to runoff at BOC and EOC for 22 European countries.

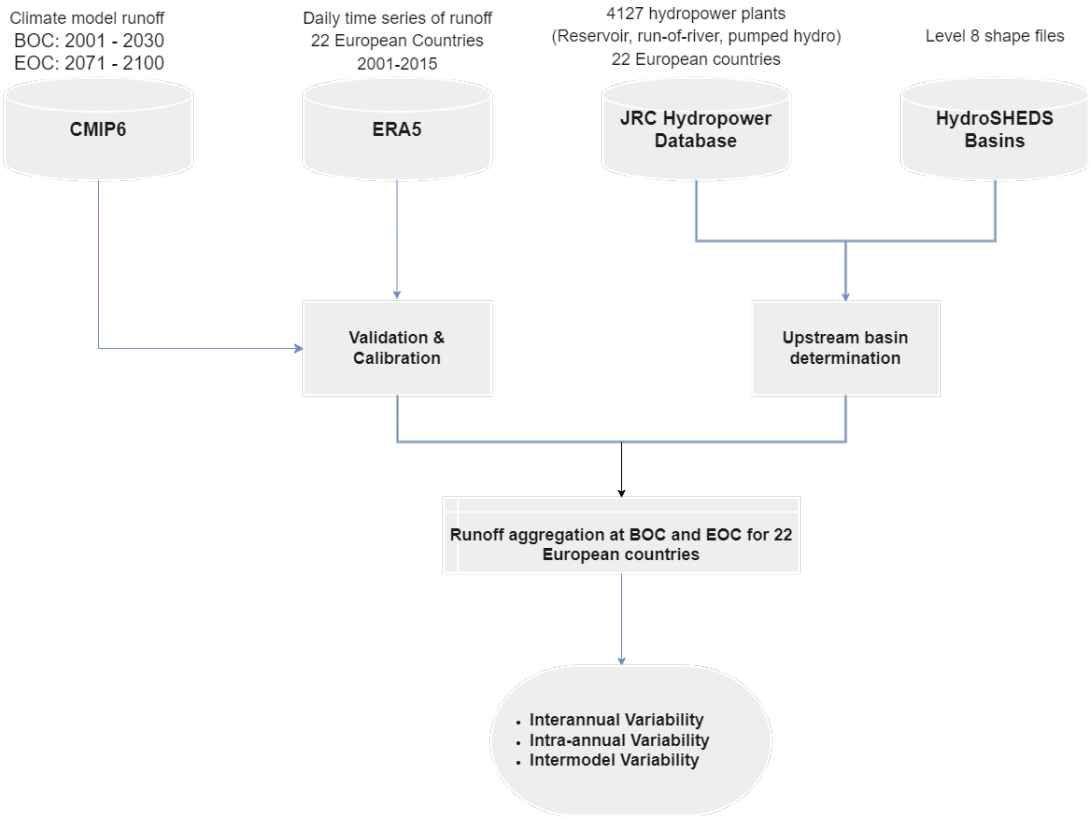

Figure 3.2: Hydro energy climate projection methodology explained with a flowchart. The validation and calibration step with ERA5 was not finalised during this Master Thesis

3.1. Models

In this Master Thesis, five GCMs are selected. These are the GCMs which have a temporal resolution of 3 hours and have all the relevant variables (rsds, rsus, tas, sfcWind, mrro) when downloading data from the ESGF portal.

Table 3.1 presents the names of these GCMs, the relevant institution and the resolution in latitude and longitude.

Table 3.1: Overview of GCMs, institution and resolution

Institution	**GCM**	**Resolution (lat x lon)**
EC-Earth-Consortium (12 European countries)	EC-Earth3	0.703° × 0.703°
JAMSTEC (Japan Agency for Marine-Earth Science and Technology) (Japan)	MIROC6	1.4° × 1.4063°
Max Planck Institute for Meteorology (Germany)	MPI-ESM1-2-LR	1.85° × 1.875°
Euro-Mediterranean Center on Climate Change (CMCC) Foundation - Italy	CMCC-ESM2	0.938° x 1.25°
Euro-Mediterranean Center on Climate Change (CMCC) Foundation - Italy	CMCC-CM2-SR5	0.938° x 1.25°

3.2. Methods

Modelled data is compared with historical values in order to determine the bias and calibrate. In addition, modelled data is also compared at BOC and EOC to understand the mean annual changes and seasonal changes.

3.2.1. Interannual daily mean

To calculate the interranual daily mean, Equation 3.1 can be used:

$$\bar{E}_d = \frac{1}{N} \sum_{y}^{n} E_{y,d} \tag{3.1}$$

where the index y refers to the year, d the day ranging from 1 to 31, $E_{y,d}$ represents a time series of daily resolution and N is the number of years investigated.

3.2.2. Interranual monthly mean

To calculate the interranual monthly mean, Equation 3.2 can be used:

$$\bar{E}_m = \frac{1}{N} \sum_{y}^{n} E_{y,m} \tag{3.2}$$

where the index y refers to the year, m the month ranging from 1 to 12, $E_{y,m}$ represents a time series of monthly resolution and N is the number of years investigated.

3.2.3. Interranual yearly mean

To calculate the interranual yearly mean, Equation 3.3 can be used:

$$\langle E_y \rangle = \frac{1}{N} \sum_{y}^{N} E_y = \frac{1}{N} \sum_{y}^{N} \sum_{m=1}^{12} E_{y,m} \tag{3.3}$$

where the index y refers to the year, m the month ranging from 1 to 12, $E_{y,m}$ represents a time series of monthly resolution and N is the number of years investigated.

3.2.4. Standard deviation

The standard deviation ca be calculated by using Equation 3.4

$$\sigma = \sqrt{\frac{1}{N} \sum_{i}^{N} \left(E_i - \bar{E}\right)^2} \tag{3.4}$$

where N is the sample size, E is the array containing the observations and $\bar{E}$ is the mean, e.g. annual, observation.

3.2.5. Normalised root mean square error

To evaluate predicted data with actual data, the mean absolute percentage error (MAPE), the root mean square error (RMSE), and the normalised root mean square error (NRMSE), can be used, as shown in Equation 3.5

$$\begin{aligned} \text{MAPE} &= \frac{1}{N} \sum_{t} \left| \frac{\hat{E}_t - E_t}{E_t} \right| \times 100 \\ RMSE &= \sqrt{\frac{1}{N} \sum_{t} \left(\hat{E}_t - E_t\right)^2} \\ NRMSE &= \frac{\sqrt{\frac{1}{N} \sum_t \left(\hat{E}_t - E_t\right)^2}}{\bar{E}}, \end{aligned} \tag{3.5}$$

where $\hat{E}_t$ is the predicted value at time t, E_t is the true value at time t, $\bar{E}$ is the average of the true observations, and N is the sample size.

3.2.6. Clearness Index

This section includes a description of the main equations used to derive the clearness index of the atmosphere according to (Victoria and Andresen, 2019; Kalogirou, 2009). The clearness index K_t measures the effect of the atmosphere and is influenced by time, location, atmospheric composition and cloud content.

$$\mathrm{K}_t = \frac{G(0,t)}{B_0(t)} \tag{3.6}$$

where G(0, t) is the global horizontal irradiance at ground level and B_0(t) is the the extraterrestrial irradiance, i.e. the irradiance at the top of the atmosphere. The extraterrestrial irradiance is absorbed, reflected and scattered when it travels through the atmosphere and it can be calculated in the following way:

$$B_0(t) = B_0\epsilon(t)\sin\gamma_s \tag{3.7}$$

where B_0 is the solar constant B_0=1367 W/m^2, ϵ is the eccentricity and γ_s is the solar altitude.

ϵ can be calculated using the following equation:

$$\epsilon = 1 + 0.033\cos\left(\frac{360d_n}{365}\right) \tag{3.8}$$

where d_n is the number of the day counted from the first day of the year. In addition, $\sin\gamma_s$ is calculated using the following equation:

$$\sin\gamma_s = \sin\delta\sin\phi + \cos\delta\cos\phi\cos\omega \tag{3.9}$$

where δ is the solar declination, ϕ is the latitude and ω is the solar angle.

The solar declination is the angular distance of the sun's rays north (or south) of the equator. Therefore, the declination is the angle between the sun-earth center line and the projection of it on the equatorial plane. It is positive north of the equation and negative in the south, within a range of +23.45°and -23.45°, and it can be defined with the following equation:

$$\delta = 23.45^\circ\sin\left(\frac{360\,(d_n + 284)}{365}\right) \tag{3.10}$$

Moreover, for any location on the Earth, the position of the Sun can be determined at any moment by using the solar altitude γ_s and the solar azimuth ψ_s, which is the angle between the projection of the Sun radio-vector over the horizontal plane and the south direction In addition, ω, the solar angle, can be defined in the following way:

$$\omega = 15^\circ(ST - 12) \tag{3.11}$$

where ST is the True Solar Time, expressed in hours, which can be calculated with the following equation:

$$\mathrm{S}T = LT + \frac{ET}{60} - \frac{\xi}{15} \tag{3.12}$$

where LT is the hour of the day (expressed in Coordinated Universal Time - UTC), ξ is the longitude and ET is a correction factor for different length of the days in a year and is used to account for the Earth's axial tilt and for the Earth's elliptical orbit.

$$\mathrm{E}T = 9.87\sin(2B) - 7.53\cos(B) - 1.5\sin(B) \tag{3.13}$$

where the factor B is given by:

$$\mathrm{B} = (d_n - 81)\,\frac{360}{364} \tag{3.14}$$

To conclude this section, the concept of diffuse fraction is also introduced and defined as the ratio between direct and global irradiance at ground level.

$$\mathrm{F} = D(0)/G(0) \tag{3.15}$$

3.2.7. Irradiance

This sections aims to explain how the different types of radiation on a tilted plane are converted into a PV time series. The irradiance $\mathrm{G}(\beta, \alpha)$ on a surface with tilt angle β and orientation α is calculated in the following way:

$$\mathrm{G}(\beta, \alpha) = \mathrm{B}(\beta, \alpha) + \mathrm{D}(\beta, \alpha) + R(\beta, \alpha) \tag{3.16}$$

where $\mathrm{B}(\beta, \alpha)$ is the direct irradiance, $\mathrm{D}(\beta, \alpha)$ is the diffuse irradiance and $\mathrm{R}(\beta, \alpha)$ is the albedo irradiance.

Figure 3.3 displays the different solar radiation components.

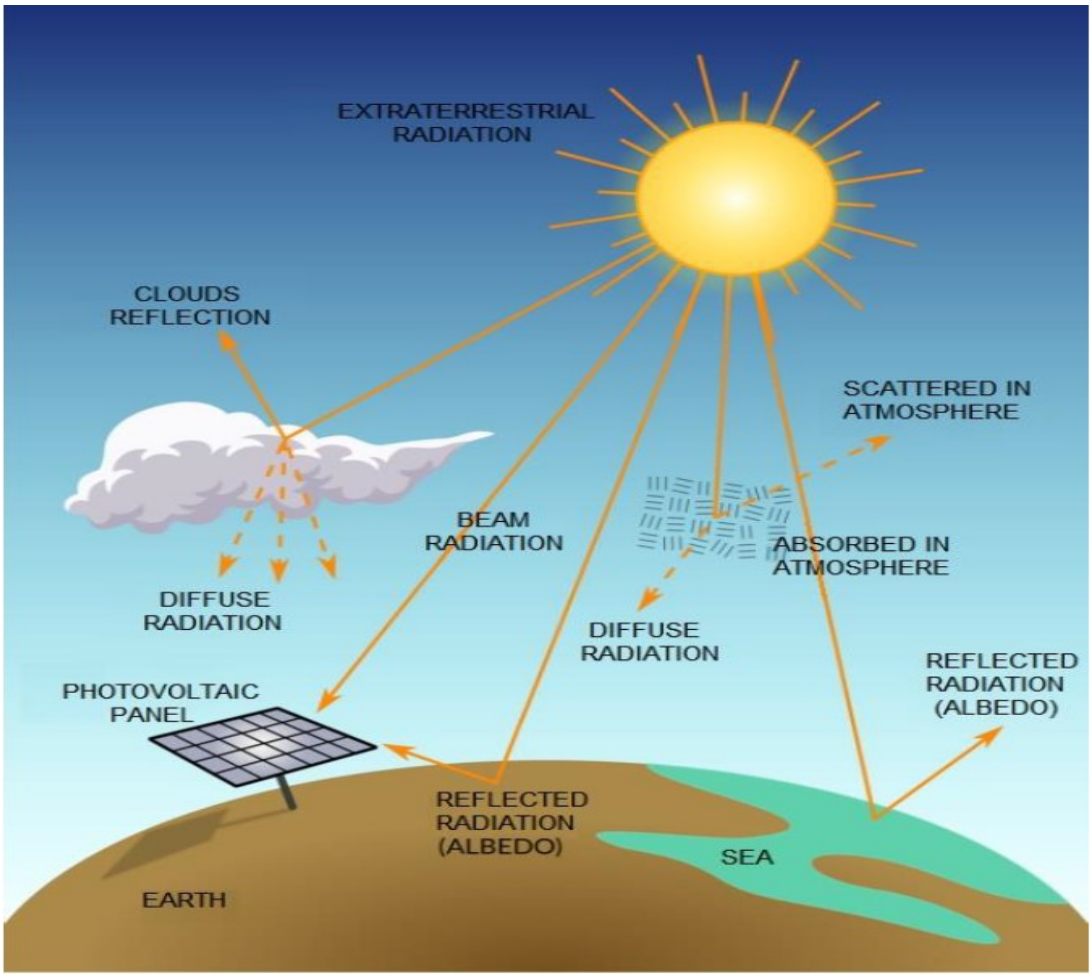

Figure 3.3: Representation of Solar Radiation Components (Souza et al., 2019)

The direct irradiance can be calculated in the following way:

$$\mathrm{B}(\beta, \alpha) = \frac{\mathrm{B}(0) \max\left(0, \cos\theta_s\right)}{\sin\gamma_s} \tag{3.17}$$

where θ_s is the incident angle which is the angle between the sun's rays and a line normal to the irradiated surface.

$$\begin{aligned} \cos\theta_s = & \sin\delta \sin\phi \cos\beta \\ & - [\mathrm{sign}(\phi)] \sin\delta \cos\phi \sin\beta \cos\alpha \\ & + \cos\delta \cos\phi \cos\beta \cos\omega \\ & + [\mathrm{sign}(\phi)] \cos\delta \sin\phi \sin\beta \cos\alpha \cos\omega \\ & + \cos\delta \sin\alpha \sin\omega \sin\beta \end{aligned} \tag{3.18}$$

The diffuse irradiance $\mathrm{D}(\beta, \alpha)$ is calculated using the anisotropic model according to (Hay and Mckay, 1985):

$$\mathrm{D}(\beta, \alpha) = \mathrm{D}_{\mathrm{circumsolar}}\left(\beta, \alpha\right) + \mathrm{D}_{\mathrm{isotropic}}\left(\beta, \alpha\right) \tag{3.19}$$

where $\mathrm{D}_{\text{circumsolar}}(\beta, \alpha)$ is the circumsolar component coming in an uninterrupted way from the Sun and $\mathrm{D}_{\text{isotropic}}(\beta, \alpha)$ is the isotropic component coming from the entire celestial hemisphere.

The circumsolar component can be calculated as:

$$\mathrm{D}_{\text{circumsolar}}(\beta, \alpha) = k_1 \frac{D(0) \max(0, \cos\theta_s)}{\sin\gamma_S} \tag{3.20}$$

where k_1 is the anistropy index defined as ratio between the direct irradiance on the ground B(0) and the irradiance at the top of the atmosphere $B_0(0)$:

$$\mathrm{k}_1 = \frac{B(0)}{B_0(0)} \tag{3.21}$$

In addition, the isotropic component can be calculated in the following way:

$$\mathrm{D}_{\text{isotropic}}(\beta, \alpha) = k_{\text{horizon}}\ (1 - k_1)\, D(0) \frac{1 + \cos\beta}{2} \tag{3.22}$$

where k_{horizon} is defined as:

$$\mathrm{k}_{\text{horizon}} = 1 + \sqrt{1 - F} \sin^3\left(\frac{\beta_{\mathrm{s}}}{2}\right) \tag{3.23}$$

To conclude, the albedo irradiance is defined as:

$$\mathrm{R}(\beta, \alpha) = \rho G(0) \frac{1 - \cos\beta}{2} \tag{3.24}$$

where ρ is defined as the reflectivity of the ground, defined as the ratio between the upward shortwave radiation at surface and downward shortwave radiation at surface:

$$\rho = \frac{R(0)}{G(0)} \tag{3.25}$$

3.2.8. PV time-series modelling

As mentioned in section 3.2.6, the irradiance on a surface with tilt angle, i.e. solar panels at an optimum slope angle, is calculated by summing up different components. Therefore, when downloading data for CMIP6 from the Earth System Grid Federation (ESGF) data portal (*WCRP* 2022), it is important to select the appropriate climate variables. These are the variables used in order to generate the PV time-series:

- Surface downward shortwave radiation flux (rsds)
- Surface upward shortwave radiation flux (rsus)
- Surface temperature (tas)

The surface temperature is an important variable for PV generation. In fact, it is directly correlated with the efficiency:

$$\eta = \eta_{\text{STC}} \left[1 - \gamma_T \left(T_{\text{cell}} - T_{\text{cell,STC}}\right)\right] \tag{3.26}$$

where η_{STC} is the conversion efficiency assumed for the PV panel under Standard Test Conditions (STC), γ_T is the efficiency thermal coefficient (equal to -0.4%/°C) and T_{cell} is the temperature of the cell under Standard Test Conditions. The capacity factors can then be calculated as the ratio between the delivered powered and the installed capacity:

$$CF_n(t, \beta, \alpha) = \eta_{system} \frac{G_n(t, \beta, \alpha)\eta}{G_{STC}\eta_{5\pi}} \tag{3.27}$$

In addition, an optimal tilt angle has been used in these analyses when computing the capacity factors and the crystalline silicon CSi PV panels have been used.

3.2.9. Wind time-series modelling

Wind power generation depends on the wind speed at wind turbine height H. This relation is represented by the following equation:

$$\text{WPD} = \frac{1}{2} \cdot \rho \cdot \text{WS}^3 \tag{3.28}$$

where ρ is the air density and WS is the wind speed.

Wind power is therefore dependent on the wind speed cubed. This indicates that even small changes in the wind speed would greatly affected the wind power generated. Therefore, a thorough analysis is necessary when deciding the placement of a wind turbine or a wind farm.

When retrieving wind data from the ESGF portal, 10 m wind data is downloaded for all GCMs. Therefore, it is necessary to extrapolate the 10 m wind speed to hub height and evaluate the power curve. In order to extrapolate the wind speed from a given height above ground to another, the following equation is used according to (Andresen, Søndergaard, and Greiner, 2015):

$$\nu(H) = \nu(10\text{ m}) \frac{\ln\left(H/z_0\right)}{\ln\left(10\text{ m}/z_0\right)} \tag{3.29}$$

where z_0 is the surface roughness. This is a simplified method as the actual wind speed profile is more complicated and depends on the stability of the atmosphere, the orography, i.e. hills and valleys, and the local obstructions such as trees or buildings. The value for the surface roughness is not available from the CMIP6 database so ERA5 roughness is used instead. Then the ERA5 data is interpolated into the resolution of the CMIP6 GCMs. This suggests that if a GCM has higher resolution, the results for wind energy will be less accurate. This is also proven in this master thesis as the wind resource results from MIROC6 and MPI-ESM1-2-LR are having a higher NRMSE compared to ERA5 reanalysis data.

In addition, the turbine Vestas V112-3.3 MW has been used (Bauer, 2022) during all the analyses and in the figure below it is possible to see its power curve:

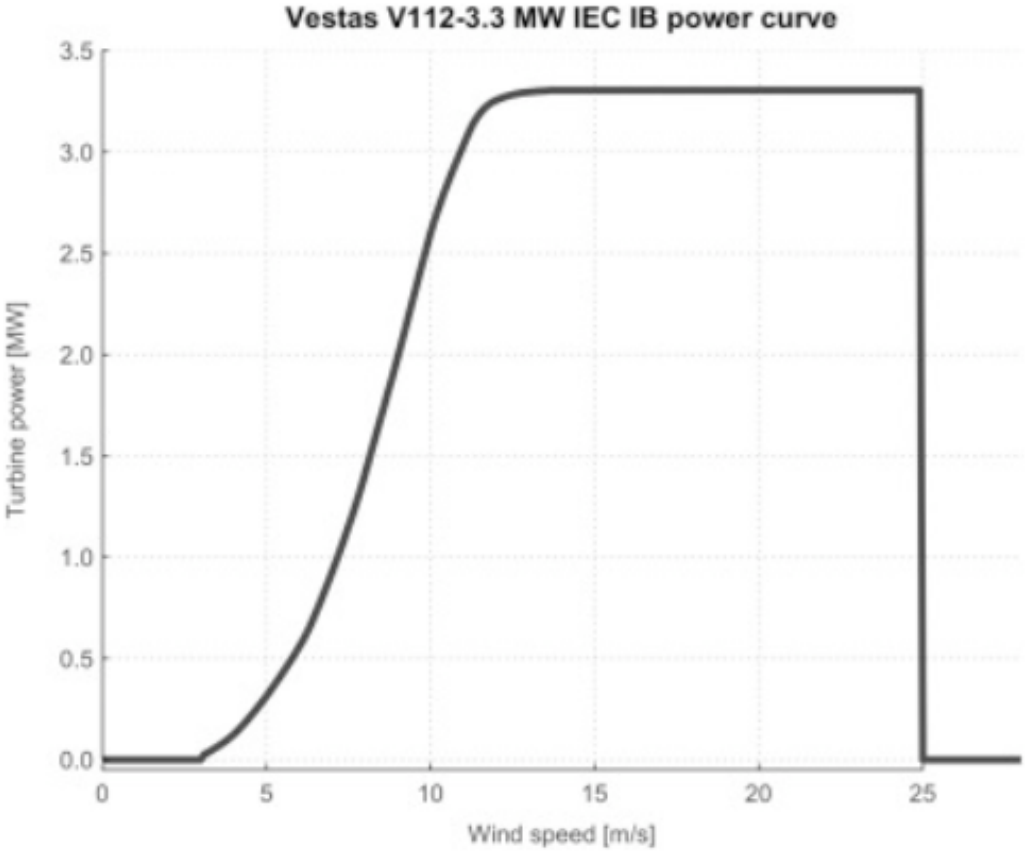

Figure 3.4: Power curve of the wind turbine Vestas V112-3.3 MW (Petrakopoulou, Robinson, and Loizidou, 2016)

A minimum wind speed is required for the turbine to produce useful power. This is called cut-in speed and is equal to 3 m/s for the considered turbine. In addition, above a certain wind speed, i.e. cut-out wind speed, the turbine is stopped in order to protect it from potential damages caused by strong wind gusts. The cut-out speed for the considered turbine is 25 m/s.

3.2.10.Upstream basin determination and runoff aggregation

This section aims to explain how the runoff is aggregated on a country level. Surface runoff (or runoff) is the excess water from precipitations or meltwater that does not enter the soil or evaporates. The runoff, due to gravity and shape of the land surface, will reach a river, a lake, a pond etc. and be collected there. A drainage basin (or basin) is the area of land that collects all the flow of water to a common outlet (*USGS* 2023; *HydroBASINS* 2023; *JRC* 2019). The topography of a basin varies based on levels, using the Pfafstetter coding scheme from (K. L. Verdin and J. P. Verdin, 1999). This code indicates the number of subdivisions and the basin type. Increasing the level, increases the resolution, which means that the size of each basin is reduced. The upstream basins are determined in this study on a level 8 basins delineation.

For each time step, the runoff is aggregate in each subbasin where a hydroelectric reservoir is located. The model calculates the time interval for the runoff within the upstream areas to reach the hydroelectric reservoirs, by assuming a runoff flow sped of 1 m/s and by calculating the distance between the runoff and the power plants. Therefore, country aggregated volumetric inflow is calculated with the following equation:

$$\mathrm{Q}_c = \sum_{b}^{M} \frac{R_{bc} A_b}{\Delta t} \tag{3.30}$$

where b is the upstream basin index, M is the number of upstream basins within country c, R_{bc} is the aggregated runoff in basin b and country c, A_b is the surface area of the basin, Δ t is the temporal resolution of the runoff data .

4 Historical validation

In this chapter, results from the hindcast analysis for solar, wind and hydro resources are presented. 5 GCMs and 3 SSPs are used to obtain time series for solar and wind capacity factors and hydro runoff (the datasets are available on Github[1]). The period of scope for the hindcast is from 2001 til 2015.

4.1. Solar energy hindcast

This sections presents the hindcast for the solar energy resource, where three countries are analysed: Spain, Norway and Germany. The results from the climate models will need to be accompanied with a skill score in order to calculate the accuracy. The results from the five GCMs are compared with the reanalysis data from ERA5. In addition, yearly capacity factors are also calculated between 2014 and 2019 by using actual historical data from IRENA. Yearly produced solar electricity generation (GWh) and electricity capacity (MW) are retrieved, which represent respectively the numerator and denominator of the capacity factor values. The capacity factors from IRENA for all 38 European countries considered are then used to cross-validate climate model results. Thereafter, the NRMSE is calculated between the climate model and reanalysis results and a correction factor is used to minimize the NRMSE. Figure 4.1 presents the yearly averaged forecast from January til December for the above mentioned countries.

[1] https://github.com/WaleedArshad98/Master-Thesis-Results

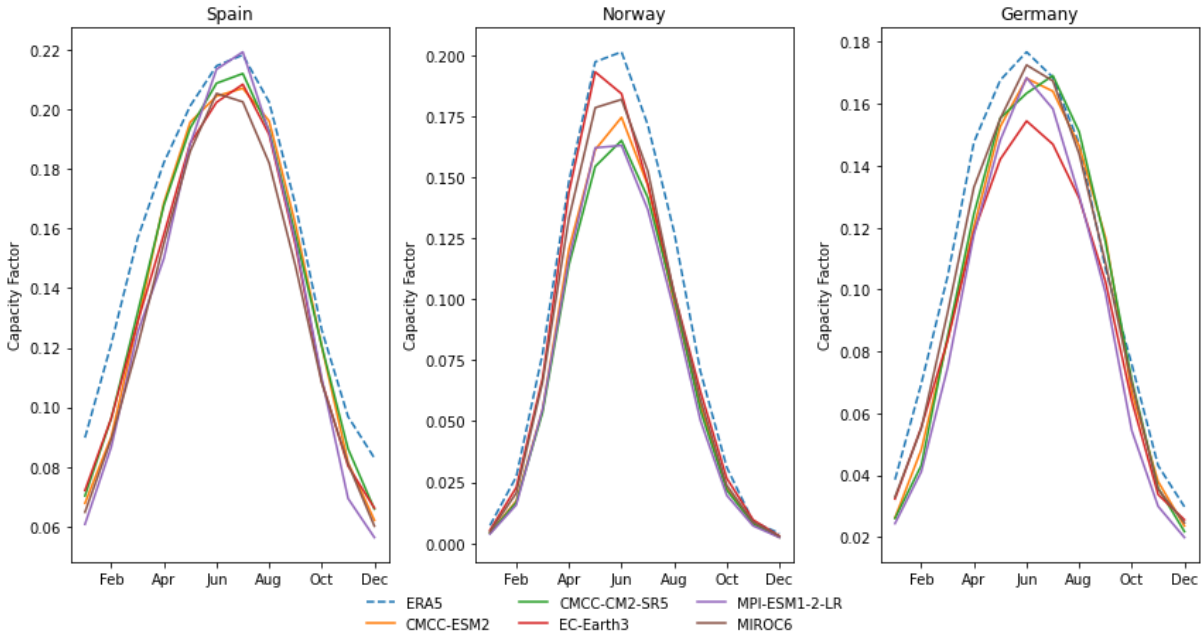

Figure 4.1: Solar energy climate model hindcast for Spain, Norway and Germany. This figure includes data for five GCMs and ERA5 prior to calibration

The models seem to resemble the reanalysis data from ERA5. However, it is noticeable that the climate models tend to underestimate the solar capacity factors. Therefore, a correction factor is used in order to correct the bias. The delta mapping approach is used and all European countries are scaled up by 13% as this value is found to minimize the NRMSE for the whole continent (see Appendix Table C.4 for more details). Figure 4.2 presents the average ensemble data after calibration and the ERA5 data.

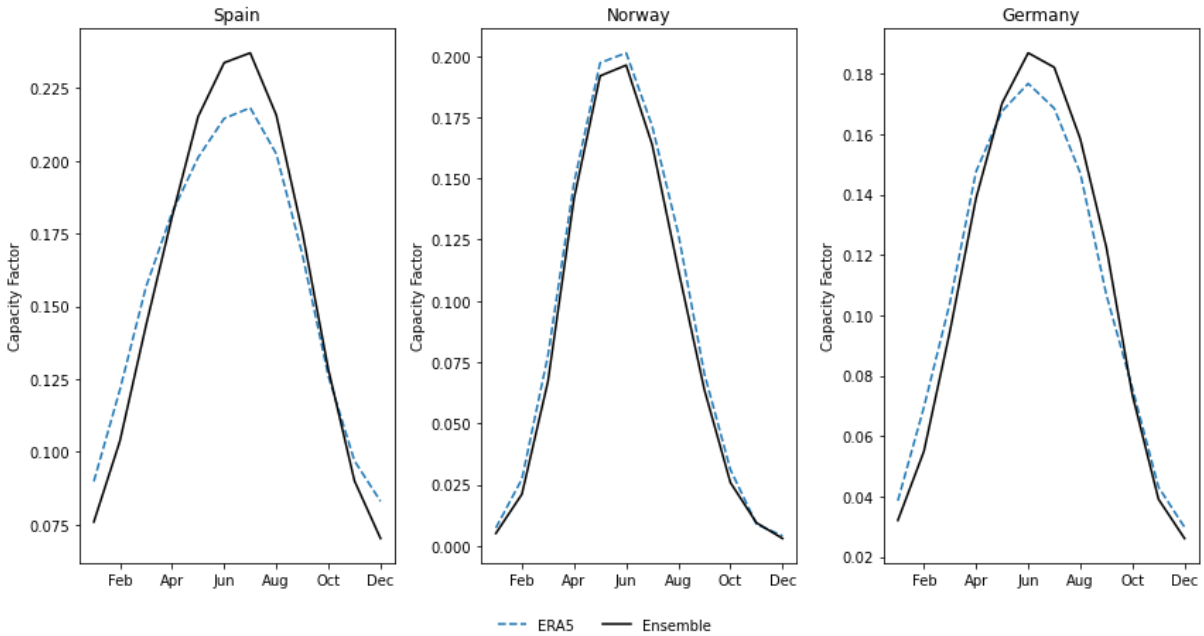

Figure 4.2: Solar energy climate model hindcast for Spain, Norway and Germany. This figure includes data for the averaged ensemble and ERA5 after calibration

4.2. Wind energy hindcast

This sections presents the hindcast for the wind energy resource, where three countries are analysed: Spain, Norway and Germany. The results from the five GCMs are compared with the reanalysis data from ERA5. The yearly capacity factors from ERA5 for all 38 European countries considered are then used to cross-validate climate model results. Figure 4.3 presents the yearly averaged forecast from January til December for the above mentioned countries.

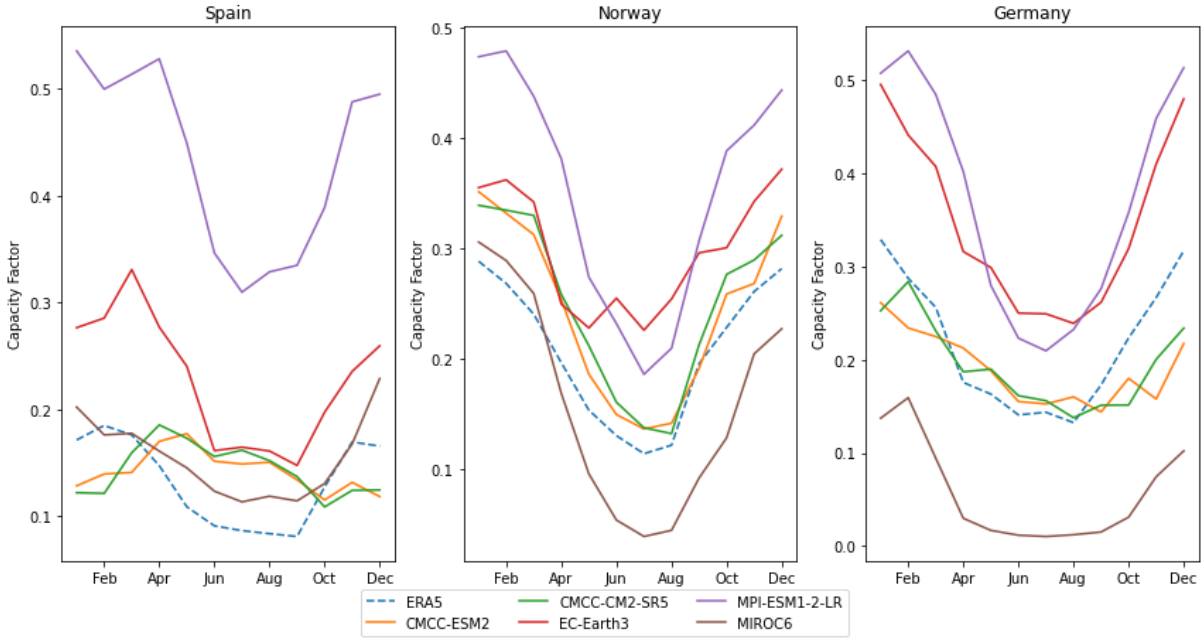

Figure 4.3: Wind energy climate model hindcast for Spain, Norway and Germany. This figure includes data for five GCMs and ERA5 prior to calibration

The hindcast reveals that two of the models (MIROC6 and MPI-ESM1-2-LR) are either underestimating or overestimating the reanalysis data from ERA5. That is owing to the fact that these models have a coarser resolution and, thus, are not able to precisely model wind energy time series in areas of high roughness (areas with mountains or many trees and buildings). When compared with other studies which are taking into account more than thirty GCMs (Carvalho, Rocha, Costoya, et al., 2021; Martinez and Iglesias, 2022), these two models are either not used due to a resolution higher than 1.25° in latitude and longitude or due to having low agreement with ERA5 reanalysis data.

In addition, it is also noticeable that the two circulation models CMCC-ESM2 abd CMCC-CM2-SR5 are showing very similar results to ERA5. However, Earth3 seems to be also overestimating the capacity factors, but with a very similar seasonal pattern. For that reasons, a yearly calibration factor is used for Earth3 on a country level to calibrate the modelled data. Thereafter, the NRMSE is calculated between the climate model and reanalysis results. After the calibration, it is possible to notice a decrease in the NRMSE (see Appendix Table C.5 for more details).

Figure 4.4 shows the average ensemble data after calibration and the ERA5 data.

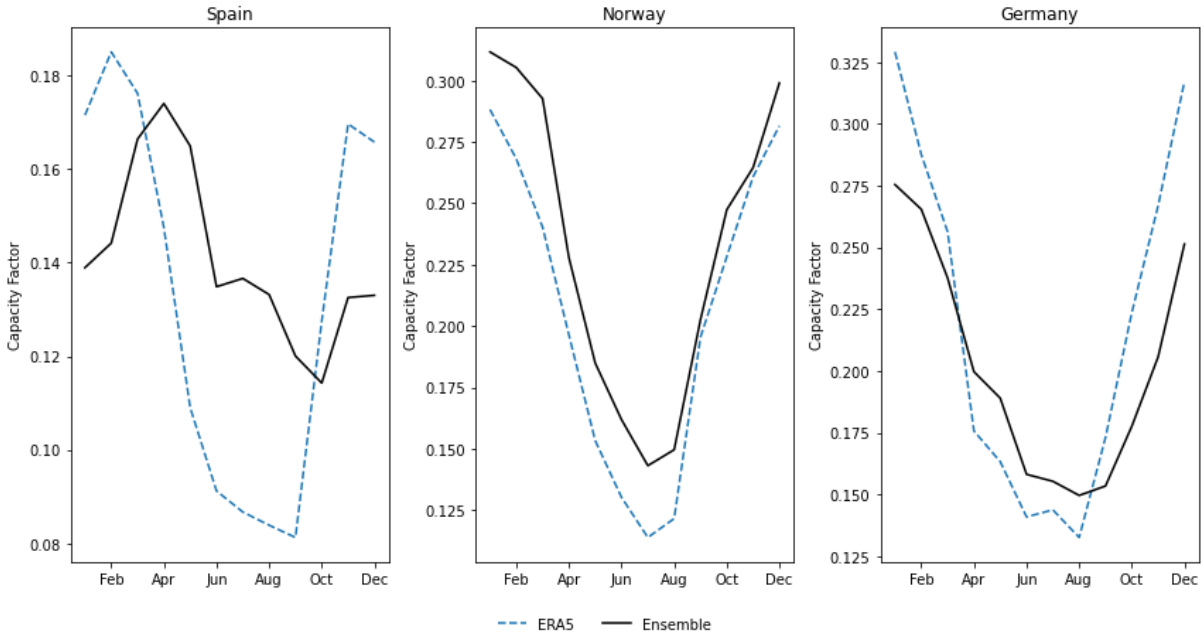

Figure 4.4: Wind energy climate model hindcast for Spain, Norway and Germany. This figure includes data for the averaged ensemble and ERA5 after calibration

4.3. Hydro energy hindcast

This section present the hydro energy hindcast. Since the validation with ERA5 was not finalised during this Master Thesis, the capacity factors for the different circulation models are plotted in Figure 4.5 to understand if they are showing a high variability. Similarly to the wind energy analysis, results from MIROC6 and MPI-ESM1-2-LR are not used for the analysis of hydro energy due to a higher resolution and also because they are showing results significantly different than the other GCMs. Meanwhile, the other three GCMs are showing results which are in good alignment and with similar seasonal pattern.

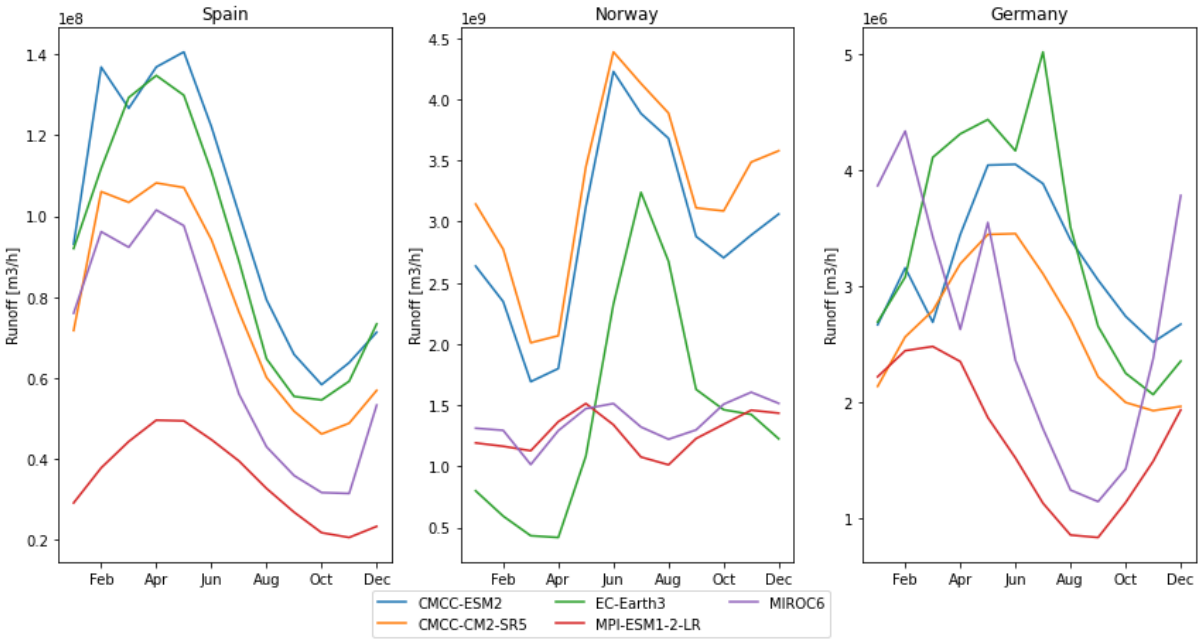

Figure 4.5: Hydro energy climate model hindcast for Spain, Norway and Germany. This figure includes data for five GCMs prior to calibration

5 Evaluation of climate change signal

This chapter presents the climate model results for solar, wind and hydro. A general BOC and EOC comparison is carried out for the three different SSPs to answer RQ2. In addition, a relevant statistical analysis is also present in order to answer RQ3.

5.1. Solar energy projection

This sections presents the projected changes for solar energy by taking into consideration five GCMs and three SSPs. The changes in PV production are displayed in terms of relative percentage. An intra-annual analysis is also present where all four seasons are considered. In addition, a statistical analysis is present in order to evaluate the interannaul variability and to analyse the changes in the clearness index. The results show that for all SSPs, the observed findings are largely in agreement with previous CMIP6 (Hou et al., 2021) and CMIP5 studies (Müller et al., 2019).

Figure 5.1 shows the ensemble relative change for PV projection from BOC til EOC for SSP5-8.5, SSP2-4.5 and SSP1-2.6. For SSP 5-8.5, the mean relative changes show a general increase for most of the European continent. Only the Scandinavian countries and east Ukraine show a decrease, whereas the increase is most pronounced for countries such as Spain, France and Germany. On the other hand, SSP2-4.5 and SSP1-2.6 show a general increase for the whole European continent. The increased energy generation is more pronounced for the mitigation scenario SSP1-2.6 as it would lead to an increase of approximately 5-10% compared with today. This suggest that a transition to an European energy system with higher penetration of renewable energies improves the climatic conditions for the renewable energies.

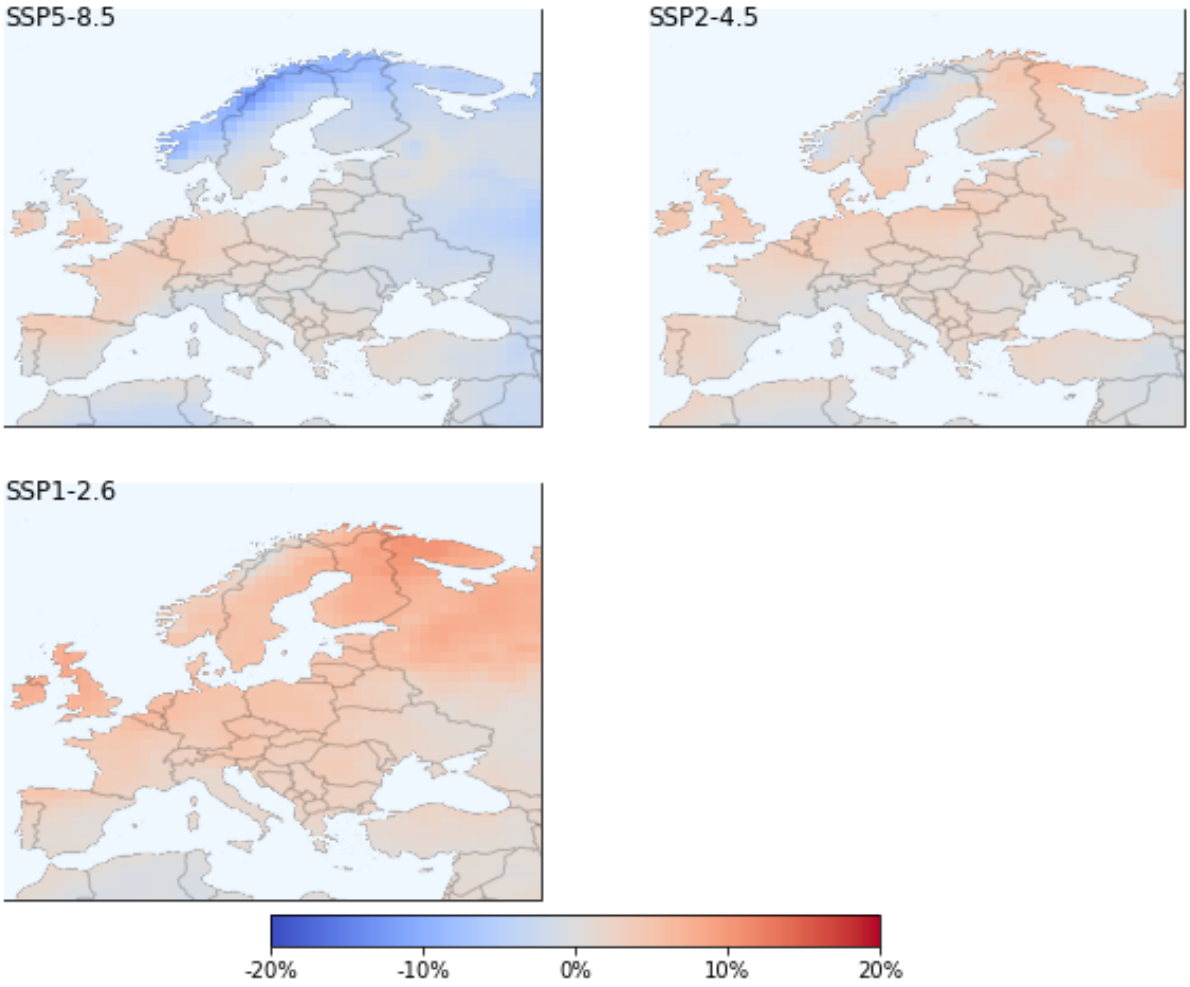

Figure 5.1: Ensemble mean relative change in capacity factors between EOC and BOC for solar energy. The results are for SSP5-8.5, SSP2-4.5 and SSP1-2.6

In addition, Figure 5.2 presents the intra-annual analysis for SSP5-8.5. The scenario with high GHG is considered in this section, while the results from the other two scenarios can be found in the Appendix section A.1.The seasonal analysis reveals different patterns of evolution throughout the year. In summer and autumn, the patter of change resembles largely the annual means. Specifically, for summer the countries that show an increase are certain areas of Germany, Poland and Czech Republic. In addition, countries that show a decrease are those at lower latitudes such as Iberia, Italy and the Balkans. On the other hand, in winter and spring the EOC projections show a higher decrease relatively to the BOC seasons for most of Europe besides around the Mediterranean. Specifically for winter, south Europe shows a relatively small increase, while most countries in north Europe, i.e. Norway, Sweden, Finland, shows a decrease ranging from 10% to 20%. A similar pattern can be seen for spring, but in weaker relative change. The decrease in north Europe suggests that this area is less suitable for large-scale PV production as limited solar radiation will be reaching the surface.

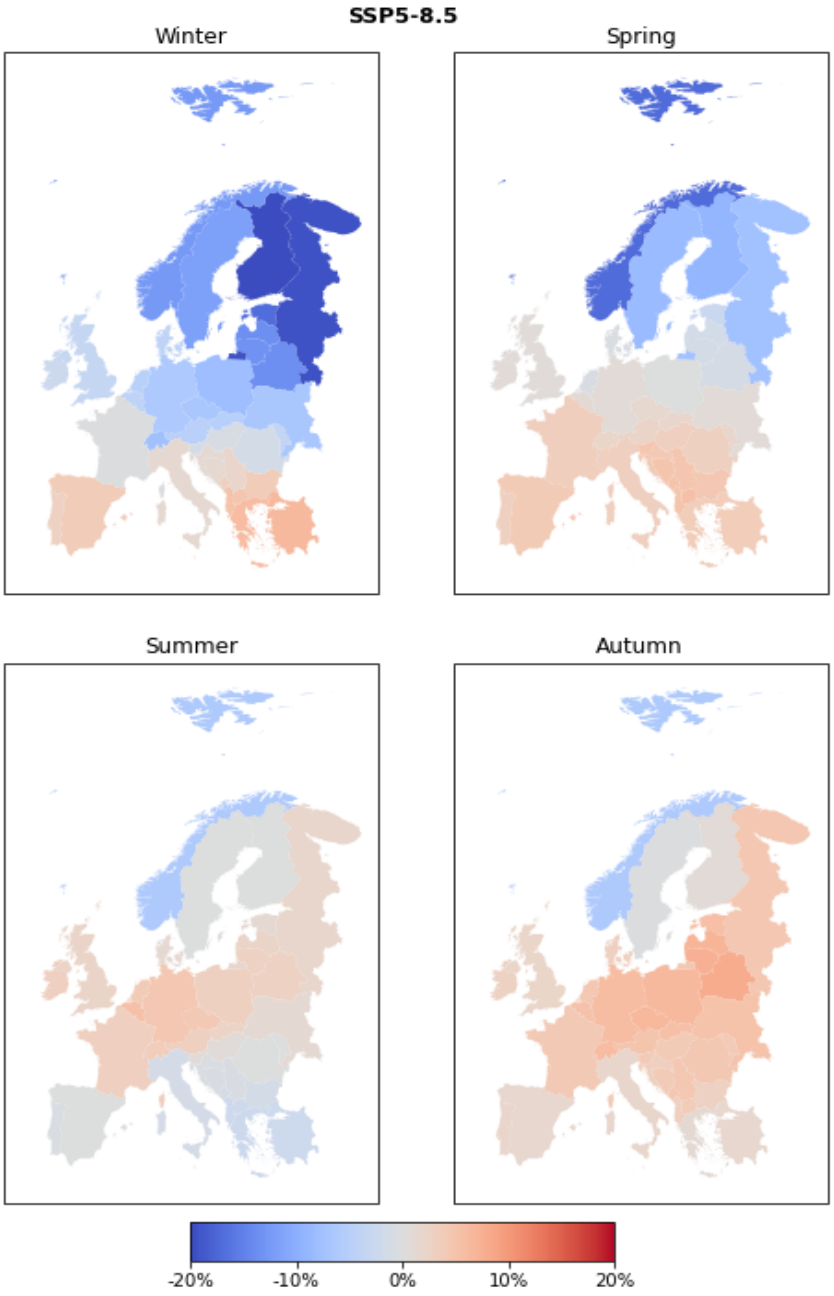

Figure 5.2: Ensemble mean intra-annual relative change in capacity factors between EOC and BOC for solar energy. The results are for SSP5-8.5

On the other hand, for SSP1-2.6 (see Appendix A.1) the projection forecasts positive changes in PV production for continental Europe. During summer, a strong increase in central Europe is noticeable, while the Mediterranean is projected to increase slightly. This pattern is reversed in winter, as the strongest increase in PV production is evident around the Nordics and in a less pronounced way in the Mediterranean. In addition, during spring, negative changes are visible for north Europe, specifically for Norway. Lastly, for autumn a similar pattern to winter is noticeable, however with a stronger increase in continental Europe. When looking at the SSP2-4.5 intra-annual analysis, a middle of the road change between SSP5-8.5 and SSP1-2.6 is forecasted, with a less pronounced decrease in north Europe when compared with SSP5-8.5 and a less pronounced

seasonal increase in comparison with SSP1-2.6. To better understand the change between BOC and EOC, a kernel density estimation (KDE) of the probability density function (PDF) has been used.

Figure 5.3 represents the KDE of the PDF of yearly averaged solar capacity factors for Spain, Norway and Germany for BOC and EOC periods based on the SSP5-8.5 scenario. This figure indicates how the annual mean changes between the two periods, but more importantly it provides a representation of the relative change in the standard deviation of the capacity factors. The standard deviation is calculated with equation 3.4 in which the sample size is N = 30. The mean yearly solar capacity factors are expected to decrease for Spain and Germany, while an increase is expected from Norway. In addition, the relative standard deviation are projected to decrease for most of the European countries, with Germany showing a decrease in variance of 18.6%, Spain of 34.4% and Norway of 4.6% (see Table C.3 for more details).

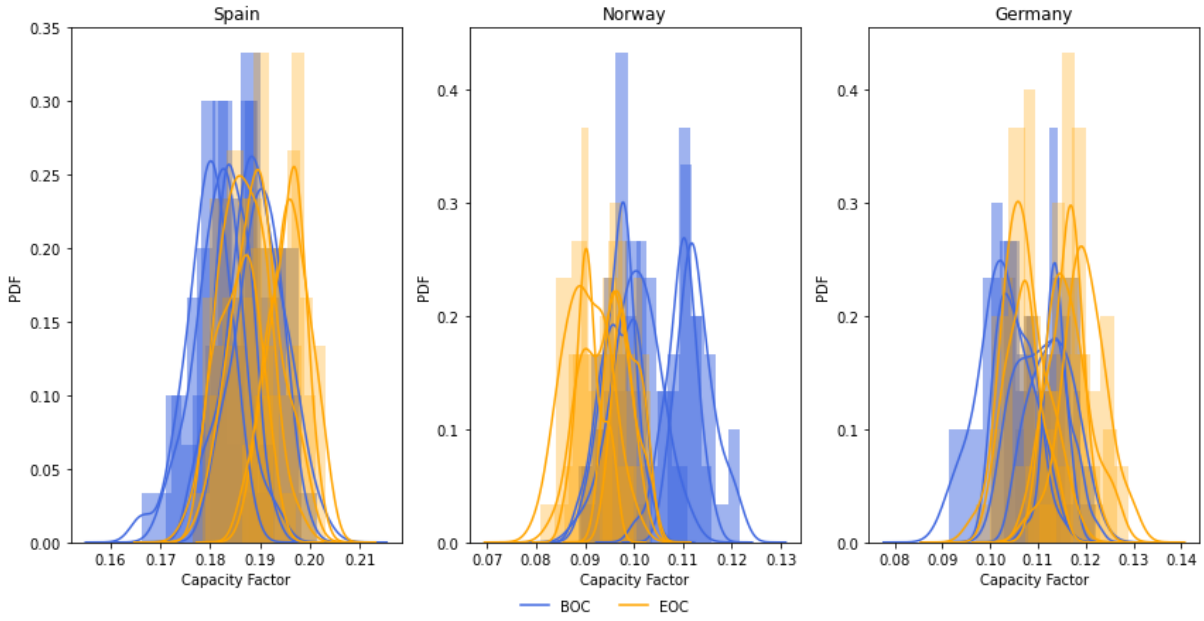

Figure 5.3: Kernel density estimations of the probability density functions for the yearly solar energy capacity factors in Spain, Norway and Germany at the BOC (blue) and EOC (yellow) periods for the SSP5-8.5 scenario

Furthermore, Figure 5.4 presents the KDE of the PDF for the daily solar energy capacity factors at BOC and EOC. The purpose of this figure is to highlight how the clearness index, i.e. measure of the sky clearness, is changing. In fact, the clearness index (see Equation 3.6) and the capacity factors (see Equation 3.27) are directly proportional as they both depend on the radiation on the ground. That means that a higher capacity factor indicates an increase in the clearness index. It is possible to notice from Figure 5.4 that in Norway the high capacity factors tend to have a lower probability density during EOC compared to BOC. This means that the clearness index will decrease for Norway for the SSP5-8.5 scenario. On the other hand, Spain and Germany are displaying an opposite behaviour: an increase of the probability density for higher capacity factors. These results can be generalized to the whole Europe by considering also the results from Figure 5.1. Countries in north Europe, i.e. Norway, Sweden and Finland, will be characterized by

a general decrease in the clearness index. While countries in continental Europe, i.e. Spain, Germany, France, will be characterized by an increase in the clearness index. This indicates that north Europe will become more isotropic and south Europe will become more circumsolar.

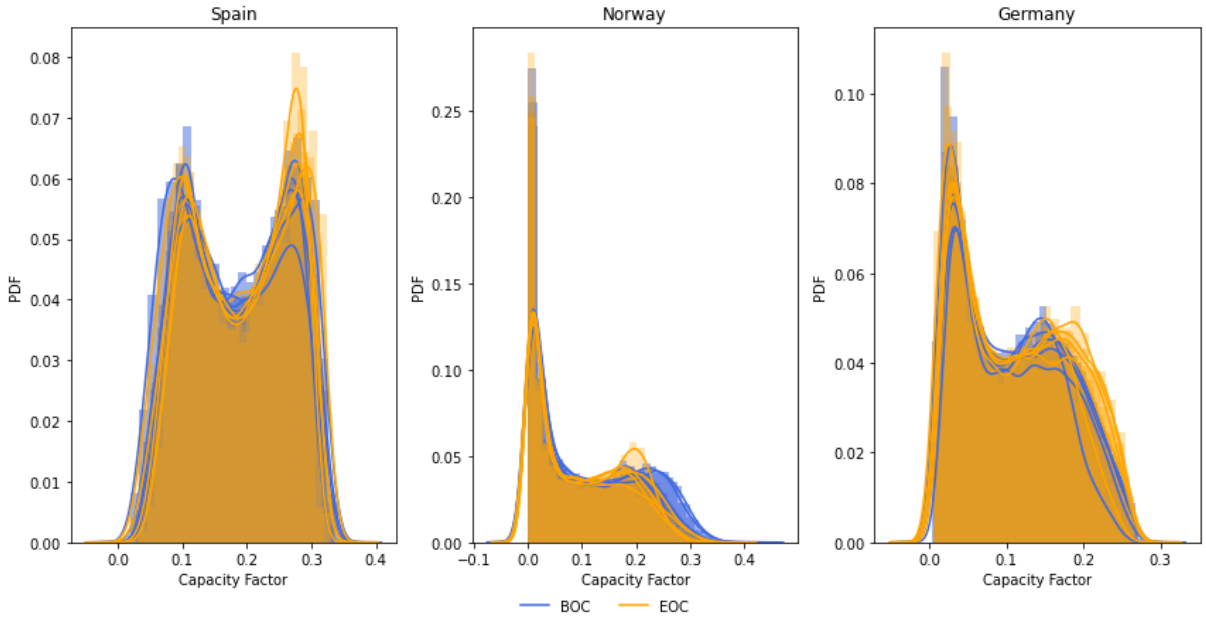

Figure 5.4: Kernel density estimations of the probability density functions for the daily solar energy capacity factors in Spain, Norway and Germany at the BOC (blue) and EOC (yellow) periods for the SSP5-8.5 scenario

5.2. Wind energy projection

This sections presents the projected changes for hydro energy by taking into consideration three GCMs and three SSPs. As mentioned in section 4.2, three GCMs out of five were selected after the hindcast analysis since two of the GCMs (MIROC6 and MPI-ESM1-2-LR) were showing very high NRMSE due to a coarse climate model resolution. The changes in wind production are displayed in terms of relative percentage. An intra-annual analysis is also present where all four seasons are considered. In addition, a statistical analysis is present in order to evaluate the interannaul variability and to analyse the changes in variance. The results show that for all SSPs, the observed findings are largely in agreement with previous CMIP6 studies (Carvalho, Rocha, Costoya, et al., 2021).

Figure 5.5 shows the ensemble relative change for Wind projection from BOC til EOC for SSP5-8.5, SSP2-4.5 and SSP1-2.6. For SSP 5-8.5, the mean relative changes show a general decrease for practically all of the European continent. A decrease ranging between 10-20% is projected, with particularly strong decrease in Northern Norway, Poland and western Ukraine (with great resemblance with (Carvalho, Rocha, Costoya, et al., 2021)) where the range is between 20 and 30%. In addition, SSP2-4.5 and SSP1-2.6 project mixed changes, with some areas experiencing an increase and others a decrease in the capacity factors values. SSP2-4.5 projects relatively small changes compared with BOC, with some areas (Poland, west France, Iberia, Northern Norway, the Alps mountains and British Isles) showing a decrease and others an increase (Southern Finland and Sweden, Germany,

eastern Ukraine and the Black Sea). Moreover, SSP1-2.6 forecasts an increase for localized areas in Iberia, Turkey, the Mediterranean Sea, Southern Finalnd and Sweden, while a decrease is forecasted for the rest of Europe with relatively higher change expected for Norway, localized areas in Poland, Ukraine and the British Isles.

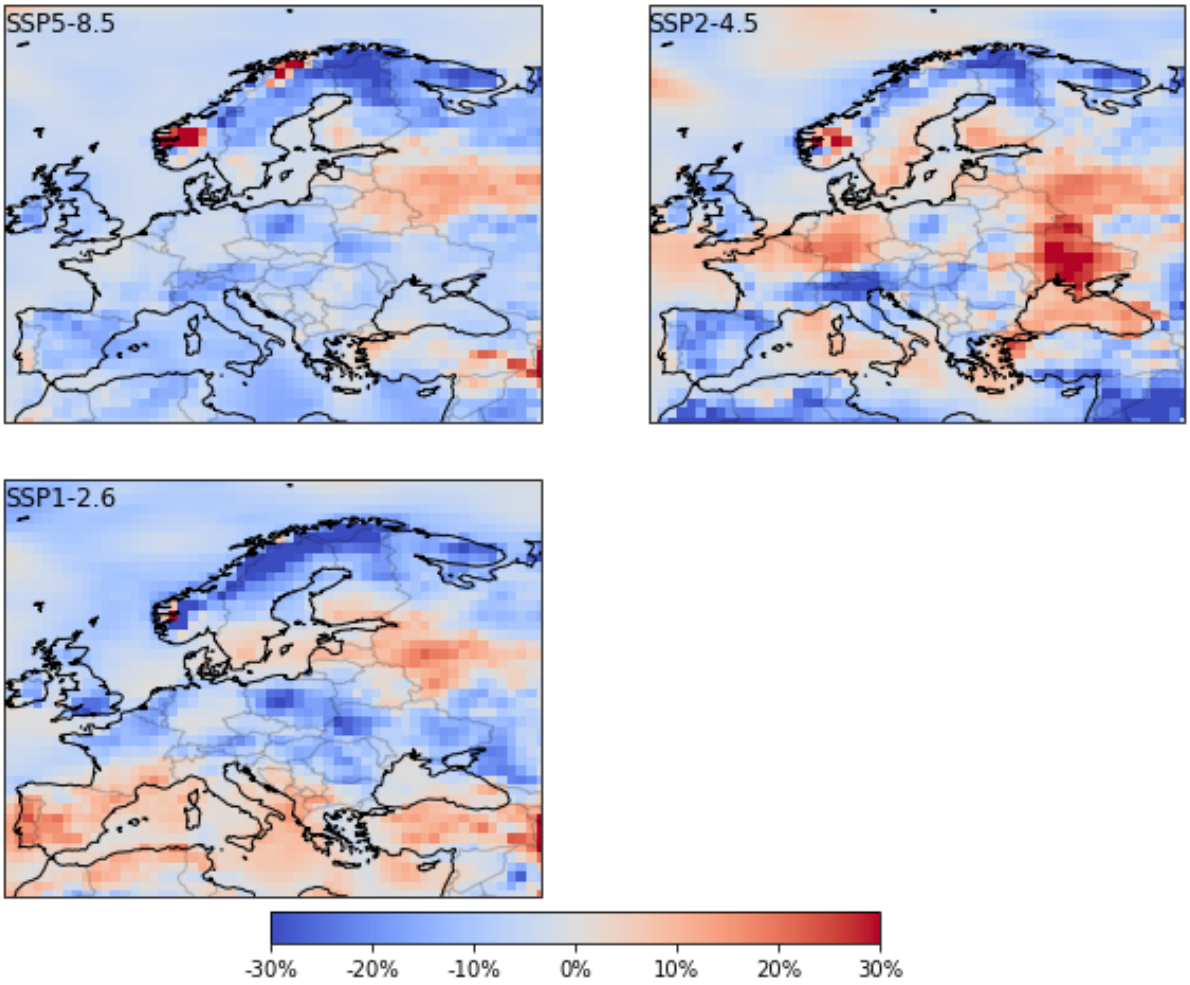

Figure 5.5: Ensemble mean relative change in capacity factors between EOC and BOC for wind energy. The results are for SSP5-8.5, SSP2-4.5 and SSP1-2.6

In addition, Figure 5.6 presents the onshore intra-annual analysis for SSP5-8.5. The scenario with high GHG is considered in this section, while the onshore results from the other two scenarios can be found in the Appendix Section B.1. SSP5-8.5 forecasts a general decrease in summer and autumn in terms of wind energy capacity factors for practically the whole of Europe, with certain countries showing relatively small increases such as Lithuania, Latvia, Estonia and Turkey. During winter and spring, a slightly different pattern is found with a relatively small increase expected for continental Europe in the range of 5-10% and a higher increase expected for the Baltics and Finland in the range of 15-25%. Furthermore, the projection shows that in Turkey and the Balkans an increase is expected only in summer, while a decrease is expected in all other seasons. The wind capacity factors change is stronger in summer and autumn compared to other seasons.

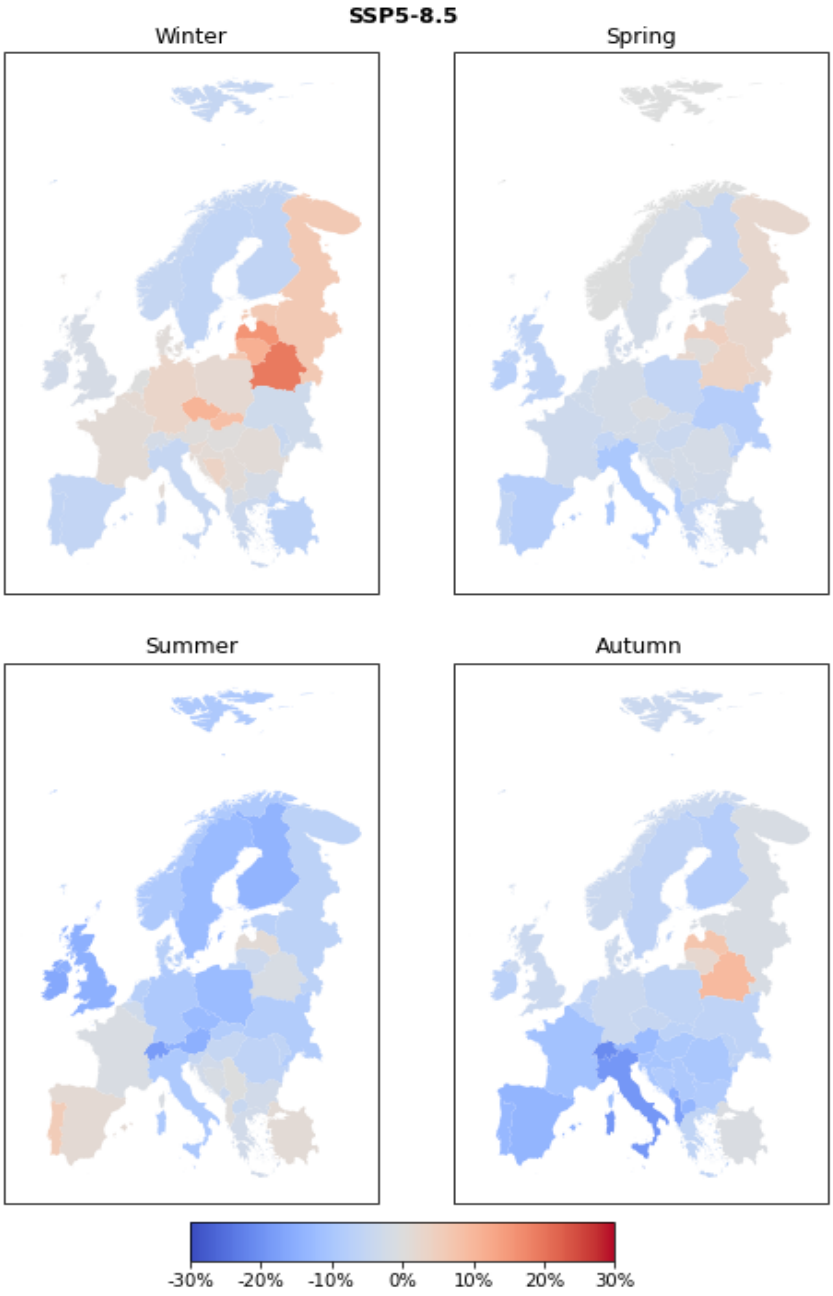

Figure 5.6: Ensemble mean intra-annual relative change in capacity factors between EOC and BOC for wind energy. The results are for SSP5-8.5

In addition, SSP2-4.5 does not forecast a clear and marked seasonality change between BOC and EOC. The main exception is represented by Iberia, where an increase is projected in summer and a decrease for all other seasons (similarly to SSP5-8.5). The Baltic countries show a consistent increase, with autumn representing the seasons with the highest relative change. On the other hand, SSP1-2.6 projects very similar results for summer and autumn, with Southern Europe being characterized by a decrease ranging between 10-20% and North-East Europe being characterized by a relatively small increase. During winter and spring, it is also possible to see a general decrease in Southern Europe, but the relative change is smaller to the other two seasons. In addition, the Baltic countries show a similar seasonal pattern to the other two SSP scenarios, with a constant increase

forecasted during all the seasons.

Furthermore, Figure 5.7 presents the KDE of the PDF for the yearly averaged wind energy capacity factors at BOC and EOC. The purpose of this figure is to highlight how the mean and the variance are changing between the two periods. Spain, Norway and Germany are all showing a decrease by EOC, as also shown in Figure 5.5. In addition, the variance, i.e. standard deviation, is expected to increase for Germany by 38.1% and decrease for Spain and Norway by respectively 5.3% and 17.7% (see more details in Appendix Table C.6).

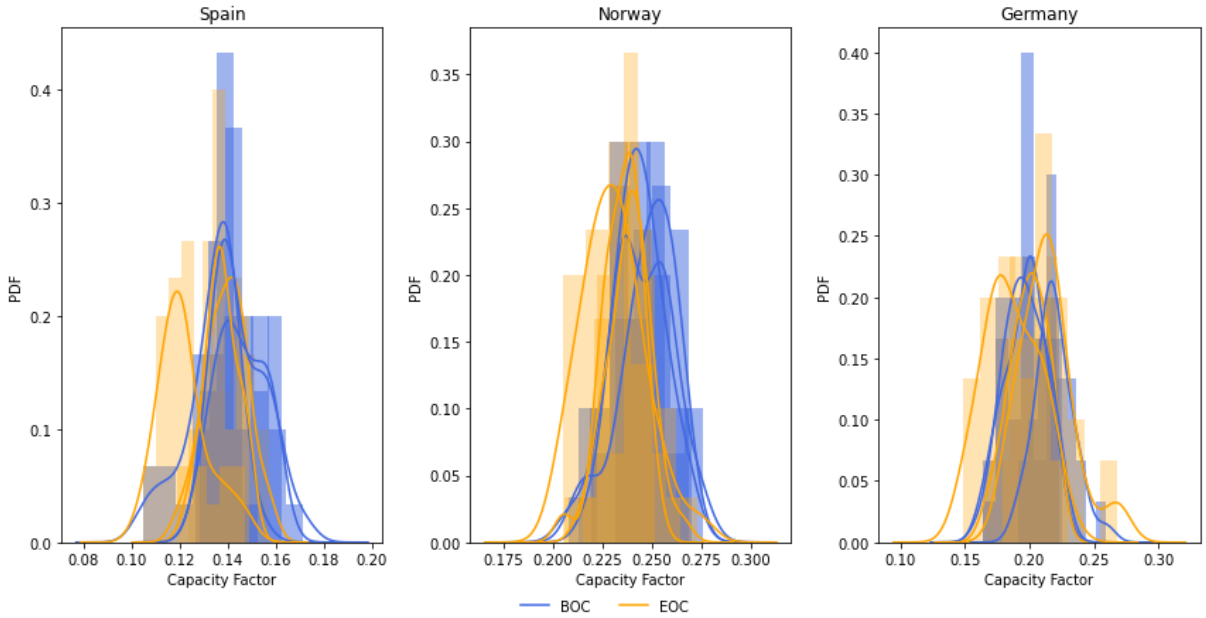

Figure 5.7: Kernel density estimations of the probability density functions for the yearly wind energy capacity factors in Spain, Norway and Germany at the BOC (blue) and EOC (yellow) periods for the SSP5-8.5 scenario

5.3. Hydro energy projection

This sections presents the projected changes for hydro energy for runoff by taking into consideration three GCMs and three SSPs. As mentioned in section 4.3, three GCMs out of five were selected after the hindcast analysis since two of the GCMs (MIROC6 and MPI-ESM1-2-LR) have a very coarse climate model resolution and significantly differ from the other GCMs with better resolution. The changes in runoff are displayed in terms of relative percentage. An intra-annual analysis is also present where all four seasons are considered. In addition, a statistical analysis is present in order to evaluate the interannual variability and to analyse the changes in variance. The results show that for all SSPs, the observed findings are largely in agreement with previous CMIP6 (Gøtske and Victoria, 2021) and CORDEX ((Schlott et al., 2018) studies.

Figure 5.8 shows the ensemble relative change for runoff projection from BOC til EOC for SSP5-8.5, SSP2-4.5 and SSP1-2.6. For SSP 5-8.5, the mean relative changes show a general decrease for Northern Europe, i.e. Norway, Sweden and Finland, in a range from 20 til 30 %, while an increase is projected for continental and Southern Europe, i.e.

Spain, Portugal, the Balkans, in a similar range from 20 til 30%. In addition, SSP2-4.5 projects similar results to SSP5-8.5 for Northern Europe with an increase in runoff change ranging from 10 til 15% instead. However, the ensemble mean relative change in runoff for continental and Southern Europe is showing slightly different results compared with SSP5-8.5. The projection shows that, for SSP2-4.5, countries such as Germany, Poland, Italy now show an increase ranging from 5 til 10%, while other countries such as Austria, Slovakia and Bosnia and Herzegovina now show an increase ranging from 20 til 30%. The low GHG emission scenario (SSP1-2.6), shows a relative change in the range of +5 and -5% compared to BOC. Therefore, it is possible to say that SSP1-2.6 does not project significant changes compared with today.

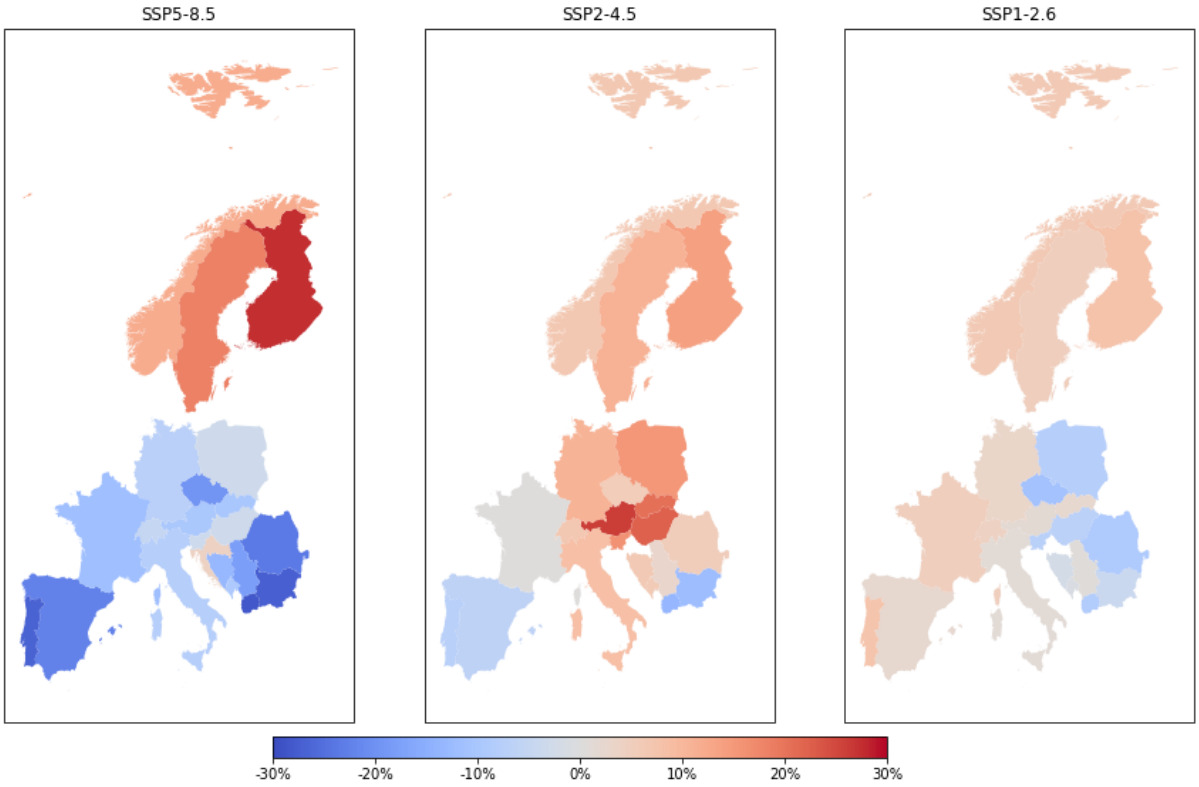

Figure 5.8: Ensemble mean relative change in runoff between EOC and BOC for hydro energy. The results are for SSP5-8.5, SSP2-4.5 and SSP1-2.6

Figure 5.9 presents the intra-annual analysis for SSP5-8.5. The scenario with high GHG is considered in this section, while the results from the other two scenarios can be found in the Appendix section C.1. SSP5-8.5 forecasts a general decrease for continental and Southern Europe with summer and autumn showing the highest change. During winter and spring an increase is projected for Northern Europe, with winter showing an increase ranging between 30 and 50% and spring showing an increase ranging between 50 and 70 %. Therefore, it is possible to say that the spring runoff generation is significantly increased for Northern Europe during winter and spring. This might be simply caused due to higher temperatures preventing rain from freezing. Moreover, during summer and autumn Northern countries show either very small increase (summer) or a very small decrease (autumn). This marks a clear seasonality for Northern Europe, as winter and spring represent the only seasons in which a noticeable increase is found.

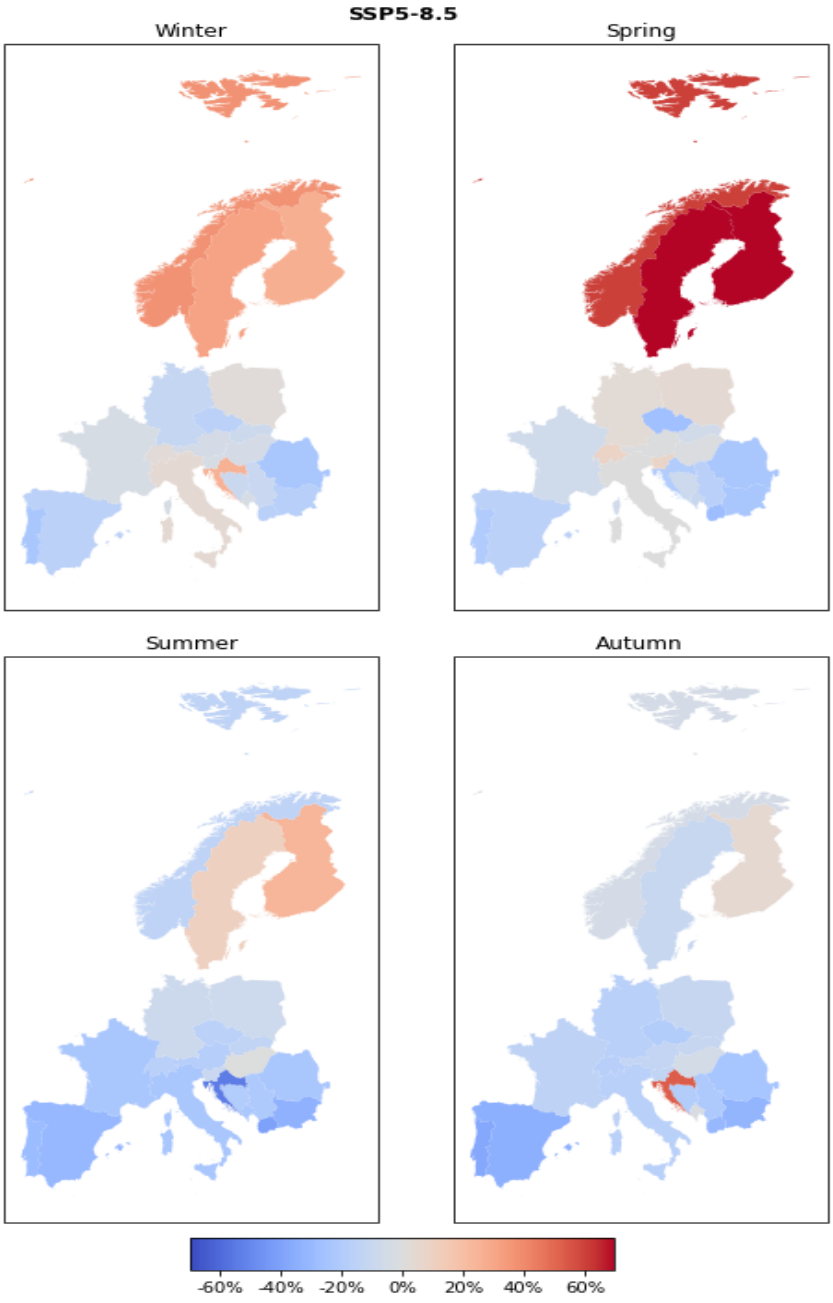

Figure 5.9: Ensemble mean intra-annual relative change in runoff between EOC and BOC for hydro energy. The results are for SSP5-8.5

Furthermore, Figure 5.10 presents the KDE of the PDF for the yearly averaged hydro energy runoff values at BOC and EOC. The purpose of this figure is to highlight how the mean and the variance are changing between the two periods. Spain is showing a decrease, Norway an increase and Germany shows very similar results to BOC, as also shown in 5.8. In addition, the variance increases for Norway and Germany respectively by 6.9% and 7.5%, while it is decreases for Spain by 3.7% (see more details in Appendix Table C.7).

Spain, Norway and Germany are all showing a decrease by EOC, as also shown in Figure 5.5. In addition, the variance, i.e. standard deviation, is expected to increase for Germany by 38.1% and decrease for Spain and Norway by respectively 5.3% and 17.7% (see more

details in Appendix Table C.6).

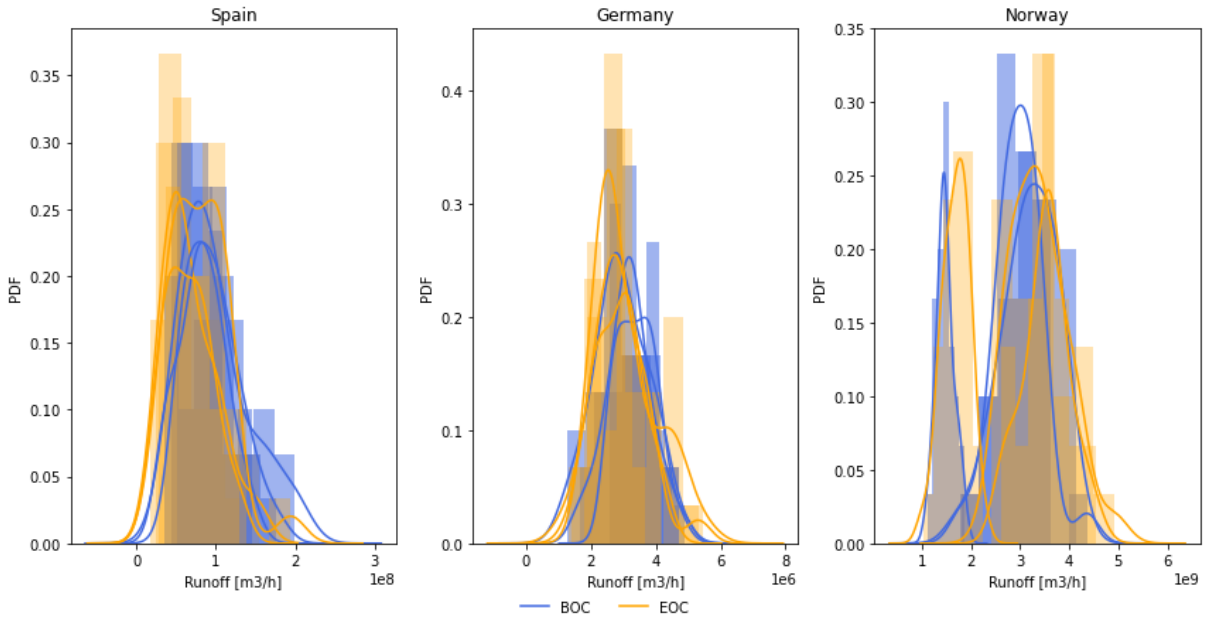

Figure 5.10: Kernel density estimations of the probability density functions for the yearly hydro energy runoff in Spain, Norway and Germany at the BOC (blue) and EOC (yellow) periods for the SSP5-8.5 scenario

6 Energy droughts and extreme events

This chapter presents the results for energy drought and extreme events for solar and wind resources. Analyses for drought and overflow are present in order to understand how the solar and wind generation patterns will change during EOC compared to BOC. The results shown are for SSP5-8.5.

6.1. Solar energy extreme events

This section presents the results for energy drought and extreme events specifically for solar energy. The results shown are for SSP5-8.5, while the results for SSP2-4.5 and SSP1-2.6 can be found respectively in Appendix A.3 and A.4.

As shown in Figure 5.1, a general decrease in solar energy capacity factors is forecasted for Northern European countries, while an increase is forecasted for Southern European countries with a higher change projected for continental European countries. During winter and spring, the decrease is much stronger compared to summer and autumn. This might be critical for the energy system of these countries, as the solar generation grows weaker during certain seasons. This section aims to analyse how many days the capacity factors for solar energy are below a predefined level, which corresponds to the number of days with drought. The low limit for the capacity factors is set at the 10^{th} percentile, which is a widely used index for drought analysis, according to (M. T. H. van Vliet et al., 2016) and (Gøtske and Victoria, 2021). Consecutive days during EOC below the 10^{th} percentile limit of BOC are what causes a drought. Therefore, a drought will be defined as a consecutive period in which the capacity factors are below the 10^{th} percentile. For solar energy, the drought analysis is carried out on a monthly level in order to take into account the seasonality. The results are then aggregated on a yearly time frame between BOC and EOC.

Figure 6.1 presents the results for the drought analysis of 38 countries for solar energy for SSP5-8.5 for BOC and EOC. In this figure, it is possible to find the mean duration of droughts on the x-axis and the mean number of sequences on the y-axis. It is shown that the data is more spread out at EOC compared to BOC, with countries such as Norway, Sweden, Finland, Romania, Latvia, Belarus, Estonia showing droughts with an increased mean duration. Particularly, Norway is showing that the droughts might have a critical impact on the energy system, as the total amount of days (product between mean sequences and mean duration) in which the capacity factors are below the pre-defined limit increases to almost 150. Moreover, the figure shows that the mean duration and mean number of sequences of droughts will decrease for Spain, Albania, North Macedonia, Portugal and Turkey. For Spain, the total amount of days with drought becomes less than 10.

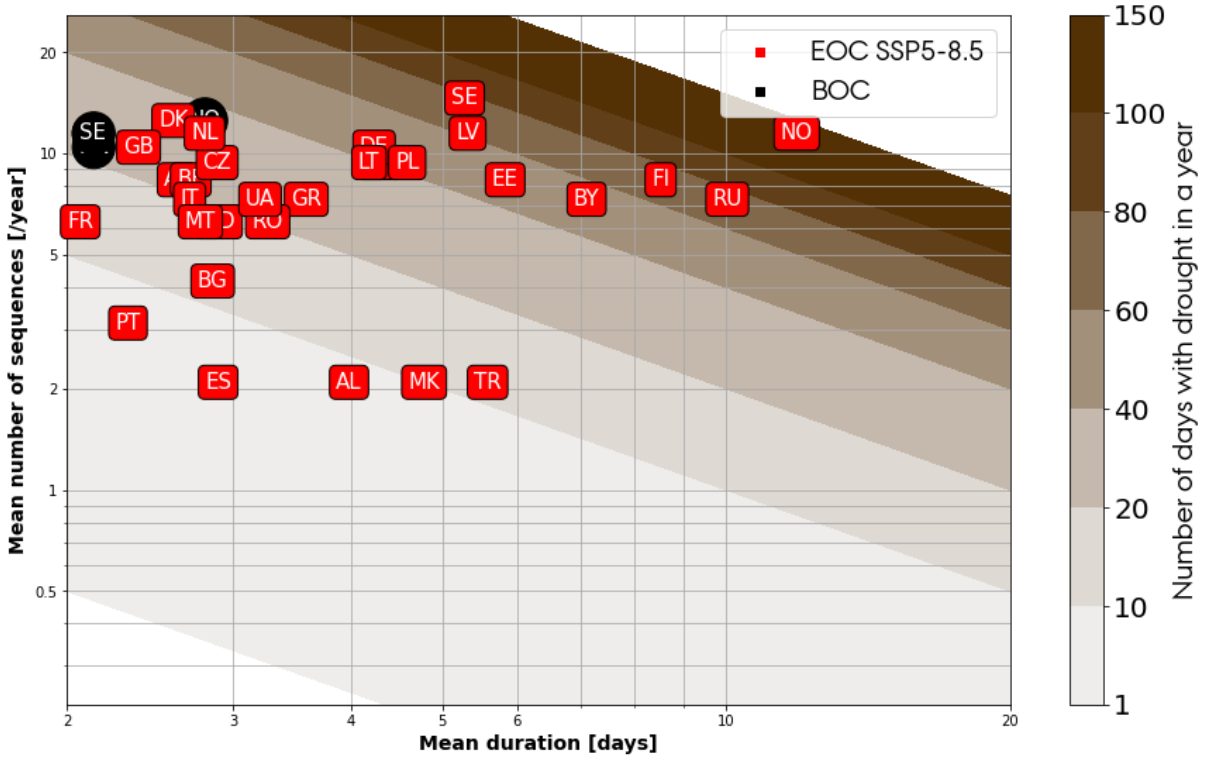

Figure 6.1: Duration and frequency of solar energy drought periods, determined as consecutive days with capacity factors less than the 10th percentile of capacity factors at the BOC, evaluated for the BOC and EOC periods under the SSP5-8.5 scenario

Furthermore, Figure 6.2 presents the results for the overflow analysis, which is defined as the periods in which the capacity factors are above the 90th percentile. This analysis is carried out in order to understand how the days with high capacity factors increase for the European countries, as this will give an insight on how the clearness index changes. The figure indicates that countries such as France, Germany, Belgium, Turkey, Austria will have higher periods of overflow with an increase in mean duration (to a higher extent) and mean number of sequences (to a lower extent). In addition, countries such as Finland and Sweden will have lower periods of overflow. This suggests that these latter countries will be characterized by a decrease in the clearness index, similarly that what is shown in Figure 5.1 and Figure 5.4.

Moreover, SSP2-4.5 and SSP1-2.6 project a decrease in the days with droughts. Particularly, SSP1-2.6 projects that practically all of the European countries will be characterized by a decrease in periods of consecutive days with capacity factors below the 10th. Only Norway is forecasted to have a similar pattern during EOC compared with BOC.

When it comes to the overflow analysis, SSP2-4.5 does not present significant changes, similarly to what is forecasted in Figure 5.1. In fact, results for BOC and EOC are very similar, with all countries showing a very small difference in the increase of mean duration and in mean number of sequences in a year. However, SSP1-2.6 projects a clear increase in countries with capacity factors above the 90th. This suggests that the clearness index will increase for the whole of Europe under the SSP1-2.6 scenario. Days with circumsolar solar radiation will increase and days with isotropic solar radiation will decrease.

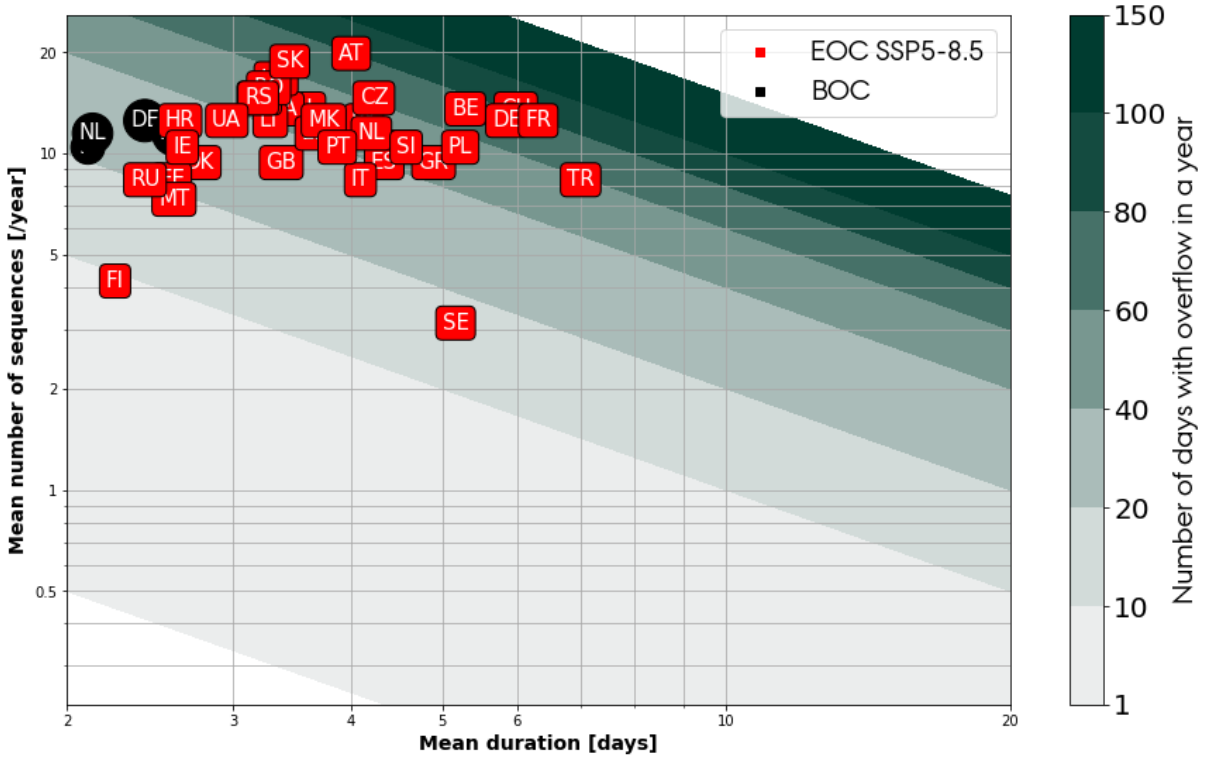

Figure 6.2: Duration and frequency of solar energy overflow periods, determined as consecutive days with capacity factors more than the 90th percentile of capacity factors at the BOC, evaluated for the BOC and EOC periods under the SSP5-8.5 scenario

6.2. Wind energy extreme events

This section presents the results for energy drought and extreme events specifically for wind energy. The results shown are for SSP5-8.5, while the results for SSP2-4.5 and SSP1-2.6 can be found respectively in Appendix B.3 and B.4.

As shown in Figure 5.5, a general decrease in wind energy capacity factors is forecasted for practically all of the European countries. During summer and autumn, the relative decrease is much stronger compared to winter and spring. This might be critical for the energy system of these countries, as the wind generation grows weaker towards the end of the century with a pronounced effect due to the seasonality.

Figure 6.4 presents the results for the drought analysis of 38 countries for wind energy for SSP5-8.5 for BOC and EOC. This analysis is done on a yearly time frame, differently than for solar energy where a monthly analysis is carried out. The figure shows that the droughts become more sever throughout the whole Europe. A critical result is found for a country like Italy, where the number of days with drought in a year significantly increase to almost 150. In addition, the mean duration of days of a drought also increases, while the mean number of sequences remains similar. This suggests that there will be prolonged periods of days with less wind. In addition, countries such as Slovenia, Germany, Estonia and Denmark will be characterized by an increase in mean number of sequences with a drought, while the mean duration will remain similar. This suggests that there will be an increase in the amount of periods of drought towards the end of the century, which will

have the same duration as during BOC. In addition, only countries such as Albania and Turkey show similar behaviour during EOC and BOC, while all the other countries are projected to have in increase in droughts.

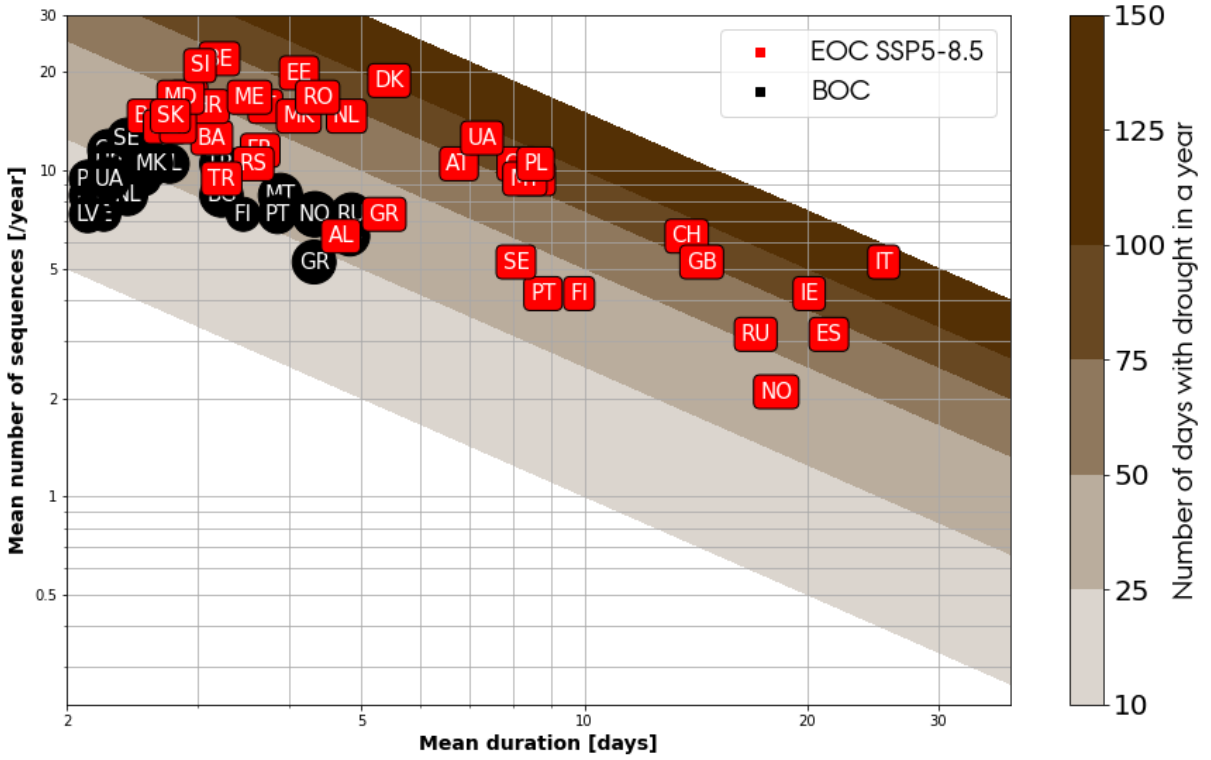

Figure 6.3: Duration and frequency of wind energy drought periods, determined as consecutive days with capacity factors less than the 10th percentile of capacity factors at the BOC, evaluated for the BOC and EOC periods under the SSP5-8.5 scenario

In addition to the drought analysis, this section also presents the overflow analysis which can be seen in Figure 6.4. Days with capacity factors above the 90^{th} percentile are critical for the wind energy system. In fact, days with very high wind suggest that a lot of the energy will not be used due to the cut-off speed of the turbines. The figure below shows that overflow periods will increase for countries such as Latvia, Lithuania, Estonia, Russia, Bosnia and Herzegovina and Czech Republic. Therefore, after comparing the results from Figure 5.5, Figure 6.4 and Figure 6.4, these countries will be characterized by a violent wind speed pattern as the mean wind speed will decrease and periods with high wind speed will become more frequent.

(Carvalho, Rocha, Costoya, et al., 2021) presents a similar research by investigating the non-useable wind speed events, which are comprised by days with wind speed below cut-in and above cut-off wind speeds. The results found are largely in agreement with this Master Thesis as countries such as Italy are forecasted to have an increase in droughts.

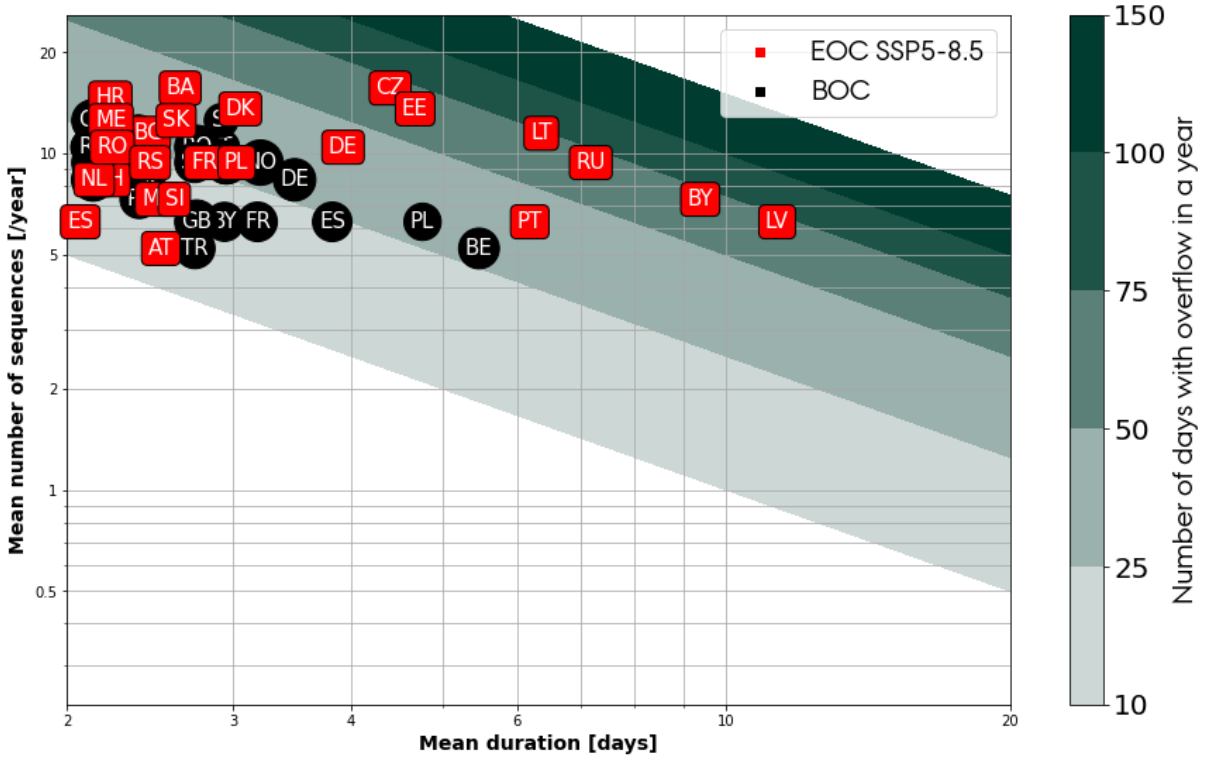

Figure 6.4: Duration and frequency of wind energy overflow periods, determined as consecutive days with capacity factors more than the 90th percentile of capacity factors at the BOC, evaluated for the BOC and EOC periods under the SSP5-8.5 scenario

In addition, SSP2-4.5 forecasts that the droughts will also increase, but not as strongly as for SPP5-8.5. The overflow periods are expected to remain very similar between BOC and EOC. On the other hand, SSP1-2.6 also projects an increase in the drought analysis for countries such as Germany, France, Denmark and Spain. The overflow analysis for SSP1-2.6 projects similar results between BOC and EOC, with the exception of Germany which represents an outlier as it displays a decrease of periods with overflow.

7 Discussion

The historical analysis from 2001 til 2015 is used to compare the modelled data from the five CMIP6 models with reanalysis data from ERA5 and actual data from IRENA. This analysis is used to confirm whether a GCM can be used to model solar, wind and hydro energy time series. Regarding solar energy, all the climate models seem to consistently underperform when compared with reanalysis and actual data. Since all the models seem to show a consistent bias, a calibration factor is used to account for that. Different approaches are possible, but a constant factor is chosen for all of Europe by calculating the average ratio between the actual and modelled data. The NRMSE is calculated before and after the calibration for the solar energy yearly average values. It is found that the NRMSE decreases for all countries after calibration. Regarding wind energy, a similar approach is followed but the calibration factor is calculated per country as the bias is not consistent. The hindcast reveals that two of the models (MIROC6 and MPI-ESM1-2-LR) are either underestimating or overestimating the reanalysis data from ERA5. That is owing to the fact that these models have a coarser resolution and, thus, are not able to precisely model wind energy time series in areas of high roughness (areas with mountains or many trees and buildings). When compared with other studies which are taking into account more than thirty GCMs (Carvalho, Rocha, Costoya, et al., 2021; Martinez and Iglesias, 2022), these two models are either not used due to a resolution higher than 1.25° in latitude and longitude or due to having low agreement with ERA5 reanalysis data. Moreover, these two GCMs are also not used for the analysis of hydro energy due to a high resolution and also because they are showing results significantly different than the other GCMs. An analysis with ERA5 data was not finalised in this Master Thesis, but that would have been a better method to validate the data from the GCMs.

After the historical analysis, a multi-model ensemble is made by averaging the considered GCMs: all five for solar and three for wind and hydro. The climate model is a simplified mathematical model of complicated nature phenomena. Various different assumptions are made when initializing, discretizing and choosing a numerical method for a climate model. Therefore, it is useful to average several different GCMs in order to minimize the uncertainties and errors of an individual GCM. By using the ensemble, a comparison between BOC and EOC periods is carried out. The results shown for solar, wind and hydro resources are in significant agreement with previous studies (Carvalho, Rocha, Costoya, et al., 2021; Hou et al., 2021; Schlott et al., 2018; Gøtske and Victoria, 2021).

For solar energy, according to (Hou et al., 2021), a decrease is forecasted for SSP5-8.5 for Northern Europe and an increase for southern Europe. In addition, for SSP1-2.6 the PV potential is forecasted to increase by around 5% across the whole of Europe. The results from this Master Thesis also highlight similar changes. Countries such as Norway, Sweden and Finland are projected to be characterized by a decrease in capacity factors, while the rest of Europe is project to have an increase. SSP1-2.6 also shows a general increase in the range of 5-10%, while SSP2-4.5 does not project any significant different

compared with today. When it comes to intra-annual analysis, the paper mentioned above shows results only for summer and winter. When comparing the results from this study with the ones from the paper, a very strong mapping is noticeable. In fact, both studies conclude that during summer the hot spots of increase are centered in Germany, Poland and Czech Republic. In addition, the PV generation decreases in the south of Iberia, Italy and the Balkans. During winter, an increase is forecasted for Southern Europe and a decrease for Northern Europe. Also, the strongest winter increase happens in the south while the stronger summer increase is found in continental Europe. For SSP1-2.6, the intra-annual analysis is projected to have very similar results with the paper mentioned above. During winter, the strongest PV electricity generation increase is found around the Mediterranean (particularly around the Apennines and Balkan peninsulas). Meanwhile, during summer the highest increase is found for central Europe, with the Mediterranean region only shows a slight increase. The novelty of this study consists in the inclusion of the drought and overflow analysis. For SSP5-8.5, the drought analysis shows that countries such as Norway, Sweden, Finland, Romania, Latvia, Belarus and Estonia show droughts with an increased mean duration. This is in alignment with the fact that the values for capacity factors decrease for Northern Europe. Moreover, droughts will decrease for Spain, Albania, North Macedonia, Portugal and Turkey. The overflow analysis indicates that countries such as France, Germany, Belgium, Turkey, Austria will have an increase in capacity factors above the 90^{th} percentile. This also suggest that for countries in Southern and continental Europe, the clearness index will decrease as the capacity factors are increasing.

Regarding wind energy, according to (Carvalho, Rocha, Costoya, et al., 2021), a general decrease is forecasted for practically all of Europe for the SSP5-8.5 scenario, similarly to the conclusion from this Master Thesis. SSP2-4.5 projects in both studies that some areas can witness a slight increase of the wind resource.

However, additional research is required for SSP1-2.6 as unexpected results are found. Even though the results for SSP1-2.6 are quite similar with the results from SSP5-8.5, certain areas are showing a high decrease in the wind resource. This could also be caused due to the uncertainty in the three models considered. Therefore, a higher number of GCMs should be considered to investigate the results from SSP1-2.6.

When it comes to intra-annual analysis, similar results to the above mentioned paper are found in this Master Thesis as well. For SSP5-8.5, the wind capacity factors change is stronger in summer and autumn compared to other seasons. A general decrease is projected during summer and autumn for the whole of Europe. In addition, during winter and spring an increase is projected for continental Europe, the Baltic countries and Finland. The drought analysis indicates a general increase in periods of drought for all of Europe, similarly to the study done in the paper mentioned above for the non-useable wind speed events. These are defined as the days with wind speed below cut-in and above cut-off wind speeds. From this paper, countries such as Italy are forecasted to have an increase in droughts, which is in alignment with the results found here. When compared with CMIP5 results, CMIP6 stronger radiative forcing scenarios enhance the differences when compared with milder scenarios and show relevant differences. CMIP5 projected an increase in the wind resource for Northern Europe and a decrease in Southern Europe. The differences between these two models could be because of the way the large-scale atmospheric circulation and boundary layer processes are simulated.

Regarding hydro energy, only runoff analysis has been finalized in this Master Thesis. When analysing energy systems, it is more suitable to calculate the inflow, which is the amount of water that remains after evaporation, infiltration and irrigation. However, when comparing with other papers, a relative analysis can be made since a high change in runoff will also cause a high change in inflow (and the opposite). According to (Schlott et al., 2018), for the emission scenario RCP8.5 (equivalent to SSP5-8.5 in CMIP6) annual inflow will decrease by 31% in Southern Europe and increase by 21% in Northern Europe. Similar results are projected in this Master Thesis where the runoff is increase for countries such as Norway, Sweden and Finland in a range from 20 to 30%. In addition, a general decrease is forecasted for continental and Southern Europe with summer and autumn showing the highest change. During winter and spring an increase is projected for Northern Europe, with winter showing an increase ranging between 30 and 50% and spring showing an increase ranging between 50 and 70 %. Therefore, it is possible to say that the spring runoff generation is significantly increased for Northern Europe during winter and spring. This might be simply caused due to higher temperatures preventing rain from freezing.

The findings for solar, wind and hydro energy suggest that the changes based on climate scenario should be taken into consideration in the planning of the energy mix and future wind farm and solar park projects. This Master Thesis provides a very thorough analysis with the inclusion of five GCMs and three SSPs. Even though the multi-model approach eliminates biases and uncertainties to a great level, some limitations of the GCMS are still present, such as the coarse grid resolution or the inaccuracy in areas with high roughness (such as mountainous regions). In order to better understand the changes on a smaller scale, regional level studies should be complemented with a large scale evaluation. Finally, a higher amount of GCMs should be considered which satisfy the conditions of having a resolution higher than 1.25° in latitude and longitude.

8 Conclusions

The rise of Earth's temperature represents one of the biggest challenges of the modern world. This study investigates the impacts of climate changes on solar, wind and hydro resources. The beginning and end of the century evolution of solar, wind and hydro resources is investigated by means of a multi-model ensemble comprised of 5 global circulation models. In addition, three SSPs are considered i.e. SSP1-2.6 , SSP2-4.5 and SSP5-8.5 from CMIP6 in order to quantify the climate risks towards the end of the century. A hindcast analysis within the period from 2001 and 2015 is carried out in order to validate and calibrate modelled data. For solar energy, a calibration is made with a constant calibration factor for all European countries in order to minimize the NRMSE. While for wind energy, the calibration is made with country dependent calibration factors.

Then a comparison for the modelled data is made for two periods: 2001 til 2030 (BOC) and 2071 til 2100 (EOC). Regarding solar energy, SSP5-8.5 predicts a decrease for Northern Europe in terms of capacity factors and an increase for Southern Europe with strong intermodel agreement. The Nordics, i.e. Norway, Sweden and Finland, encounter a decrease in relative capacity factors within the range from -7% to -11%. Meanwhile, the Alps, i.e. France, Switzerland, Austria and Italy show an increase within the range from +3% to +5%. The Mediterranean, i.e. Spain and Portugal, show an increase ranging from +5% to +7%. This study also finds that for SSP1-2.6, mitigating emissions improves solar power generation by 5%, while no significant changes are noticeable for SSP2-4.5. When it comes to intra-annual analysis, the seasonality of PV production becomes more pronounced as the generation grows in summer and decreases in winter (SSP 5-8.5). With the exception that for Southern Europe PV generation decreases in summer while it increases in winter for SSP5-8.5. The reduction in the capacity factors that occurs in the Nordics, causes more frequent and longer periods of drought. In addition, Mediterranean countries also forecast an increase in days with a higher clearness index, i.e. days with clear-sky radiation, while the Nordics forecast the opposite.

Moreover, when it comes to the wind resource, SSP5-8.5 projects a decrease, despite large interannual and intermodel variability, across the whole European continent (10-20%), particularly for the Nordics and the British Isles. Even though, SSP1-2.6 and SSP2-4.5 predict that towards the end of the century small localized areas might experience an increase in wind energy (15%-30% in eastern Ukraine and Turkey), all other European countries will experience a significant decrease (5%-15%). The general decrease in the capacity factors that occurs for SSP5-8.5, causes more frequent and longer periods of drought for all countries with Italy representing the country with highest number of total days of drought. In addition, the results also indicate an increase in the frequency and duration of overflow periods (defined as $> 90^{\text{th}}$ percentile of historical values) for Northeast Europe, i.e.Latvia, Russia, Lithuania, Estonia, while a decrease for Southern Europe, i.e. Spain, Austria. This study also suggests an increase in the intra-annual variability in the British Isles, Turkey, Iberia and Northeast Europe.

Furthermore, hydro energy also is expected to significantly change towards the end of the century. SSP5-8.5 suggests an increase in annual runoff in Northern Europe by 20-30% and a decrease in Southern Europe in a similar range. Intra-annual analysis forecasts that runoff decreases during spring and summer, while it increases during fall and winter.

9 Future Work

This Master Thesis only used five general circulation models, which could be a low number in order to have a high certainty of the climate model predictions. Future work could involve using all available general circulation models which satisfy specific requirements for resolution in terms of latitude and longitude. In addition, to understand the changes on a smaller scale, general circulation models should be used in combination with regional climate models. This will help in understanding the changes for wind energy around areas with high roughness, such as mountainous areas.

The applied climate model data is not bias adjusted with ERA5 reanalysis data for hydro energy. The next step would be to validate and calibrate hydro modelled data with a higher number of general circulation models. This will decrease to a high level the uncertainty in the displayed results.

The results for solar, wind and hydro resource should be used in order to investigate a future European energy system. A change in the production of any energy source will affect the configuration of an optimal European energy system.

Bibliography

Andresen, G. B., A. A. Søndergaard, and M. Greiner (Dec. 2015). "Validation of Danish wind time series from a new global renewable energy atlas for energy system analysis". In: *Energy* 93, pp. 1074–1088. ISSN: 0360-5442. DOI: 10.1016/j.energy.2015.09.071.

Bartók, B., M. Wild, D. Folini, D. Lüthi, S. Kotlarski, C. Schär, R. Vautard, S. Jerez, and Z. Imecs (Oct. 2017). "Projected changes in surface solar radiation in CMIP5 global climate models and in EURO-CORDEX regional climate models for Europe". In: *Clim. Dyn.* 49.7, pp. 2665–2683. ISSN: 1432-0894. DOI: 10.1007/s00382-016-3471-2.

Bauer, L. (Dec. 2022). *Vestas V112-3.3 - 3,30 MW - Wind turbine*. [Online; accessed 30. Dec. 2022].

Carvalho, D., A. Rocha, X. Costoya, M. deCastro, and M. Gómez-Gesteira (2021). "Wind energy resource over Europe under CMIP6 future climate projections: What changes from CMIP5 to CMIP6". In: *Renewable and Sustainable Energy Reviews* 151, p. 111594. ISSN: 1364-0321. DOI: https://doi.org/10.1016/j.rser.2021.111594.

Carvalho, D., A. Rocha, M. Gómez-Gesteira, and C. Silva Santos (2017). "Potential impacts of climate change on European wind energy resource under the CMIP5 future climate projections". In: *Renewable Energy* 101, pp. 29–40. ISSN: 0960-1481. DOI: https://doi.org/10.1016/j.renene.2016.08.036.

Crook, J. A., L. A. Jones, P. M. Forster, and R. Crook (2011). "Climate change impacts on future photovoltaic and concentrated solar power energy output". In: *Energy Environ. Sci.* 4 (9), pp. 3101–3109. DOI: 10.1039/C1EE01495A.

CSI (2022). *The Greenhouse Effect*. URL: http://www.ces.fau.edu/nasa/module-2/how-greenhouse-effect-works.php. (visited: 14.12.2022).

EU (2020). *Stepping up Europes 2030 climate ambition - Investing in a climate-neutral future for the benefit of our people*. URL: https://eur-lex.europa.eu/legal-content/EN/TXT/PDF/?uri=CELEX:52020DC0562&from=EN. (visited: 14.12.2022).

Gaetani, M., T. Huld, E. Vignati, F. Monforti-Ferrario, A. Dosio, and F. Raes (2014). "The near future availability of photovoltaic energy in Europe and Africa in climate-aerosol modeling experiments". In: *Renewable and Sustainable Energy Reviews* 38, pp. 706–716. ISSN: 1364-0321. DOI: https://doi.org/10.1016/j.rser.2014.07.041.

Gøtske, E. K. and M. Victoria (2021). "Future operation of hydropower in Europe under high renewable penetration and climate change". In: *iScience* 24.9, p. 102999. ISSN: 2589-0042. DOI: https://doi.org/10.1016/j.isci.2021.102999.

Gutiérrez, C., S. Somot, P. Nabat, M. Mallet, L. Corre, E. van Meijgaard, O. Perpiñán, and M. Á. Gaertner (Mar. 2020). "Future evolution of surface solar radiation and photovoltaic potential in Europe: investigating the role of aerosols". In: *Environ. Res. Lett.* 15.3, p. 034035. ISSN: 1748-9326. DOI: 10.1088/1748-9326/ab6666.

Hay, J. E. and D. C. Mckay (Sept. 1985). "Estimating Solar Irradiance on Inclined Surfaces: A Review and Assessment of Methodologies". In: *International Journal of Solar Energy* 3.4-5, pp. 203–240. ISSN: 0142-5919. DOI: 10.1080/01425918508914395.

Hou, X., M. Wild, D. Folini, S. Kazadzis, and J. Wohland (Nov. 2021). "Climate change impacts on solar power generation and its spatial variability in Europe based on

CMIP6". In: *Earth Syst. Dyn.* 12.4, pp. 1099–1113. ISSN: 2190-4979. DOI: 10.5194/esd-12-1099-2021.

HydroBASINS (Jan. 2023). [Online; accessed 3. Jan. 2023]. URL: https://www.hydrosheds.org/products/hydrobasins.

IEA (Dec. 2020). *Shares of electricity production by source in OECD countries, 2020 – Charts – Data & Statistics - IEA*. [Online; accessed 15. Dec. 2022].

IRENA (2022). *Tools*. URL: https://www.irena.org/Data/Downloads/Tools. (visited: 15.12.2022).

Jerez, S., I. Tobin, R. Vautard, J. P. Montávez, J. M. López-Romero, F. Thais, B. Bartok, O. B. Christensen, A. Colette, M. Déqué, G. Nikulin, S. Kotlarski, E. van Meijgaard, C. Teichmann, and M. Wild (Dec. 2015). "The impact of climate change on photovoltaic power generation in Europe". In: *Nat. Commun.* 6.10014, pp. 1–8. ISSN: 2041-1723. DOI: 10.1038/ncomms10014.

JRC (Apr. 2019). [Online; accessed 3. Jan. 2023]. URL: https://data.jrc.ec.europa.eu/dataset/52b00441-d3e0-44e0-8281-fda86a63546d.

Kalogirou, S. A. (2009). *Solar Energy Engineering*. Elsevier, Academic Press. ISBN: 978-0-12-374501-9. DOI: 10.1016/B978-0-12-374501-9.X0001-5.

Martinez, A. and G. Iglesias (2022). "Climate change impacts on wind energy resources in North America based on the CMIP6 projections". In: *Science of The Total Environment* 806, p. 150580. ISSN: 0048-9697. DOI: https://doi.org/10.1016/j.scitotenv.2021.150580.

Müller, J., D. Folini, M. Wild, and S. Pfenninger (2019). "CMIP-5 models project photovoltaics are a no-regrets investment in Europe irrespective of climate change". In: *Energy* 171, pp. 135–148. ISSN: 0360-5442. DOI: https://doi.org/10.1016/j.energy.2018.12.139.

Nazarenko, L. S., N. Tausnev, G. L. Russell, D. Rind, R. L. Miller, G. A. Schmidt, S. E. Bauer, M. Kelley, R. Ruedy, A. S. Ackerman, I. Aleinov, M. Bauer, R. Bleck, V. Canuto, G. Cesana, Y. Cheng, T. L. Clune, B. I. Cook, C. A. Cruz, A. D. Del Genio, G. S. Elsaesser, G. Faluvegi, N. Y. Kiang, D. Kim, A. A. Lacis, A. Leboissetier, A. N. LeGrande, K. K. Lo, J. Marshall, E. E. Matthews, S. McDermid, K. Mezuman, L. T. Murray, V. Oinas, C. Orbe, C. P. Garcıa-Pando, J. P. Perlwitz, M. J. Puma, A. Romanou, D. T. Shindell, S. Sun, K. Tsigaridis, G. Tselioudis, E. Weng, J. Wu, and M.-S. Yao (July 2022). "Future Climate Change Under SSP Emission Scenarios With GISS-E2.1". In: *J. Adv. Model. Earth Syst.* 14.7, e2021MS002871. ISSN: 1942-2466. DOI: 10.1029/2021MS002871.

Panagea, I. S., I. K. Tsanis, A. G. Koutroulis, and M. G. Grillakis (July 2014). "Climate Change Impact on Photovoltaic Energy Output: The Case of Greece". In: *Adv. Meteorol.* 2014. ISSN: 1687-9309. DOI: 10.1155/2014/264506.

Petrakopoulou, F., A. Robinson, and M. Loizidou (Oct. 2016). "Simulation and evaluation of a hybrid concentrating-solar and wind power plant for energy autonomy on islands". In: *Renewable Energy* 96, pp. 863–871. ISSN: 0960-1481. DOI: 10.1016/j.renene.2016.05.030.

Pryor, S. and R. Barthelmie (2010). "Climate change impacts on wind energy: A review". In: *Renewable and Sustainable Energy Reviews* 14.1, pp. 430–437. ISSN: 1364-0321. DOI: https://doi.org/10.1016/j.rser.2009.07.028.

Reyers, M., J. Moemken, and J. G. Pinto (Feb. 2016). "Future changes of wind energy potentials over Europe in a large CMIP5 multi-model ensemble". In: *Int. J. Climatol.* 36.2, pp. 783–796. ISSN: 0899-8418. DOI: 10.1002/joc.4382.

Riahi, K., D. P. van Vuuren, E. Kriegler, J. Edmonds, B. C. O'Neill, S. Fujimori, N. Bauer, K. Calvin, R. Dellink, O. Fricko, W. Lutz, A. Popp, J. C. Cuaresma, S. KC, M. Leimbach, L. Jiang, T. Kram, S. Rao, J. Emmerling, K. Ebi, T. Hasegawa, P. Havlik, F. Humpenöder, L. A. Da Silva, S. Smith, E. Stehfest, V. Bosetti, J. Eom, D. Gernaat, T. Masui, J. Rogelj, J. Strefler, L. Drouet, V. Krey, G. Luderer, M. Harmsen, K. Takahashi, L. Baumstark, J. C. Doelman, M. Kainuma, Z. Klimont, G. Marangoni, H. Lotze-Campen, M. Obersteiner, A. Tabeau, and M. Tavoni (2017). "The Shared Socioeconomic Pathways and their energy, land use, and greenhouse gas emissions implications: An overview". In: *Global Environmental Change* 42, pp. 153–168. ISSN: 0959-3780. DOI: https://doi.org/10.1016/j.gloenvcha.2016.05.009.

Schlott, M., A. Kies, T. Brown, S. Schramm, and M. Greiner (2018). "The impact of climate change on a cost-optimal highly renewable European electricity network". In: *Applied Energy* 230, pp. 1645–1659. ISSN: 0306-2619. DOI: https://doi.org/10.1016/j.apenergy.2018.09.084.

Souza, M., E. Tonolo, R. Yang, G. Tiepolo, and J. Urbanetz (Jan. 2019). "Determination of Diffused Irradiation from Horizontal Global Irradiation - Study for the City of Curitiba". In: *Brazilian Archives of Biology and Technology* 62. DOI: 10.1590/1678-4324-smart-2019190014.

UN (2015). *Paris Agreement*. URL: https://sustainabledevelopment.un.org/content/documents/17853paris_agreement.pdf. (visited: 14.12.2022).

UNFCCC (2022). *The Paris Agreement*.

USGS (Jan. 2023). [Online; accessed 3. Jan. 2023]. URL: https://www.usgs.gov/special-topics/water-science-school/science/watersheds-and-drainage-basins?qt-science_center_objects=0#qt-science_center_objects.

Van Vliet, M., S. Vögele, and D. Rübbelke (Sept. 2013). "Water constraints on European power supply under climate change: Impacts on electricity prices". In: *Environmental Research Letters* 8, p. 035010. DOI: 10.1088/1748-9326/8/3/035010.

Van Vliet, M. T. H., J. Sheffield, D. Wiberg, and E. F. Wood (Dec. 2016). "Impacts of recent drought and warm years on water resources and electricity supply worldwide". In: *Environ. Res. Lett.* 11.12, p. 124021. ISSN: 1748-9326. DOI: 10.1088/1748-9326/11/12/124021.

Verdin, K. L. and J. P. Verdin (May 1999). "A topological system for delineation and codification of the Earth's river basins". In: *J. Hydrol.* 218.1, pp. 1–12. ISSN: 0022-1694. DOI: 10.1016/S0022-1694(99)00011-6.

Victoria, M. and G. B. Andresen (July 2019). "Using validated reanalysis data to investigate the impact of the PV system configurations at high penetration levels in European countries". In: *Prog. Photovoltaics Res. Appl.* 27.7, pp. 576–592. ISSN: 1062-7995. DOI: 10.1002/pip.3126.

WCRP (May 2022). [Online; accessed 29. Dec. 2022]. URL: https://esgf-data.dkrz.de/projects/esgf-dkrz.

Wild, M., D. Folini, F. Henschel, N. Fischer, and B. Müller (2015). "Projections of long-term changes in solar radiation based on CMIP5 climate models and their influence on energy yields of photovoltaic systems". In: *Solar Energy* 116, pp. 12–24. ISSN: 0038-092X. DOI: https://doi.org/10.1016/j.solener.2015.03.039.

Appendices

A Solar energy

A.1. Intra-annual analysis for SSP2-4.5

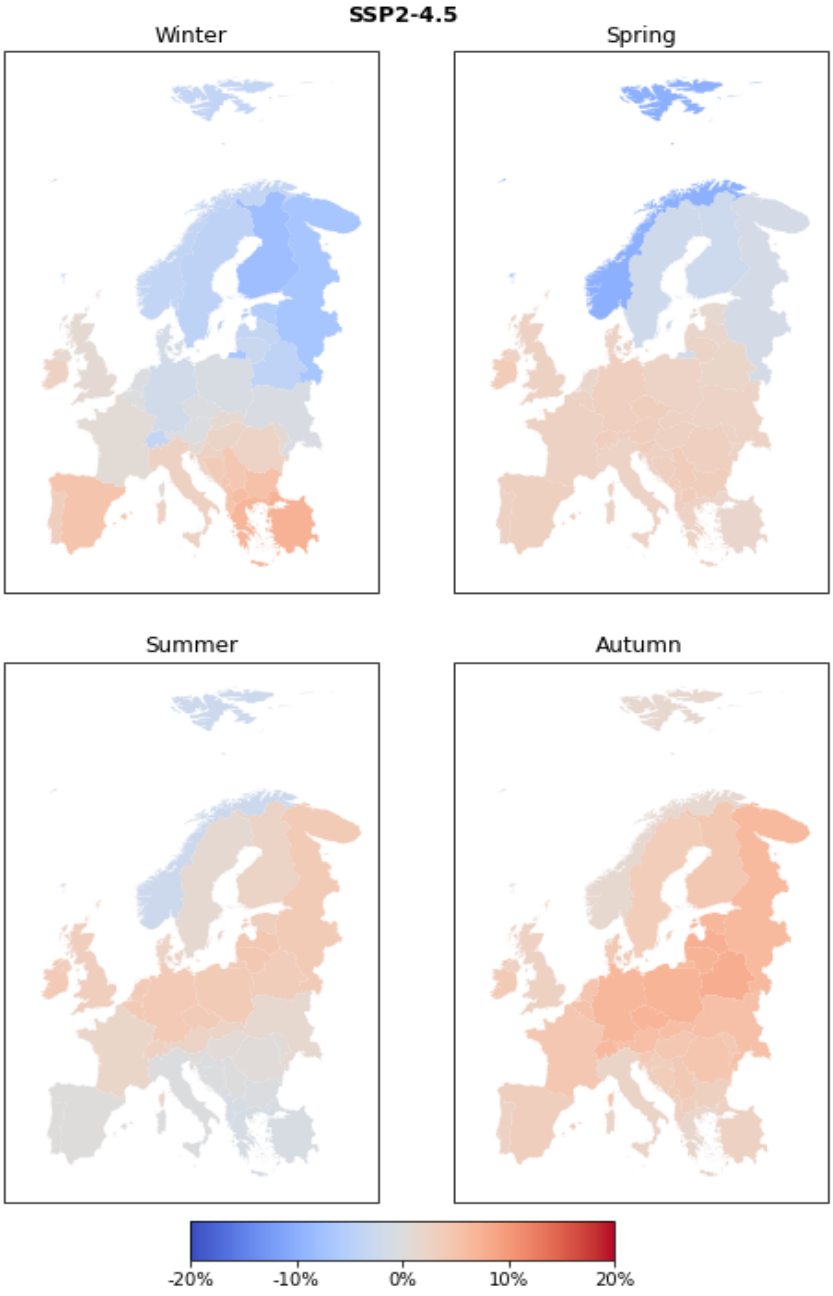

Figure A.1: Ensemble mean intra-annual relative change in capacity factors between EOC and BOC for solar energy. The results are for SSP2-4.5

A.2. Intra-annual analysis for SSP1-2.6

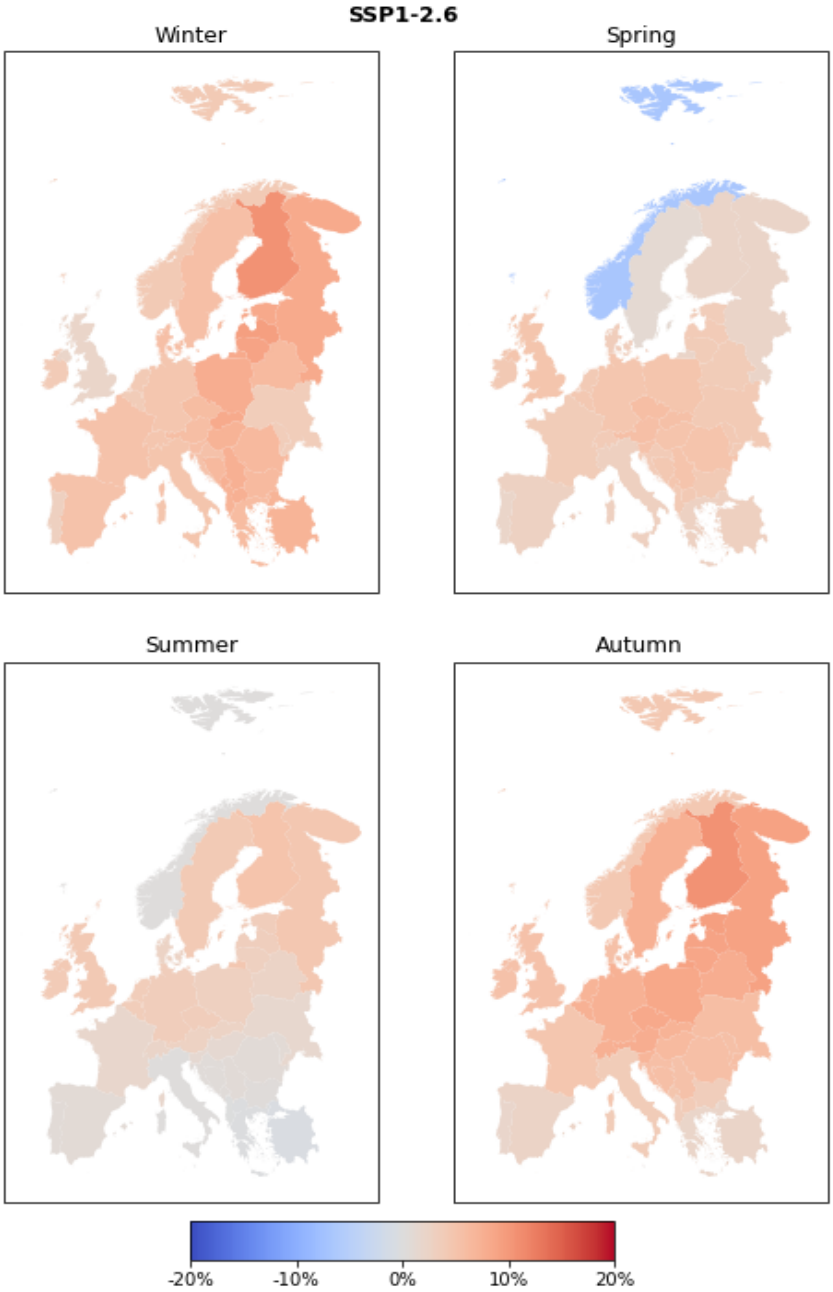

Figure A.2: Ensemble mean intra-annual relative change in capacity factors between EOC and BOC for solar energy. The results are for SSP1-2.6

A.3. Energy droughts and extreme events for SSP2-4.5

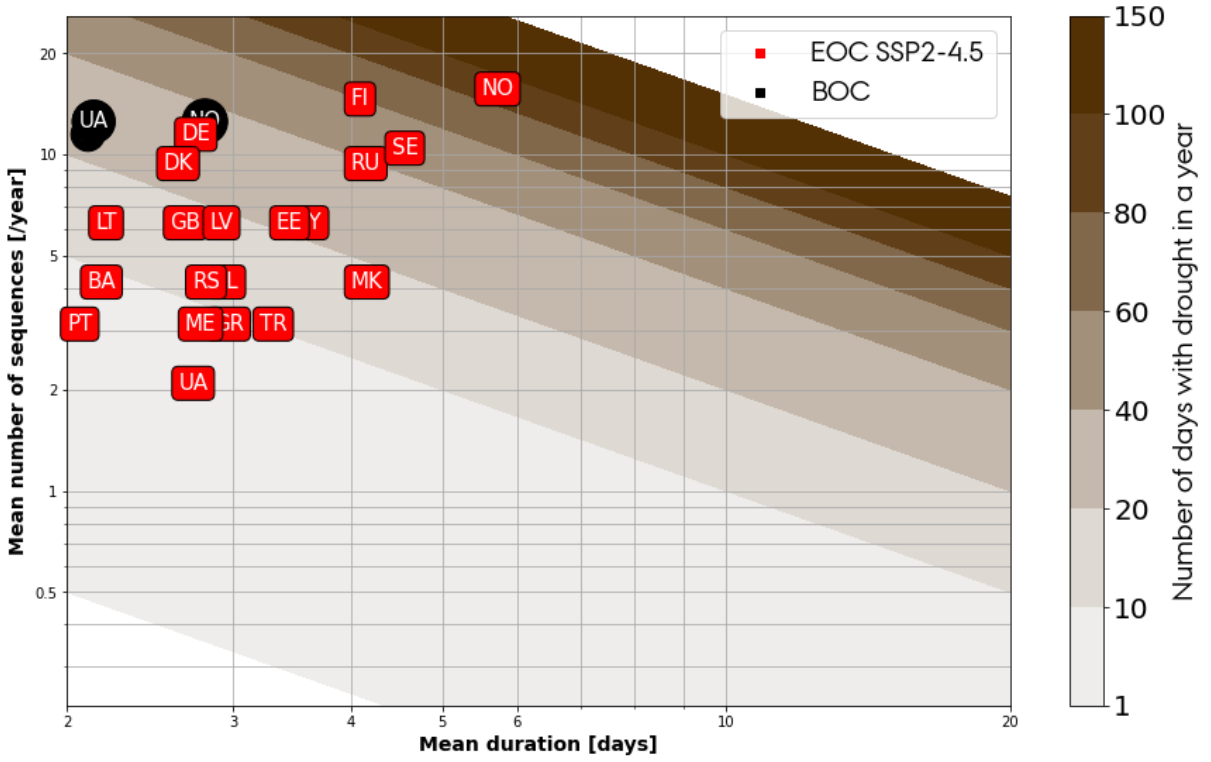

Figure A.3: Duration and frequency of solar energy drought periods, determined as consecutive days with capacity factors less than the 10th percentile of capacity factors at the BOC, evaluated for the BOC and EOC periods under the SSP2-4.5 scenario

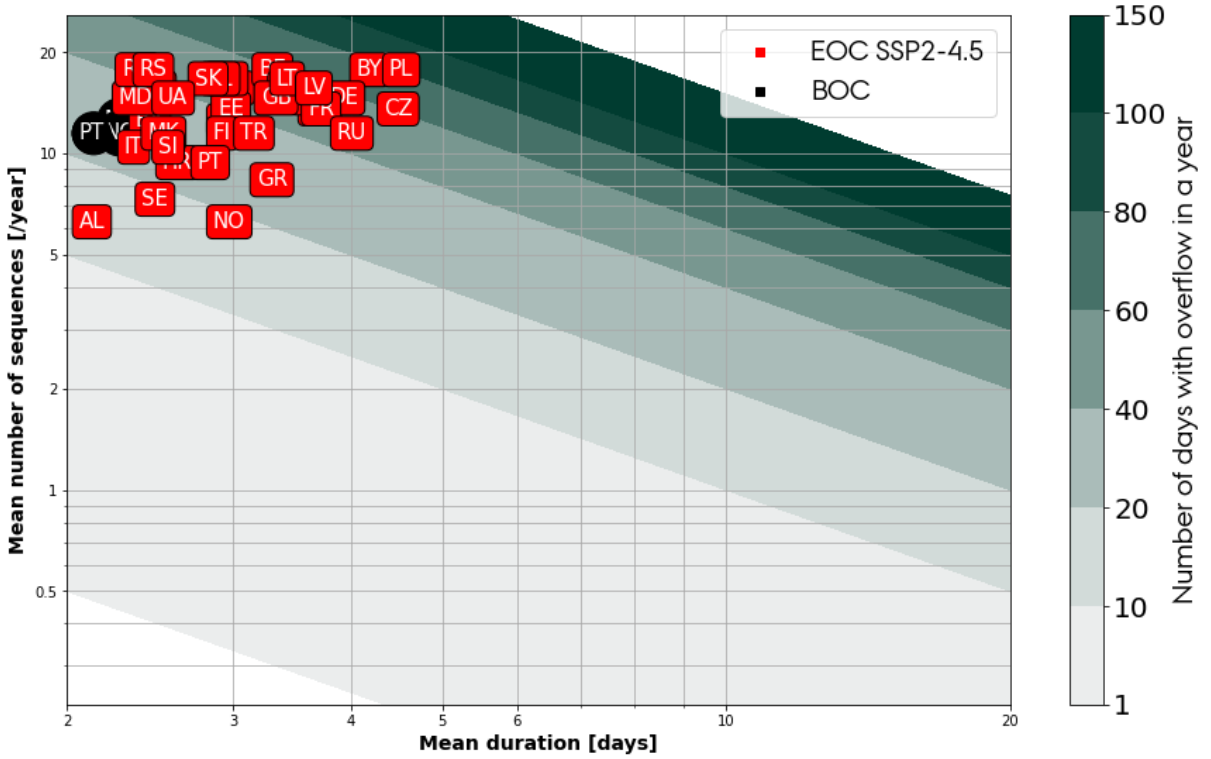

Figure A.4: Duration and frequency of solar energy overflow periods, determined as consecutive days with capacity factors more than the 90th percentile of capacity factors at the BOC, evaluated for the BOC and EOC periods under the SSP2-4.5 scenario

A.4. Energy droughts and extreme events for SSP1-2.6

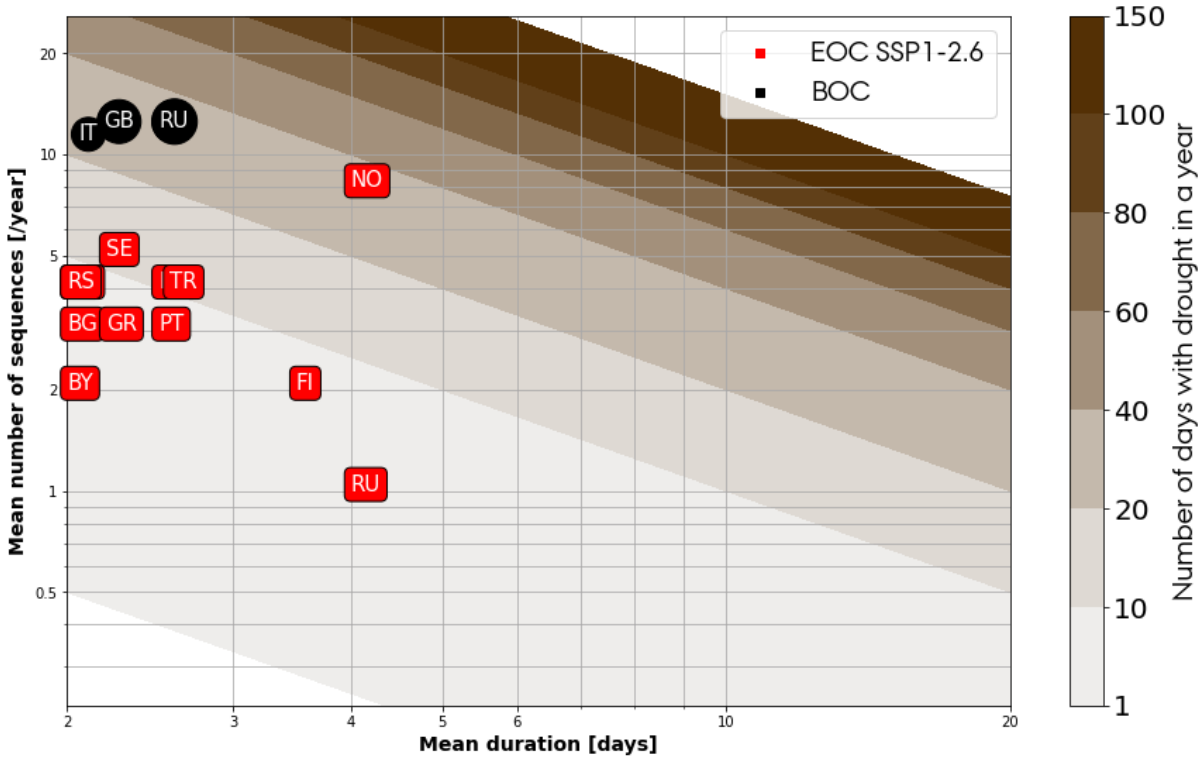

Figure A.5: Duration and frequency of solar energy drought periods, determined as consecutive days with capacity factors less than the 10th percentile of capacity factors at the BOC, evaluated for the BOC and EOC periods under the SSP1-2.6 scenario

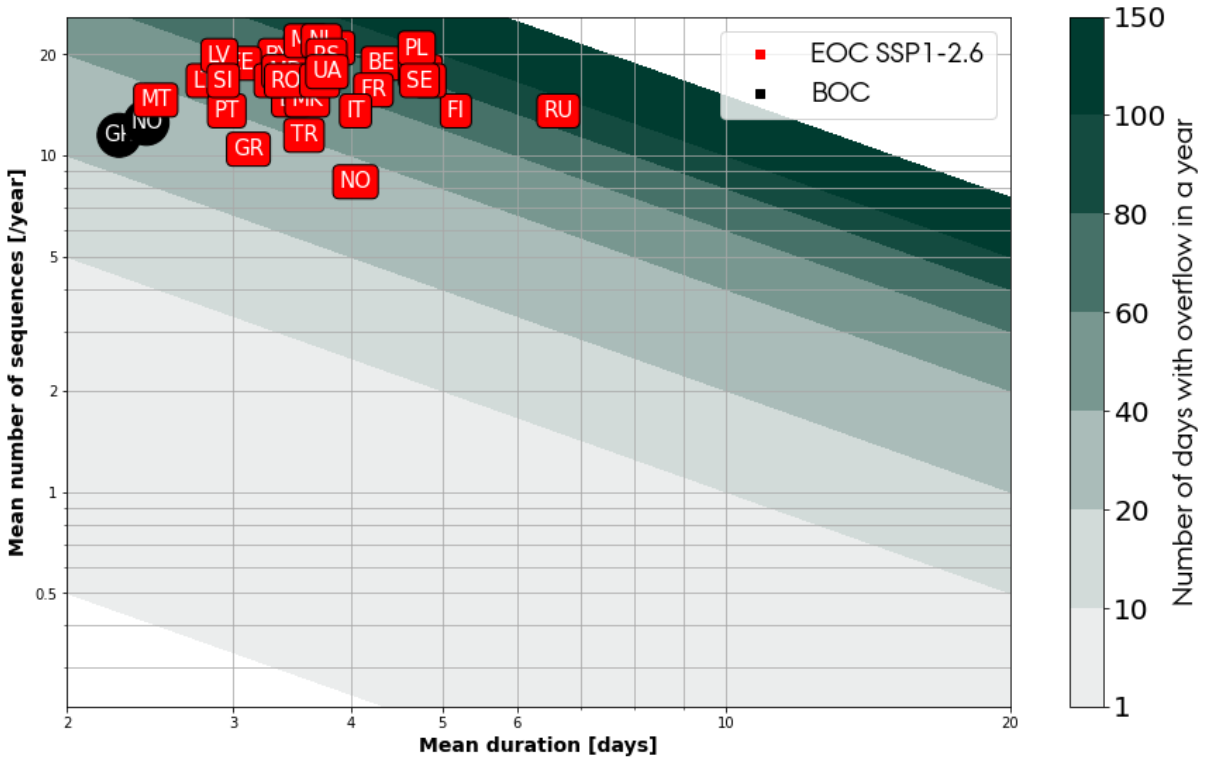

Figure A.6: Duration and frequency of solar energy overflow periods, determined as consecutive days with capacity factors more than the 90th percentile of capacity factors at the BOC, evaluated for the BOC and EOC periods under the SSP1-2.6 scenario

B Wind energy

B.1. Intra-annual analysis for SSP2-4.5

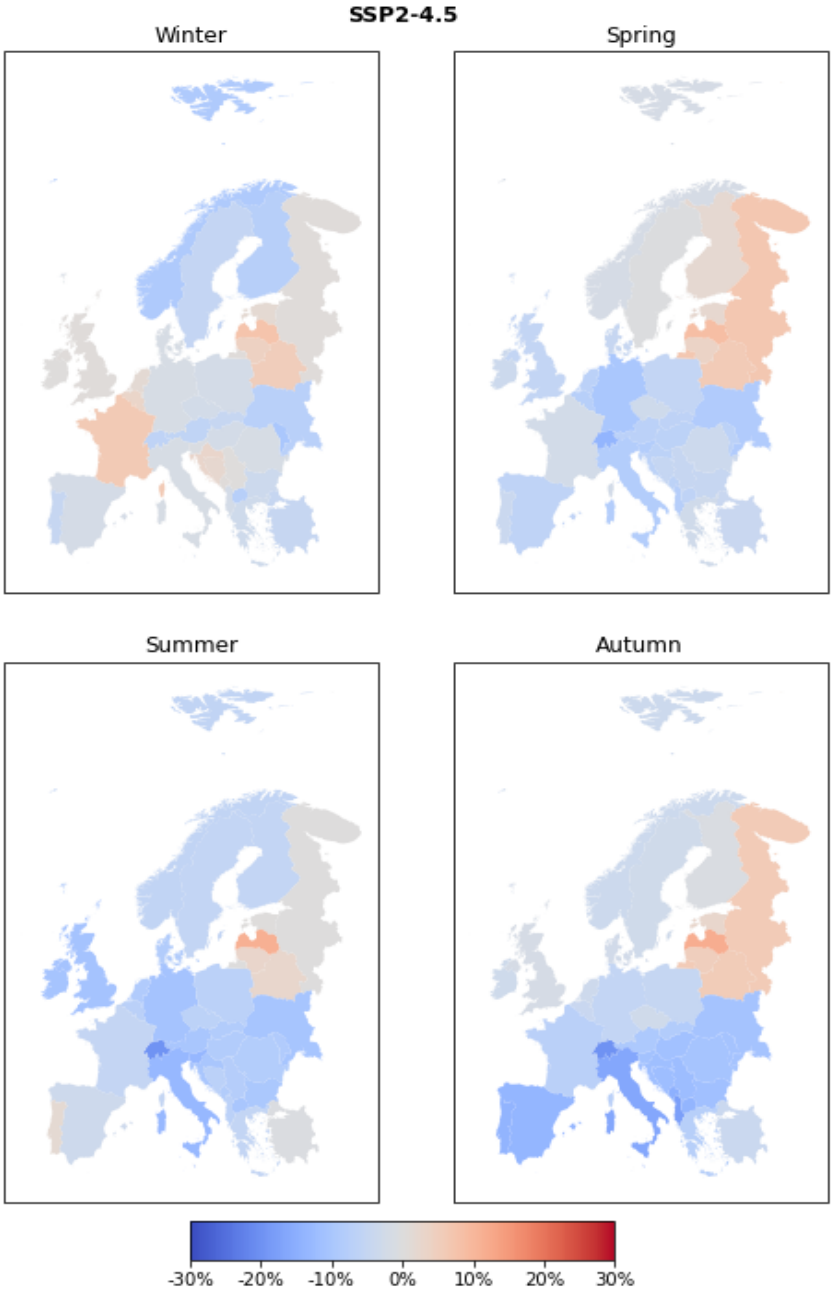

Figure B.1: Ensemble mean intra-annual relative change in capacity factors between EOC and BOC for wind energy. The results are for SSP2-4.5

B.2. Intra-annual analysis for SSP1-2.6

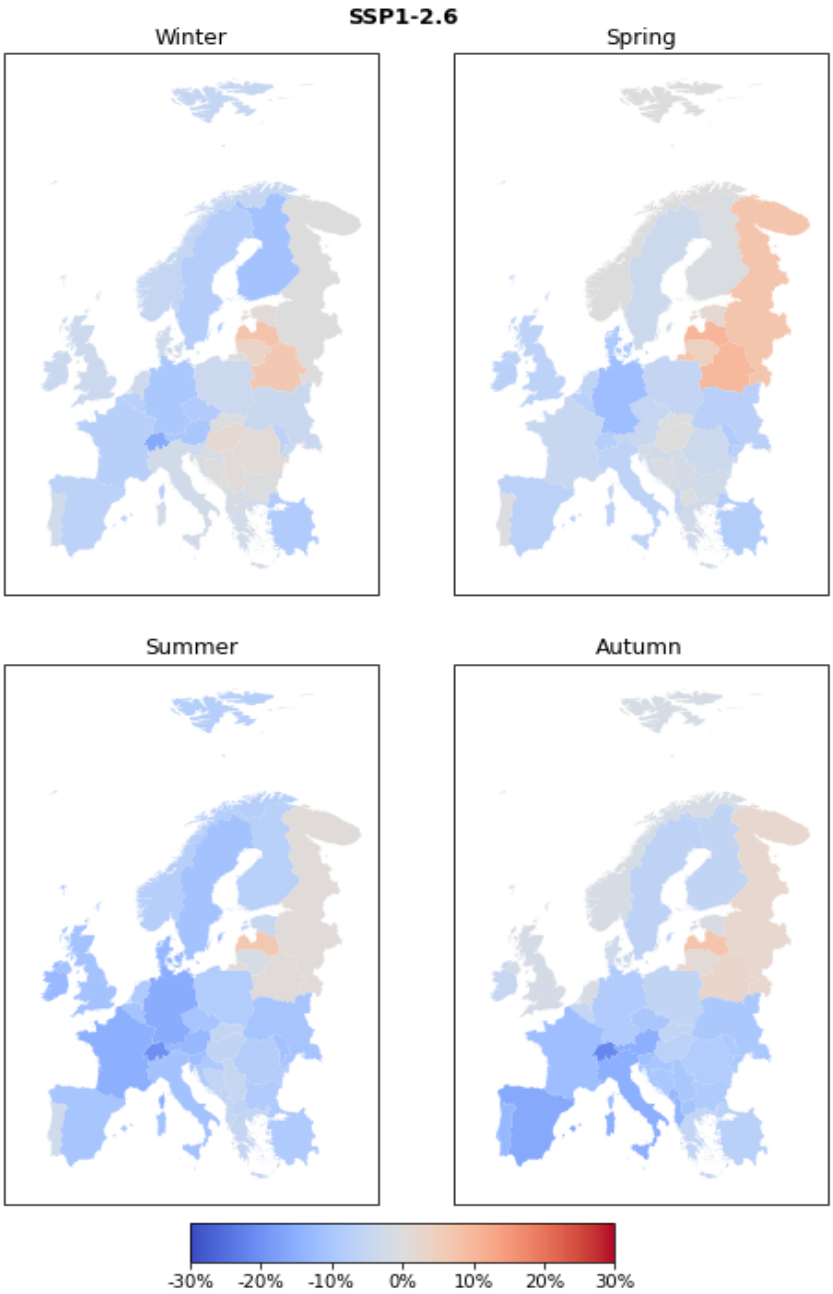

Figure B.2: Ensemble mean intra-annual relative change in capacity factors between EOC and BOC for wind energy. The results are for SSP1-2.6

B.3. Energy droughts and extreme events for SSP2-4.5

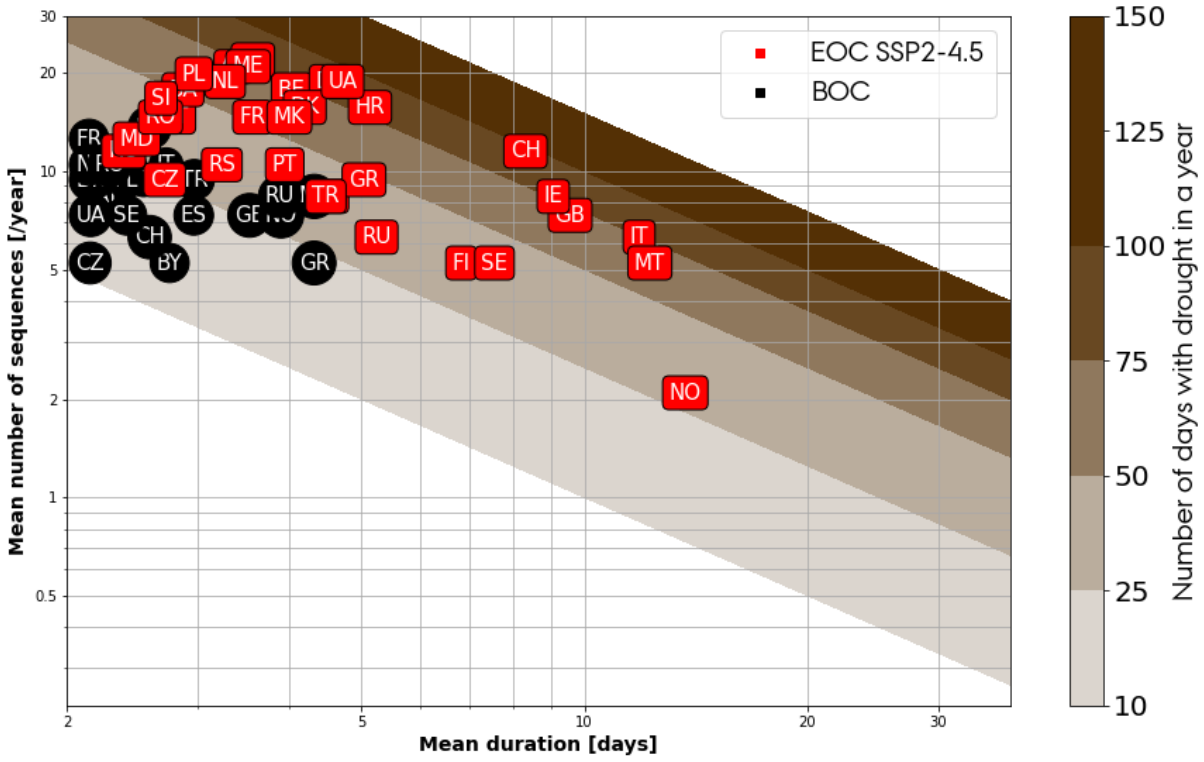

Figure B.3: Duration and frequency of wind energy drought periods, determined as consecutive days with capacity factors less than the 10th percentile of capacity factors at the BOC, evaluated for the BOC and EOC periods under the SSP2-4.5 scenario

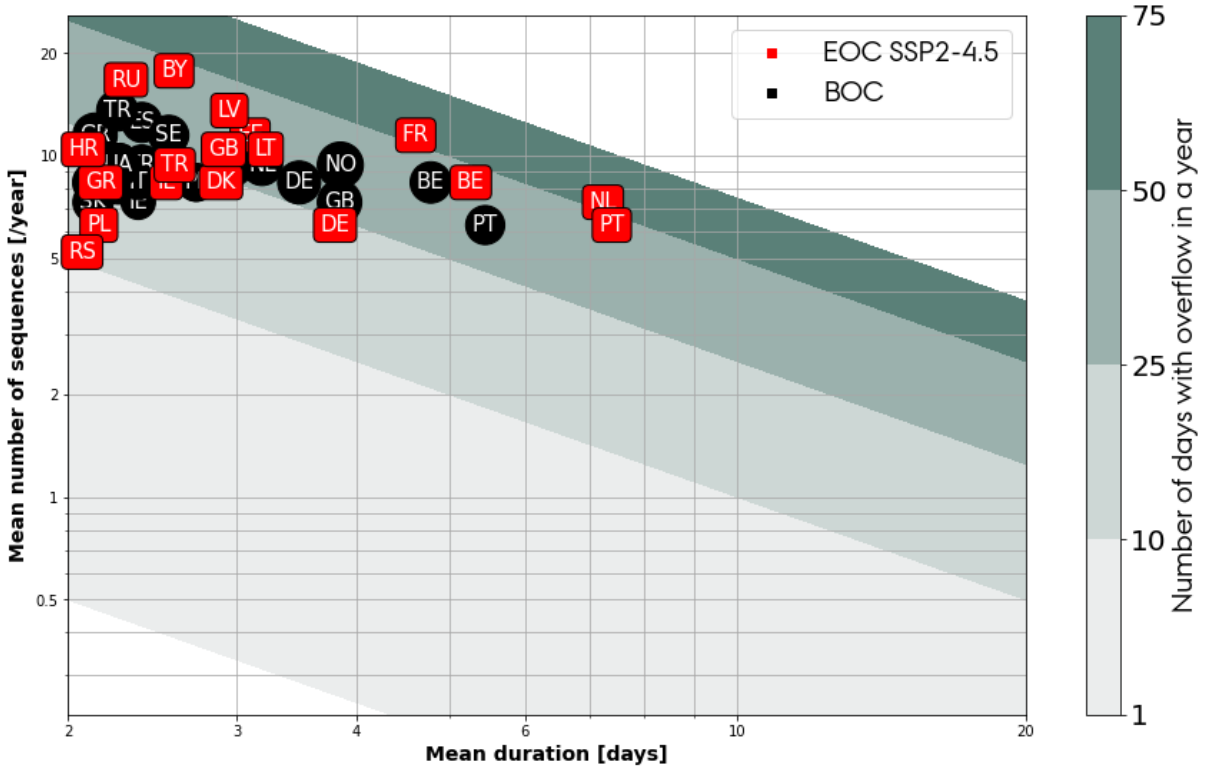

Figure B.4: Duration and frequency of wind energy overflow periods, determined as consecutive days with capacity factors more than the 90th percentile of capacity factors at the BOC, evaluated for the BOC and EOC periods under the SSP2-4.5 scenario

B.4. Energy droughts and extreme events for SSP1-2.6

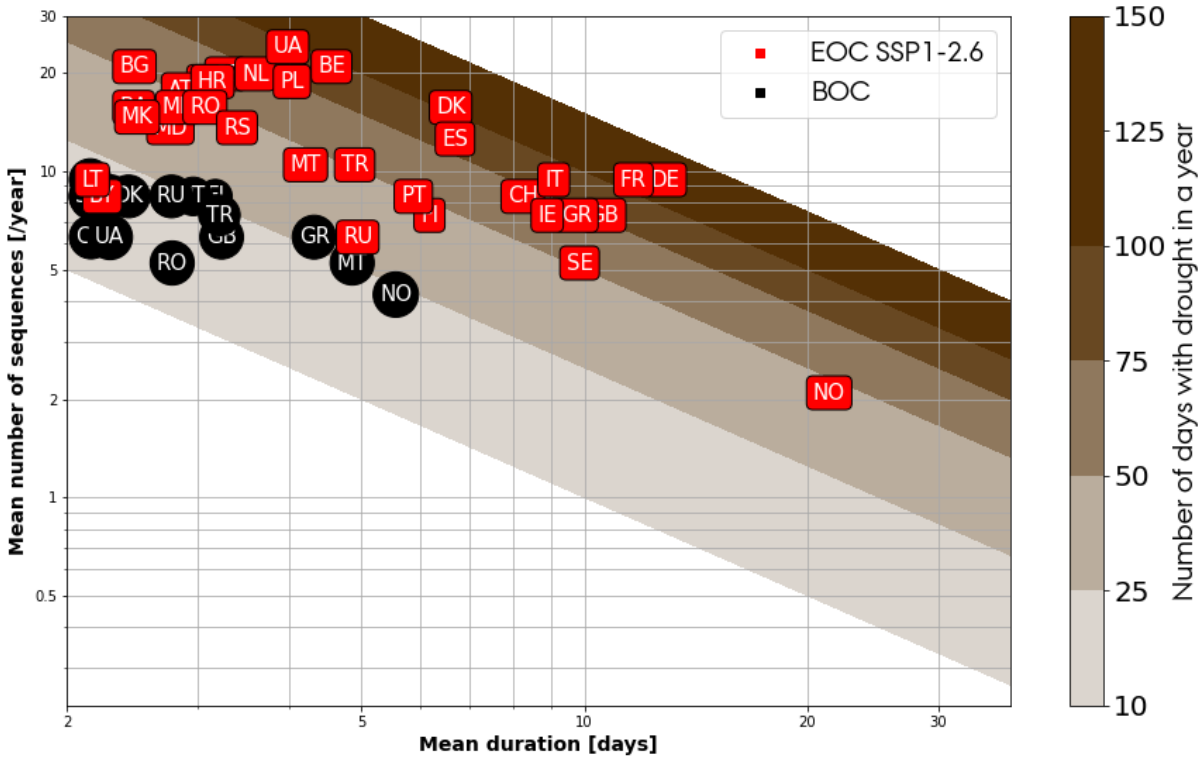

Figure B.5: Duration and frequency of wind energy drought periods, determined as consecutive days with capacity factors less than the 10th percentile of capacity factors at the BOC, evaluated for the BOC and EOC periods under the SSP1-2.6 scenario

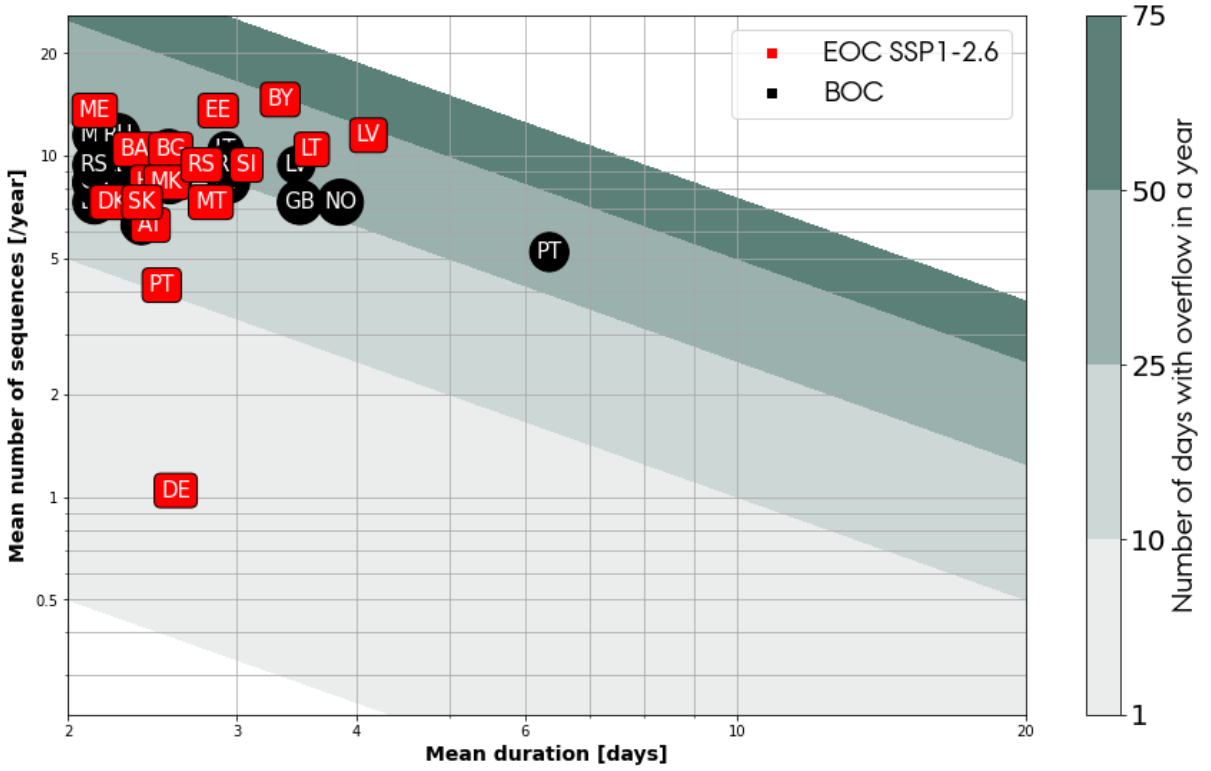

Figure B.6: Duration and frequency of wind energy overflow periods, determined as consecutive days with capacity factors more than the 90th percentile of capacity factors at the BOC, evaluated for the BOC and EOC periods under the SSP1-2.6 scenario

C Hydro energy

C.1. Intra-annual analysis for SSP2-4.5

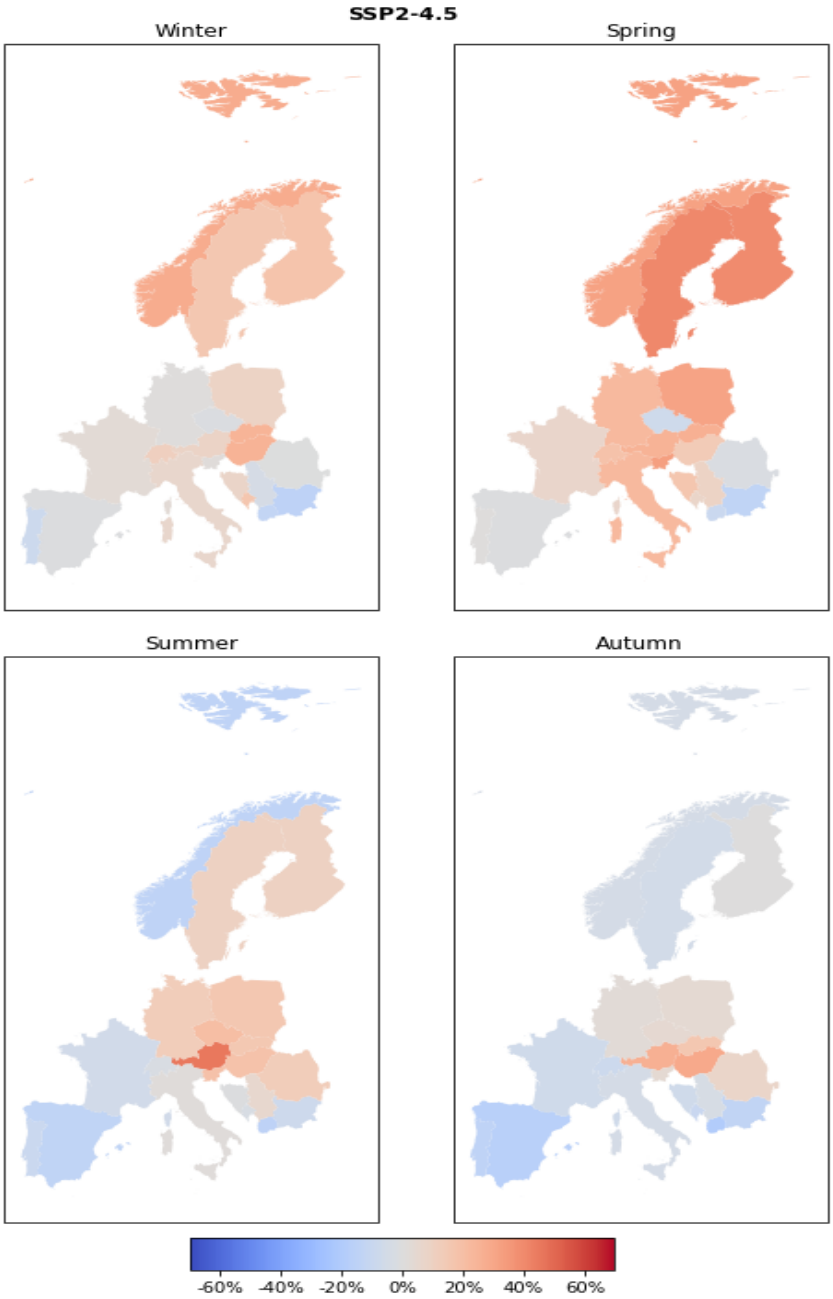

Figure C.1: Ensemble mean intra-annual relative change in runoff between EOC and BOC for hydro energy. The results are for SSP2-4.5

C.2. Intra-annual analysis for SSP1-2.6

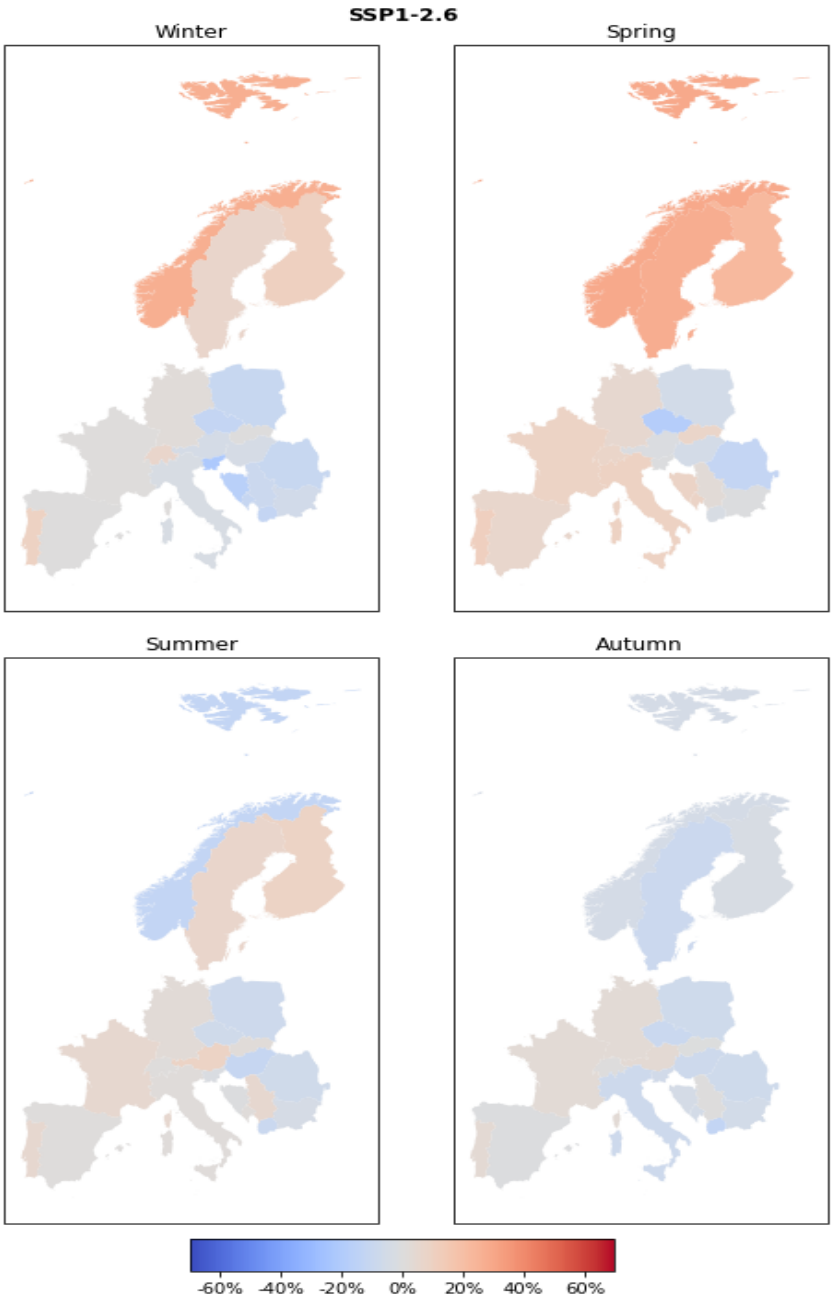

Figure C.2: Ensemble mean intra-annual relative change in runoff between EOC and BOC for hydro energy. The results are for SSP1-2.6

Country Code	Countries	2014	2015	2016	2017	2018	2019	Average
AL	Albania	0.16	0.16	0.16	0.14	0.15	0.18	0.16
AD	Andorra	0.12	0.12	0.12	0.12	0.06	0.04	0.10
AT	Austria	0.11	0.11	0.11	0.11	0.11	0.11	0.11
BY	Belarus	0.05	0.14	0.07	0.13	0.13	0.13	0.11
BE	Belgium	0.11	0.11	0.11	0.10	0.11	0.10	0.11
BA	Bosnia Herzg	0.13	0.13	0.19	0.15	0.13	0.15	0.15
BG	Bulgaria	0.14	0.15	0.15	0.15	0.15	0.16	0.15
HR	Croatia	0.12	0.14	0.13	0.15	0.13	0.11	0.13
CY	Cyprus	0.15	0.19	0.20	0.18	0.19	0.16	0.18
CZ	Czechia	0.12	0.12	0.12	0.12	0.13	0.13	0.12
DK	Denmark	0.11	0.09	0.10	0.09	0.11	0.10	0.10
EE	Estonia	0.10	0.10	0.11	0.11	0.11	0.07	0.10
FI	Finland	0.08	0.08	0.06	0.07	0.07	0.08	0.07
FR	France	0.12	0.12	0.13	0.13	0.13	0.13	0.13
DE	Germany	0.11	0.11	0.11	0.11	0.12	0.11	0.11
GR	Greece	0.17	0.17	0.17	0.17	0.16	0.18	0.17
HU	Hungary	0.09	0.09	0.12	0.12	0.10	0.12	0.11
IS	Iceland	0.09	0.09	0.09	0.09	0.09	0.09	0.09
IE	Ireland	0.17	0.17	0.12	0.08	0.08	0.08	0.12
IT	Italy	0.14	0.14	0.13	0.14	0.13	0.13	0.13
LV	Latvia	0.06	0.13	0.06	0.07	0.07	0.11	0.08
LT	Lithuania	0.12	0.12	0.11	0.11	0.12	0.13	0.12
LU	Luxembourg	0.10	0.10	0.09	0.10	0.10	0.09	0.10
MT	Malta	0.14	0.14	0.16	0.17	0.16	0.16	0.16
MD	Moldova Rep	0.11	0.17	0.09	0.11	0.11	0.07	0.11
ME	Montenegro	0.15	0.15	0.15	0.15	0.15	0.15	0.15
NL	Netherlands	0.08	0.08	0.09	0.09	0.09	0.08	0.09
MK	North Macedonia	0.11	0.15	0.16	0.16	0.13	0.10	0.14
NO	Norway	0.10	0.10	0.10	0.10	0.10	0.10	0.10
PL	Poland	0.03	0.06	0.08	0.07	0.06	0.05	0.06
PT	Portugal	0.17	0.20	0.19	0.19	0.17	0.17	0.18
RO	Romania	0.14	0.17	0.15	0.15	0.15	0.15	0.15
RS	Serbia	0.05	0.08	0.08	0.08	0.07	0.07	0.07
SK	Slovakia	0.13	0.11	0.11	0.11	0.14	0.11	0.12
SI	Slovenia	0.13	0.13	0.13	0.13	0.12	0.13	0.13
ES	Spain	0.20	0.20	0.20	0.21	0.19	0.12	0.19
SE	Sweden	0.09	0.11	0.11	0.11	0.11	0.11	0.10
CH	Switzerland	0.09	0.09	0.09	0.10	0.10	0.10	0.10
GB	UK	0.08	0.09	0.10	0.10	0.11	0.11	0.10
UA	Ukraine	0.12	0.12	0.11	0.11	0.09	0.07	0.11

Table C.1: Overview of yearly (2014-2019) solar energy historical capacity factors from IRENA for 38 European countries

Country Code	Countries	IRENA	Ensemble	% Difference
AL	Albania	0.16	0.13	19%
AT	Austria	0.11	0.11	8%
BY	Belarus	0.11	0.09	18%
BE	Belgium	0.11	0.1	11%
BA	Bosnia Herzg	0.15	0.12	22%
BG	Bulgaria	0.15	0.13	20%
HR	Croatia	0.13	0.12	7%
CZ	Czechia	0.12	0.1	25%
DK	Denmark	0.1	0.09	9%
EE	Estonia	0.1	0.09	17%
FI	Finland	0.07	0.08	-5%
FR	France	0.13	0.11	13%
DE	Germany	0.11	0.1	15%
GR	Greece	0.17	0.14	20%
HU	Hungary	0.11	0.11	-6%
IE	Ireland	0.12	0.08	43%
IT	Italy	0.13	0.13	2%
LV	Latvia	0.08	0.09	-3%
LT	Lithuania	0.12	0.09	30%
MT	Malta	0.16	0.15	0%
MD	Moldova Rep	0.11	0.11	-1%
ME	Montenegro	0.15	0.12	22%
NL	Netherlands	0.09	0.1	-10%
MK	North Macedonia	0.14	0.13	6%
NO	Norway	0.1	0.07	40%
PT	Portugal	0.18	0.14	28%
RO	Romania	0.15	0.11	33%
SK	Slovakia	0.12	0.1	14%
SI	Slovenia	0.13	0.12	12%
ES	Spain	0.19	0.14	33%
SE	Sweden	0.1	0.08	31%
CH	Switzerland	0.1	0.11	-10%
GB	UK	0.1	0.08	19%
UA	Ukraine	0.11	1	0%

Table C.2: Overview of IRENA and ensemble solar energy capacity factors with relative percentage difference for 38 European countries

Countries	Standard Deviation BOC	Standard Deviation EOC	Δ in %
AL	0.0020	0.0013	-37.1
AT	0.0025	0.0014	-44.1
BA	0.0026	0.0012	-53.5
BE	0.0020	0.0016	-21.8
BG	0.0020	0.0014	-30.0
BY	0.0021	0.0019	-10.2
CH	0.0022	0.0017	-23.0
CZ	0.0024	0.0015	-38.7
DE	0.0018	0.0014	-18.6
DK	0.0014	0.0013	-6.3
EE	0.0017	0.0015	-12.0
ES	0.0019	0.0012	-34.4
FI	0.0013	0.0013	2.0
FR	0.0019	0.0014	-25.8
GB	0.0013	0.0016	24.6
GR	0.0016	0.0012	-26.4
HR	0.0025	0.0011	-53.7
HU	0.0025	0.0011	-54.1
IE	0.0016	0.0018	13.9
IT	0.0018	0.0010	-41.6
LT	0.0019	0.0016	-12.0
LV	0.0017	0.0016	-6.3
MD	0.0022	0.0018	-20.1
ME	0.0024	0.0013	-46.7
MK	0.0022	0.0015	-32.4
MT	0.0011	0.0011	7.9
NL	0.0017	0.0016	-5.0
NO	0.0013	0.0013	-4.6
PL	0.0021	0.0015	-27.4
PT	0.0019	0.0014	-25.4
RO	0.0023	0.0014	-38.2
RS	0.0024	0.0013	-47.8
RU	0.0012	0.0013	15.3
SE	0.0011	0.0013	17.6
SI	0.0025	0.0014	-45.7
SK	0.0026	0.0014	-46.3
TR	0.0018	0.0014	-20.9
UA	0.0023	0.0018	-21.0

Table C.3: Overview of yearly averaged solar energy capacity factors standard deviation at BOC and EOC with relative percentage change column

Countries	NRMSE before calibration	NRMSE after calibration
AL	16.5%	9.8%
AT	19.4%	12.1%
BA	13.0%	10.7%
BE	12.5%	11.5%
BG	14.7%	10.3%
BY	15.9%	9.4%
CH	24.9%	16.3%
CZ	16.5%	8.8%
DE	14.7%	9.1%
DK	15.5%	7.6%
EE	20.0%	9.3%
ES	13.6%	8.4%
FI	14.9%	6.9%
FR	15.2%	11.7%
GB	20.7%	11.4%
GR	13.0%	7.7%
HR	11.8%	9.0%
HU	14.7%	9.2%
IE	25.1%	13.8%
IT	12.1%	8.5%
LT	16.1%	8.5%
LV	18.5%	9.1%
MD	12.7%	9.1%
ME	18.1%	11.9%
MK	17.2%	11.0%
MT	13.7%	5.7%
NL	12.6%	9.9%
NO	25.3%	8.5%
PL	14.4%	8.9%
PT	12.4%	7.6%
RO	17.0%	10.4%
RS	16.6%	10.6%
RU	16.2%	8.3%
SE	15.5%	6.4%
SI	11.6%	10.0%
SK	15.1%	10.0%
TR	15.6%	10.7%
UA	13.5%	9.9%

Table C.4: Overview of NRMSE values for solar energy before and after calibration. The calibration significantly improves the match with ERA5 data

Country	NRMSE before calibration	NRMSE after	Calibration factor
AL	75.6%	68.1%	0.27
AT	27.4%	26.7%	0.45
BA	67.4%	56.5%	0.30
BE	10.6%	14.1%	0.83
BG	40.4%	27.1%	0.47
BY	30.7%	25.0%	0.92
CH	63.3%	47.1%	0.29
CZ	28.0%	26.7%	0.65
DE	15.2%	8.0%	0.64
DK	9.5%	6.7%	0.81
EE	7.4%	6.0%	0.81
ES	29.7%	27.2%	0.60
FI	38.1%	16.2%	0.42
FR	12.4%	8.1%	0.68
GB	13.2%	7.8%	0.73
GR	56.1%	46.4%	0.45
HR	49.7%	34.4%	0.41
HU	18.2%	14.8%	0.62
IE	35.2%	21.4%	0.55
IT	54.9%	43.4%	0.44
LT	20.8%	16.4%	0.69
LV	14.7%	6.1%	0.71
MD	31.3%	19.2%	0.46
ME	58.4%	48.0%	0.41
MK	68.1%	55.1%	0.27
MT	11.1%	10.8%	0.91
NL	22.0%	18.1%	0.85
NO	22.3%	12.7%	0.69
PL	17.9%	15.3%	0.78
PT	34.7%	27.6%	0.62
RO	33.8%	21.6%	0.47
RS	42.9%	29.8%	0.41
RU	24.5%	24.5%	1.00
SE	34.3%	14.2%	0.44
SI	62.5%	47.8%	0.30
SK	30.1%	24.0%	0.49
TR	41.6%	41.6%	1.00
UA	17.2%	15.9%	0.61

Table C.5: Overview of NRMSE values for wind energy before and after calibration. The calibration significantly improves the match with ERA5 data

Countries	Standard Deviation BOC	Standard Deviation EOC	Δ in %
AL	0.0099	0.0080	-18.7%
AT	0.0041	0.0059	43.2%
BA	0.0081	0.0059	-27.4%
BE	0.0151	0.0170	12.5%
BG	0.0076	0.0059	-22.3%
BY	0.0082	0.0098	18.6%
CH	0.0037	0.0049	32.6%
CZ	0.0072	0.0101	41.1%
DE	0.0103	0.0142	38.1%
DK	0.0146	0.0173	17.9%
EE	0.0155	0.0128	-17.8%
ES	0.0071	0.0067	-5.3%
FI	0.0144	0.0105	-26.7%
FR	0.0084	0.0105	25.6%
GB	0.0145	0.0164	13.1%
GR	0.0074	0.0063	-15.0%
HR	0.0082	0.0070	-15.3%
HU	0.0064	0.0073	13.1%
IE	0.0135	0.0189	39.9%
IT	0.0075	0.0075	0.6%
LT	0.0143	0.0129	-9.7%
LV	0.0150	0.0126	-16.1%
MD	0.0081	0.0080	-1.4%
ME	0.0089	0.0054	-39.4%
MK	0.0061	0.0038	-38.3%
MT	0.0172	0.0178	3.7%
NL	0.0176	0.0178	1.3%
NO	0.0090	0.0074	-17.7%
PL	0.0095	0.0107	12.8%
PT	0.0100	0.0114	14.5%
RO	0.0062	0.0056	-9.5%
RS	0.0069	0.0051	-27.0%
RU	0.0133	0.0087	-34.2%
SE	0.0113	0.0105	-6.9%
SI	0.0063	0.0066	4.1%
SK	0.0058	0.0082	42.4%
TR	0.0059	0.0056	-5.0%
UA	0.0059	0.0068	14.8%

Table C.6: Overview of yearly averaged wind energy capacity factors standard deviation at BOC and EOC with relative percentage change column

Countries	Standard Deviation BOC	Standard Deviation EOC	Δ in %
SE	1.6E+08	1.8E+08	14.1%
ES	2.1E+07	2.1E+07	-3.7%
NO	3.1E+08	3.3E+08	6.9%
AT	2.6E+07	3.1E+07	19.6%
BG	4.2E+06	6.8E+06	64.4%
FI	2.9E+07	3.3E+07	15.5%
HR	1.1E+05	1.9E+05	79.6%
ME	3.9E+05	4.3E+05	10.4%
PT	1.6E+07	1.3E+07	-20.8%
RO	2.9E+07	2.8E+07	-5.0%
CH	1.9E+07	2.4E+07	31.3%
FR	1.4E+07	1.9E+07	40.0%
IT	1.2E+07	1.8E+07	48.7%
DE	3.8E+05	4.1E+05	7.5%
CZ	4.4E+06	5.6E+06	27.3%
HU	6.8E+06	6.1E+06	-9.5%
PL	9.9E+05	1.0E+06	2.4%
SK	1.8E+07	1.5E+07	-15.6%
BA	5.1E+06	5.4E+06	5.3%
MK	7.5E+05	8.3E+05	10.3%
RS	2.6E+06	2.9E+06	12.5%
SI	1.5E+06	2.0E+06	26.5%

Table C.7: Overview of yearly averaged hydro energy capacity factors standard deviation at BOC and EOC with relative percentage change column